
Doctoral Dissertations

Student Theses and Dissertations

Spring 2020

Geophysical characteristics of nickel and copper deposits in Wadi Al Khadra prospect, southwestern of Saudi Arabia

Abdulrahman Ahmed Aljabbab

Follow this and additional works at: https://scholarsmine.mst.edu/doctoral_dissertations



Part of the [Geological Engineering Commons](#), and the [Geophysics and Seismology Commons](#)

Department: Geosciences and Geological and Petroleum Engineering

Recommended Citation

Aljabbab, Abdulrahman Ahmed, "Geophysical characteristics of nickel and copper deposits in Wadi Al Khadra prospect, southwestern of Saudi Arabia" (2020). *Doctoral Dissertations*. 3030.

https://scholarsmine.mst.edu/doctoral_dissertations/3030

This thesis is brought to you by Scholars' Mine, a service of the Missouri S&T Library and Learning Resources. This work is protected by U. S. Copyright Law. Unauthorized use including reproduction for redistribution requires the permission of the copyright holder. For more information, please contact scholarsmine@mst.edu.

GEOPHYSICAL CHARACTERISTICS OF NICKEL AND COPPER DEPOSITS IN
WADI AL KHADRA PROSPECT, SOUTHWESTERN OF SAUDI ARABIA

by

ABDULRAHMAN AHMED ALJABBAB

A DISSERTATION

Presented to the Graduate Faculty of the

MISSOURI UNIVERSITY OF SCIENCE AND TECHNOLOGY

In Partial Fulfillment of the Requirements for the Degree

DOCTOR OF PHILOSOPHY

in

GEOLOGICAL ENGINEERING

2020

Approved by:

Neil Anderson, Advisor

J. David. Rogers

Kelly Liu

Ralph Flori

Abdulrahman Alotaibi

© 2020

ABDULRAHMAN AHMED ALJABBAB

All Rights Reserved

ABSTRACT

Three geophysical datasets (self-potential, magnetics, and time - domain electromagnetics) were acquired at Wadi Al Khadra Ni-Cu prospect in southwest Saudi Arabia, and were processed and interpreted for the Saudi Geological Survey. The primary objectives were to map the distribution of metallic mineralization, map structures, verify the integration of the geophysical interpretations and its signatures in conjunction with boreholes information, distinguish the similarities and differences in the integrated interpretation of geophysical data, and design optimal processing and interpretation data parameters. The self-potential tool was used to map the variation in natural surface potential differences to map lateral variations in the distribution of shallow metallic minerals, specifically copper and nickel, qualitatively. The time-domain electromagnetic tool was utilized to measure the lateral and vertical variations in the conductivity of the subsurface to map the distribution of metallic mineralization to depths approximately 140 meters and structures (faults) that control the distribution of mineralization qualitatively. A magnetic tool was used to map lateral variations in the magnetic field of the earth to map the distribution of magnetically susceptible mineralization (magnetite and nickel) and structures (faults) that control the distribution of mineralization and to map structures qualitatively. Surface-based geologic data and core hole control were used to constrain the interpretation of the geophysical data.

The investigation was successful. The interpreted geophysical data sets are consistent with one another (re: distribution of metallic mineralization) and consistent with surface-based geologic control and core hole data.

ACKNOWLEDGMENTS

In the beginning, I am grateful to the Almighty God for helping me to complete this dissertation successfully and to obtain a Ph.D. degree; thanks to God. I extend my sincere thanks to my country, the Kingdom of Saudi Arabia, represented by my employer, King Abdulaziz City for Science and Technology (KACST), which give me the opportunity to complete the Ph.D. degree with full scholarship.

I would like to express my deepest appreciation and thanks to my advisor, Dr. Neil Anderson, for his expertise, support, valuable guidance, technical and editorial advice, and encouragement. His contributions were essential to the completion of this dissertation and provided me with different and important perspectives with respect to academic research in general. I would also like to extend my deepest thanks and gratitude to Dr. Abdulrahman Alotaibi for continually following up on my research progress and for constructive input that significantly improved the contents of the dissertation. My thanks also go to my other committee members, Dr. J. David. Rogers, Dr. Kelly Liu, and Dr. Ralph Flori, for perusing drafts of the dissertation and providing valuable comments.

I would like to thank the Saudi Geological Survey (SGS) for its support and for providing me with all necessary geophysical and geological data.

Last, but not least, I'm deeply indebted to my parents and extend my deepest gratitude and love for their dedicated support throughout my life. My success would not have been possible without the support and nurturing I received from my wife and my son, Ahmed. I deeply and especially thank them for their understanding, lasting cooperation and love during the past few years. God bless you.

TABLE OF CONTENTS

	Page
ABSTRACT.....	iii
ACKNOWLEDGMENTS	iv
LIST OF ILLUSTRATIONS.....	xi
LIST OF TABLES	xvi
 SECTION	
1. INTRODUCTION.....	1
1.1. OVERVIEW OF THE RESEARCH	1
1.2. SIGNIFICANCE OF THIS RESEARCH AND OBJECTIVES.....	3
1.3. PREVIOUS STUDIES OF THE WADI AL KHADRA AND JABAL IBRAHIM QUADRANGLE.....	4
1.4. PREVIOUS GEOPHYSICAL STUDIES CASES OF NICKEL AND COPPER DEPOSITS	5
1.4.1. Geophysics of the Voisey’s Bay Ni-Cu-Co Deposits (SEG, 1998)	5
1.4.2. Geophysical Response of the Munali Ni-Cu Deposit (ASEG/PESA Conference, 2009).....	6
1.4.3. Time Domain EM and Magnetic Mapping of the Ferguson Lake Nickel-Copper-Cobalt-PGE Property (SEG, 2002).....	6
1.4.4. Geophysical Signature of the Jinchuan Ni-Cu-PGE Deposit, Gansu Province, China.....	7
2. GEOLOGY OF THE STUDY AREA	8
2.1. INTRODUCTION OF GEOLOGY OF SAUDI ARABIA	8
2.2. OVERVIEW OF THE ARABIAN SHIELD	9
2.3. LOCATION OF THE WADI AL KHADRA Ni-Cu PROSPECT.....	12

2.4. GEOLOGY OF THE WADI AL KHADRA PROSPECT	13
2.5. STRUCTURE TRENDS.....	18
2.5.1. The Northwest to Southeast Trends (Red Sea Trend).....	18
2.5.2. The Northeast to Southwest Trends (Aqaba Trends)	19
2.6. DRILL HOLES DATA OF WADI AL KHADRA PROSPECT	20
2.6.1. Well (KAD-1).....	20
2.6.2. Well (KAD-2).....	22
2.6.3. Well (KAD-3).....	22
2.6.4. Well (KAD-4).....	22
3. DISTRIBUTION OF MINERAL DEPOSITS IN SAUDI ARABIA	25
3.1. BRIEFLY INTRODUCTION OF MINERAL DEPOSITS	25
3.2. PROPERTIES OF NICKEL	27
3.2.1. Occurrences of Nickel	27
3.2.2. Occurrences of Nickel in Saudi Arabia	28
3.2.2.1. Stratiform massive sulfide mineralization in volcanoclastic rocks.	29
3.2.2.2. Disseminated massive sulfides in mafic and ultramafic rocks.	30
3.2.2.3. Gossans	31
3.3. PROPERTIES OF COPPER.....	31
3.3.1. Occurrences of Copper	32
3.3.2. Occurrences of Copper in Saudi Arabia.....	32
3.3.2.1. Jabal Sayid copper – zinc deposit.....	33
3.3.2.2. Kutam copper – zinc deposit.	33

3.3.2.3. Jabal Ash Shizm copper prospects.....	33
3.3.2.4. Umm Ad Damar copper prospect	33
4. GEOPHYSICAL METHODOLOGY	35
4.1. INTRODUCTION OF GEOPHYSICAL METHODS IN MINERAL EXPLORATION	35
4.2. SELF-POTENTIAL METHOD.....	35
4.2.1. Occurrence of SP and Electrical Potentials	36
4.2.2. Mechanism of Self-Potential	37
4.3. MAGNETIC METHOD	38
4.3.1. Magnetic Field of the Earth.....	40
4.3.2. Magnetic Susceptibility.....	43
4.3.3. Types of Magnetic Materials.....	44
4.4. TIME-DOMAIN ELECTROMAGNETIC METHOD.....	47
5. GEOPHYSICAL DATA ACQUISITION AND PROCESSING	53
5.1. INTRODUCTION OF DATA ACQUISITION	53
5.2. SELF-POTENTIAL SURVEY DATA ACQUISITION	53
5.3. SP DATA PROCESSING	55
5.4. MAGNETIC SURVEY DATA ACQUISITION	55
5.5. MAGNETIC DATA PROCESSING.....	56
5.5.1. Reduction to the Pole (RTP)	57
5.5.2. First Vertical Derivative.....	57
5.5.3. Tilt Derivative	60
5.5.4. Upward Continuation Filtering	61

5.5.5. Analytical Signal Derivative (AS)	62
5.5.6. Regional and Residual Magnetic Maps	62
5.5.7. 3-D Euler Deconvolution	62
5.5.8. Radially Average Power Spectrum	63
5.5.9. 2D Modeling.....	63
5.6. TIME-DOMAIN ELECTROMAGNETIC SURVEY DATA ACQUISITION	64
5.7. TDEM DATA PROCESSING	65
6. GEOPHYSICAL DATA RESULTS AND INTERPRETATIONS	68
6.1. SELF-POTENTIAL RESULTS	68
6.1.1. Self-Potential Mapping.....	68
6.1.2. Self-Potential Profiling.....	69
6.2. MAGNETIC DATA RESULTS.....	73
6.2.1. Overview of Magnetic Results	73
6.2.2. Qualitative Interpretation of the Potential Field.....	74
6.2.2.1. Nature of the observed magnetic anomalies	75
6.2.2.2. Description of the detailed ground magnetic data	76
6.2.2.3. Regional and residual maps of the ground magnetic data	79
6.2.2.4. Structural trend analysis.....	80
6.2.3. Quantitative Interpretation of the Potential Field Data	83
6.2.3.1. Spectral analysis methods.....	83
6.2.3.2. Analytical signal derivative	90
6.2.3.3. 3D euler deconvolution method.....	90

6.2.3.4. 2D modeling.	91
6.2.3.5. Magnetic susceptibility	94
6.3. TIME-DOMAIN ELECTROMAGNETIC RESULTS	94
6.3.1. Overview of TDEM Results.....	94
6.3.2. Two Dimension Sounding (Resistivity Profiles).....	100
6.3.3. Two Dimension of Electrical Resistivities Change with the Depth..	104
6.3.4. 3D Dimension.....	104
7. DISCUSSION, CONCLUSION, AND RECOMMENDATIONS	108
7.1. GEOPHYSICAL METHODS CAN BE USED TO MAP THE DISTRIBUTION OF METALLIC MINERALLIZATION.....	108
7.2. GEOPHYSICAL METHODS CAN BE USED TO MAP THE ORIENTATION FAULTS.....	109
7.3. BOREHOLE AND SURFICIAL GEOLOGICAL DATA TO VERIFY THE REASONABLENESS OF THE SP, MAGNETIC, AND TDEM INTERPRETATIONS SIGNATURES	109
7.4. THE DIFFERENCES AND SIMILARITIES BETWEEN THE INTERPRETATIONS OF THE OF THE SP, MAGNETIC AND TDEM DATA.....	119
7.5. OPTIMAL ACQUISITION PARAMETERS BASED ON THE ASSESSMENT OF THE ACQUIRED DATA.....	119
7.6. OPTIMAL PROCESSING PARAMETERS BASED ON THE ASSESSMENT OF THE ACQUIRED DATA.....	120
7.7. OPTIMAL INTERPRETATION PARAMETERS BASED ON THE ASSESSMENT OF THE ACQUIRED DATA.....	125
7.8. STRENGTHS AND LIMITATIONS OF THE GEOPHYSICAL METHODS.....	126
7.9. CONCLUSIONS	128
7.10. RECOMMENDATIONS.....	132

APPENDICES

A. SURFICIAL SAMPLES ASSAY RESULTS OF NICKEL AND COPPER IN WADI AL KHADRA PROSPECT AREA.....	133
B. MINERALIZATION ZONES OF DRILL HOLES IN WADI AL KHADRA PROSPECT AREA	154
REFERENCES	159
VITA.....	165

LIST OF ILLUSTRATIONS

	Page
Figure 2.1 Map of geological divisions of the Kingdom of Saudi Arabia, Sourced by SGS.....	8
Figure 2.2 Distribution of exposed Precambrian rocks in the Arabian Peninsula and adjacent parts of northeast Africa.....	9
Figure 2.3 Stratigraphic intervals in the Proterozoic showing the periods represented by the Proterozoic rocks in Saudi Arabia	10
Figure 2.4 Arabian shield's terranes and sutures	11
Figure 2.5 Location map of the study area in Saudi Arabia.	12
Figure 2.6 Geology map of Jabal Ibrahim quadrangle.	17
Figure 2.7 Geological map of Wadi Al Khadra prospect, SGS, 2013	21
Figure 2.8 1) Location map of drilled well on RTP map of the study area, 2) Satellite map of location drill holes of the study area.	23
Figure 2.9 The distribution of the copper and nickel concentrations in the drilled holes.	24
Figure 3.1 Map distribution of metallic minerals deposits in Saudi Arabia, Data sources by SGS.....	25
Figure 3.2 Map distribution of nonmetallic minerals deposits in Saudi Arabia, Data sources by SGS	26
Figure 3.3 1) Nickel, and 2) Nickel-Copper-Platinum Ore Locality.	28
Figure 3.4 Map of nickel deposits and prospects drilled localities, sourced by SGS. ...	29
Figure 3.5 1) Copper from Bisbee, Arizona, and 2.Chalcopyrite, the most important ore of copper.....	32
Figure 3.6 Map of Copper deposits and prospects drilled localities.....	34
Figure 4.1 A schematic model of the origin of the self-potential anomaly of an orebody.	39

Figure 4.2 Earth's magnetic field depicted as the field of a bar magnet.	41
Figure 4.3 Schematic diagram of geomagnetic field elements	42
Figure 4.4 Magnetic susceptibility of common rocks, Exploration geophysics	45
Figure 4.5 Magnetic properties of some materials.....	47
Figure 4.6 Illustrates generally the resistivities and electrical conductivities of most rock groups.....	48
Figure 4.7 Transmitter current wave-form in TEM method, EPA.	49
Figure 4.8 System of equivalent current filaments at various times after current interruption in the transmitter loop, showing their downward and outward movement. EPA	50
Figure 4.9 Log plot-receiver output voltage versus time (one transient).....	51
Figure 5.1 Map of SP data acquisition of Wadi Al Khadra Prospect.	54
Figure 5.2 Elrec Lite instruments were using of SP survey, IRIS Company, France....	55
Figure 5.3 Map of Magnetic data acquisition of Wadi Al Khadra Prospect.....	58
Figure 5.4 G-858 Portable Cesium Magnetometer was using of magnetic survey /Gradiometer, Geometrics.	59
Figure 5.5 IGRF model of the study area, geomag.bgs.ac.uk/data	59
Figure 5.6 Effects of using the reduction-to-pole correction	60
Figure 5.7 Map of TDEM acquisition data of Wadi Al Khadra Prospect	66
Figure 5.8 GDP-32 receiver used for TDEM survey, A Zonge.....	67
Figure 5.9 Layout of TEM survey, adapted from Zonge International.	67
Figure 6.1 SP contour map of Wadi Al Khadra Prospect.	70
Figure 6.2 Self-potential anomaly in line 325 associated with grounded monitoring instruments.....	71
Figure 6.3 Self-potential anomaly in line 425 associated with grounded monitoring instruments	71

Figure 6.4 Self-potential anomaly in line 525 associated with grounded monitoring instruments.....	71
Figure 6.5 Self-potential anomaly in line 625 associated with grounded monitoring instruments.....	71
Figure 6.6 Self-potential anomaly in line 725 associated with grounded monitoring instruments.....	72
Figure 6.7 Self-potential anomaly in line 825 associated with grounded monitoring instruments.....	72
Figure 6.8 Self-potential anomaly in line 925 associated with grounded monitoring instruments.....	72
Figure 6.9 Self-potential anomaly in line 1025 associated with grounded monitoring instruments.....	72
Figure 6.10 Self-potential anomaly in line 1100 associated with grounded monitoring instruments.....	73
Figure 6.11 Map of total magnetic intensity (TMI) of Wadi Al Khadra Prospect.	78
Figure 6.12 Reduce to the pole (RTP) map of the Wadi AL Khadra Prospect.....	81
Figure 6.13 Tilt derivative (contour at zero level) map of the Wadi Al Khadra Prospect.	84
Figure 6.14 First vertical derivative map of Wadi Al Khadra Prospect.	85
Figure 6.15 Residual anomaly map from Upward continuation.....	86
Figure 6.16 Regional anomaly (low pas map).....	87
Figure 6.17 Residual anomaly (High pass map).....	88
Figure 6.18 Rose diagram shows analyzed and plotted structure trends systems in the study area.....	89
Figure 6.19 2D radially averaged power spectrum for magnetic survey.....	89
Figure 6.20 Analytical signal map of magnetic survey.	93
Figure 6.21 The elevation map of the study area.....	95
Figure 6.22 Map of Euler Deconvolution.....	96

Figure 6.23 RTP of magnetic anomaly map, showing location of the selected profiles for 2D modeling.	97
Figure 6.24 Two-dimension magnetic model along the profile A-A'	98
Figure 6.25 Two-dimension magnetic model along the profile B-B'	98
Figure 6.26 Map of Magnetic Susceptibility in the study area.	99
Figure 6.27 TDEM sounding No. 350 in the Wadi Al Khadra prospect survey.....	101
Figure 6.28 TDEM sounding No. 375 in the Wadi Al Khadra prospect survey.....	102
Figure 6.29 TDEM sounding No. 400 in the Wadi Al Khadra prospect survey.....	102
Figure 6.30 TDEM sounding No. 575 in the Wadi Al Khadra prospect survey.....	102
Figure 6.31 TDEM sounding No. 650 in the Wadi Al Khadra prospect survey.....	103
Figure 6.32 TDEM sounding No. 725 in the Wadi Al Khadra prospect survey.....	103
Figure 6.33 TDEM sounding No. 1025 in the Wadi Al Khadra prospect survey.....	103
Figure 6.34 2D TDEM sounding maps in different depth level shows the distribution of resistivity values.	106
Figure 6.35 3D TDEM sounding maps in different depth shows the distribution of resistivity values.	107
Figure 7.1 SP map showing the distribution of negative SP anomalies of the study area.	111
Figure 7.2 RTP map showing the distribution of positive magnetic anomalies of the study area.	112
Figure 7.3 TDEM map shows a distribution at depth between 25m – 75m.	113
Figure 7.4 Maps from three methods showing the interpreted distribution of metallic minerals in the study area.....	114
Figure 7.5 Interpreted fault trends superposed on 1) SP map, 2) RTP map, and 3) TDEM map.	115
Figure 7.6 TDEM soundings showing the interpreted faults.....	116
Figure 7.7 The main fault trends interpreted from geophysical data.....	117

Figure 7.8 Maps showing distribution of Ni and Cu in parts per million based on surficial samples acquired in the study area.	121
Figure 7.9 Map showing the distribution of Nickel/Copper deposits in the study area from surficial samples and using integrated geophysical data from SP, Mag, and TDEM methods.	122
Figure 7.10 SP map shows all lines of survey, a line 425 SP profile showing negative values.	123
Figure 7.11 RTP map shows all magnetic lines compared with Euler depth map, a line 425 magnetic profile showing high positive amplitudes values.....	124
Figure 7.12 TDEM Sounding 400 showing the lithological.	125

LIST OF TABLES

	Page
Table 3.1 Nickel deposits and prospects tested by drill holes.	30
Table 4.1 Types of SP anomalies and their respective geological sources.....	36
Table 4.2 Magnetic susceptibility of various rocks and minerals $\chi 10^3$ SI.....	46

1. INTRODUCTION

1.1. OVERVIEW OF THE RESEARCH

In 2016, Saudi Arabia launched the “2030 Vision” statement, including several initiatives, one of which is to improve the mining sector by exploration, extraction, and alloying. Based on this initiative, relevant departments at universities, academic institutes, and private mining companies focus their research efforts on this topic. Covering approximately 2 million km², Saudi Arabia is the largest country in the Middle East and the 14th largest country in the world. Saudi Arabia’s size and geology make it rich in minerals, oil, and gas - key raw materials for manufacturing and industrial development. These mineral resources represent one of the most important economic resources of Saudi Arabia, supporting the anticipation that the mining sector will become the third pillar of the Saudi economy after oil and petrochemicals.

The exposed Proterozoic rocks of the Arabian Shield, in the western part of the kingdom, contain most metallic minerals (such as nickel and copper). The Wadi Al Khadra nickel-copper prospect (the study area for this research) lies in the Al Baha region in the southwest.

The Al Baha Region contains many sources of precious metals such as gold and silver, as well as base metals such as copper and zinc, in addition to some industrial metal ores. Long abandoned mining excavations such as pits, exploration adits, and shallow mining shafts, drifts, and tunnels lie in the Wadi Al Khadra prospect area. Some people assume that the mine works are more than 200 years old.

The Wadi Al Khadra prospect area interests copper-nickel explorers because metagabbro rocks, characterized by coarse-grained metamorphosed gabbro and minor anorthosite, are present. The area also contains syngenetic copper and nickel minerals disseminated within thin-layered, ultramafic to mafic lava flows that range from normal flows to agglomerates.

These mineral assemblages mainly consist of copper in oxidized and sulfide form and nickel, expressed by chalcopyrite, pyrite, niccolite, pentlandite, and arsenopyrite. Mineralization orebody is defined on the surface by a gossan-or iron-comprising brownish red oxidation and elongated zone containing mainly hematite, goethite, and limonite, and this orebody occurs in layered zones in mafic rocks of variable composition as veinlets, clusters, patches, and stringers along the foliation or fractures and mineralization.

In terms of work related to the new mining initiative, this dissertation advances the processing and interpretation of geophysical data. This dissertation contains seven sections with the first section consisting of the introduction, significance, and objectives of this research. Section 2 presents a brief geology of Saudi Arabia and the geology of the study area. Section 3 consists of the distribution of mineral deposits in Saudi Arabia, while Section 4 contains the geophysics methodology. Section 5 identifies the geophysics acquisitions and processing. Section 6 presents the geophysical results. Finally, Section 7 consists of the discussion and interpretation of the results and contains conclusions from the findings and suggested recommendations.

1.2. SIGNIFICANCE OF THIS RESEARCH AND OBJECTIVES

The main aim of this research is to enhance the exploration of nickel and copper mineralization occurrences using three geophysical survey tools: self-potential, magnetic, and time domain-electromagnetics. These geophysical data were acquired in 2009 by the Saudi Geological Survey (SGS) across the Wadi al Khadra prospect area to assess the area's nickel-copper prospect. . This study will assist the mineral exploration and effort; the results will be of genuine interest to those engaged in mineral exploration in Saudi Arabia and elsewhere.

Based on advanced processing and quantitative and qualitative interpretation of the integrated data of three geophysical datasets, nine primary specific objectives are addressed in this research in order to:

- I. Demonstrate that SP, MAG and TDEM data can be used to map the distribution of metallic mineralization.
- II. Demonstrate that geophysical methods can be used to map the orientation faults.
- III. Demonstrate that Borehole and Surficial geological data verify the reasonableness of the SP, MAG, and TDEM interpretations signatures.
- IV. Demonstrate and explain the differences / similarities between the interpretations of the SP, MAG and TDEM data.
- V. Design optimal acquisition interpretation parameters based on the assessment of the acquired data.
- VI. Design optimal processing parameters based on the assessment of the acquired data.

- VII. Design optimal interpretation parameters based on the assessment of the acquired data.
- VIII. Summarize the strengths and limitations of the geophysical methods.
- IX. Develop recommendations for further exploration activities.

1.3. PREVIOUS STUDIES OF THE WADI AL KHADRA AND JABAL IBRAHIM QUADRANGLE

In 1973, a team of geoscientists from the United States Geological Survey (USGS) visited the Wadi al Khadra area. Sample assay results and observations were obtained and described (Greenwood, a 1975). In 1979, USGS geologists revisited the area and carried out mapping and detailed sampling that consisted of 24 grab, 50 spot, and 10 channel samples (Worl & Wynn, 1979). Based on all available data at that time, USGS geologists Worl and Wynn in 1979 recommended a drilling program over an identified oxidation zone in the Wadi al Khadra area (Worl & Wynn, 1982) (From SGS,2015). In 1978, the Arabian Geophysical and Surveying Company (ARGAS) acquired geophysical data, including an electromagnetic and self-potential survey. A magnetic survey was also conducted by the USGS. These surveys were part of a regional study to evaluate airborne electromagnetic geophysical anomalies previously identified in the Wadi Bidah area (ARGAS, 1978).

In between 1985 and 1986, the USGS, in cooperation with the Deputy Ministry for Mineral Resources of Saudi Arabia, conducted an integrated structural and geochemical study of the northern Nabitah fault zone in the Wadi Al Khadra area. The Nabitah fault system is a significant tectonic element of the Arabian Shield. This study

was conducted to more accurately determine relationships between structural and geochemical data and to develop structural and petrochemical evidence to define the tectonic role of the Nabitah fault (Quick & Bosch 1990).

In 2009, the Saudi Geological Survey (SGS) carried out a detailed exploration program at the Wadi al Khadra Cu-Ni prospect to evaluate the encouraging results of 1979. Exploration work included surface sampling, surveying, mapping, geophysical surveys, and core drilling. (Aljahdali, .at el, 2015).

The geology of the Jabal Ibrahim quadrangle has been mapped in reconnaissance at 1:500,000 scale by Brown et al. (1963) and at 1:100,000 scale by Greenwood (1975a, c), Cater (1977), Hadley and Fleck (1980), and Greene and Gonzalez (1980). In 1980, the explanatory notes to the geologic map of the Jabal Ibrahim Quadrangle were written by Fred. Cater and Peter. Johnson, and the manuscript was approved by Ministry of Petroleum and Mineral Resources; Deputy Ministry for Mineral Recourses in Jeddah, Saudi Arabia (1986).

1.4. PREVIOUS GEOPHYSICAL STUDIES CASES OF NICKEL AND COPPER DEPOSITS

There are many studies cases that include the geophysical methods which have been used for this dissertation, perhaps the most of these studies as follows:

1.4.1. Geophysics of the Voisey's Bay Ni-Cu-Co Deposits (SEG, 1998). In Ontario, Canada, the Voisey's Bay Ni-Cu-Co deposits were discovered in 1994. Geophysical surveys were conducted using methods including - low - frequency EM, surface time-domain electromagnetic TDEM, total magnetic field, and horizontal loop

EM. The EM method helped in easily identifying these deposits because of the high conductivity of the Ni-Cu sulphides. In detecting the conductive Ni-Cu sulfides to a 100 m depth, the horizontal loop EM method was used in an effective manner. It was also successful in detecting the conductive mineralization to a 50m depth using 100-m coil spacing and to 100m depth using 200-m coil spacing. To detect the deep and large Ni-Cu sulfide systems at this deposit, surface TDEM proved to be the most effective geophysical tool. The features of Ni-Cu sulfide deposits were not always well defined by the total magnetic field anomalies. (Balch et al. 1998).

1.4.2. Geophysical Response of the Munali Ni-Cu Deposit (ASEG/PESA Conference, 2009). In 1960 in southern Zambia, the Munali nickel – copper deposit was discovered. A geophysical survey was conducted using airborne techniques and ground techniques. The airborne techniques involved the Versatile Time Domain Electromagnetic (VTEM) system. Ground techniques involved magnetic, ground gravity, and fixed loop time-domain EM. The gabbro was determined to be anomalous conductivity, as evident from the data of the grid of the VTEM EM (Witherly, 2009).

1.4.3. Time Domain EM and Magnetic Mapping of the Ferguson Lake Nickel-Copper-Cobalt-PGE Property (SEG, 2002). In the Ferguson Lake of Manitoba, Canada, a large deposit of gabbroic-hosted Ni-Cu-CO-PGE was discovered in 1950. A geophysical survey was conducted using methods such as the magnetic and the time domain electromagnetic TDEM. The current geophysical surveys and drillings have modified the site extensively to a large tonnage deposit. The presence of major structure near the surface magnetic anomaly along with the western extent of the EM survey is evident from the original drilling and the magnetic data. The magnetics

indicated that the mineralization also produced a significant magnetic response, which was later determined to have likely been caused by the associated magnetite and not the pyrrhotite. The EM survey indicated that the massive pyrrhotite, chalcopyrite, and pentlandite mineralization was extremely conductive > 2000 mhos and that the depth extent ranged from a few meters to a few hundred meters. (Visser, et al, 2002).

1.4.4. Geophysical Signature of the Jinchuan Ni-Cu-PGE Deposit, Gansu Province, China. In 1958, the Jinchuan Ni-Cu-PGE deposit was discovered in Gansu, China. The geophysical survey completed several times. In the 1960s to the 1970s, the ground vertical magnetic data were collected. The aeromagnetic survey was done in 1984. A self-potential survey was done in some areas of the deposit. Also, there are other geophysical methods that have been surveyed including gravity, time domain IP, resistivity, and seismic tomography. According to the results and conclusions from these geophysics surveys, the bouger gravity anomaly was not able to give helpful information regarding the mineralization but the residual anomaly proved to be effective in defining the host intrusion and it might be able to directly detect the orebodies. The regional scale aeromagnetic of the deposit was useful for mapping the ultramafic intrusion. Ground magnetics are able to define responses caused by blind mineralization during the intrusion. The self-potential survey gave strong anomalies on the mineralized body during the intrusion over the graphite-bearing country rocks (Guo& Dentith, 1998).

2. GEOLOGY OF THE STUDY AREA

2.1. INTRODUCTION OF GEOLOGY OF SAUDI ARABIA

Saudi Arabia covers an area of about 2.25 million km². Geologically, it has been divided into four distinct and extensive geological terrains: the Arabian Shield in the Precambrian age, which is located in the western part and is comprised of the igneous; the metamorphic basement, the Arabian shelf from Cambrian to recent age, which covers the eastern and northern parts and contains sedimentary rocks; the tertiary 'harrats' (extensive basalt plateaus) mainly overlying the Arabian Shield; and the Red Sea rift basin which is comprised mainly of Tertiary and Quaternary sedimentary rocks and coral reefs (Figure 2.1).

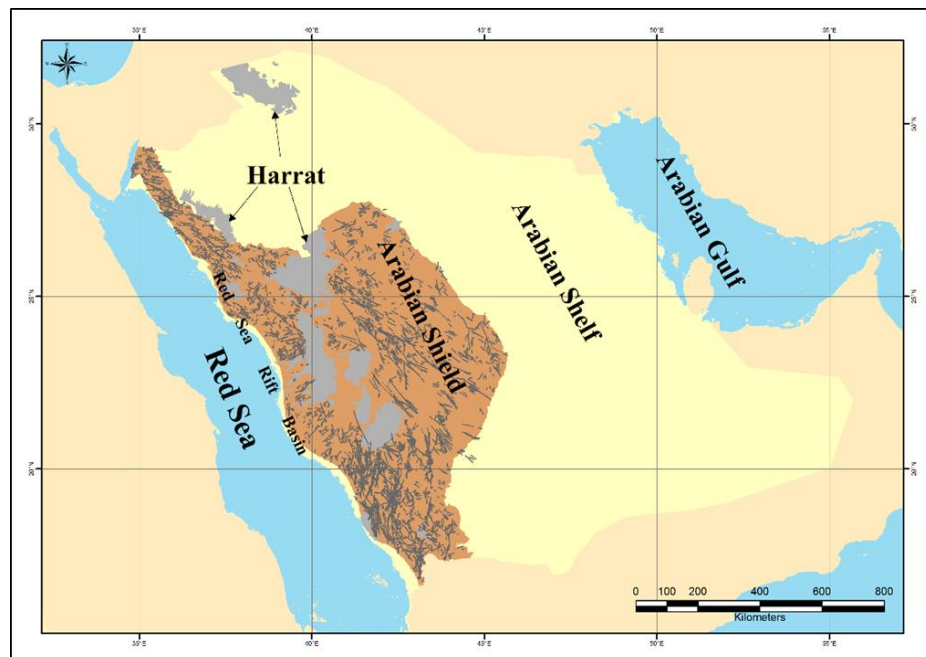


Figure 2.1 Map of geological divisions of the Kingdom of Saudi Arabia, (Sourced by SGS).

2.2. OVERVIEW OF THE ARABIAN SHIELD

The Arabian Shield is a part of the Arabian-Nubian Shield, which covers all or parts of several countries, including Saudi Arabia, Egypt, Jordan, Eritrea, Ethiopia, Somalia, Sudan, and Yemen (Figure 2.2). The Arabian Shield is separated from the Nubian Shield by the Red Sea Rift in the early Tertiary age and represents the basement igneous and metamorphic Precambrian rocks which form 1/3 (about 575000km²) of the area in the west, northwest, and southwest parts of the Saudi Arabia and hold the highest potential for metallic mineral sources (Al-Zahrani,2014). The Arabian Shield is narrow in the north and south parts. The width in the north is about 50-100 km and about 200 km in the south. In the middle, the width reaches about 700 km.

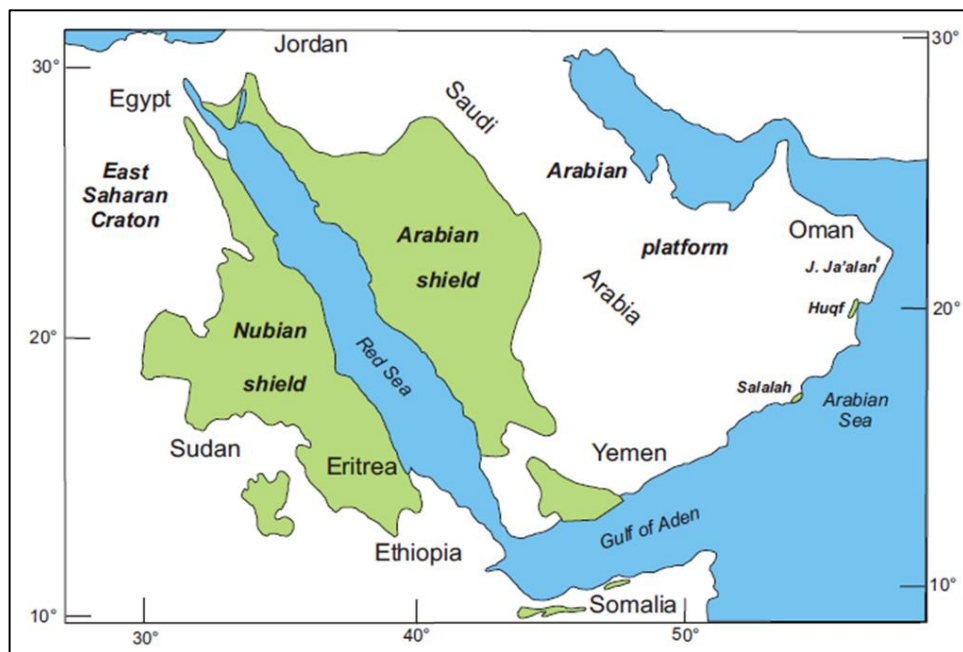


Figure 2.2 Distribution of exposed Precambrian rocks in the Arabian Peninsula and adjacent parts of northeast Africa, (Johnson, 2006)

The Arabian shield is comprised primarily of two types of Proterozoic rocks: layered rocks, which are mainly volcanic and clastic sediments, and plutonic rocks. These Proterozoic rocks range from 1600 MA to 450 MA in age (Alshanti, 2009) (Figure 2.3).

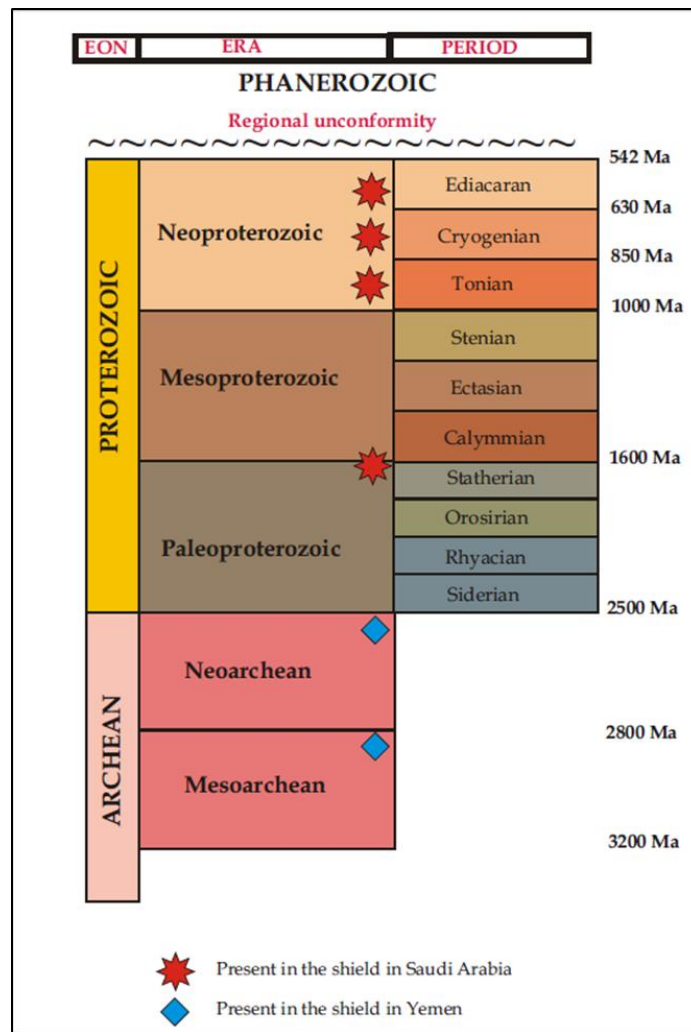


Figure 2.3 Stratigraphic intervals in the Proterozoic (after Gradstein and others, 2004), showing the periods represented by the Proterozoic rocks in Saudi Arabia, PETER R. JOHNSON, SGS-TR-2006-4.

The Arabian Shield has been divided tectonically into eight tectonostratigraphic geologic terranes separated by zones of intense deformation (sutures). The geological terranes consist of two different groups in form and origin, one of these was formed of interoceanic island arc terranes and represents the western part of the Arabian shield which includes Asir, Hijaz, Jeddah, and Midyan (Figure 2.4).

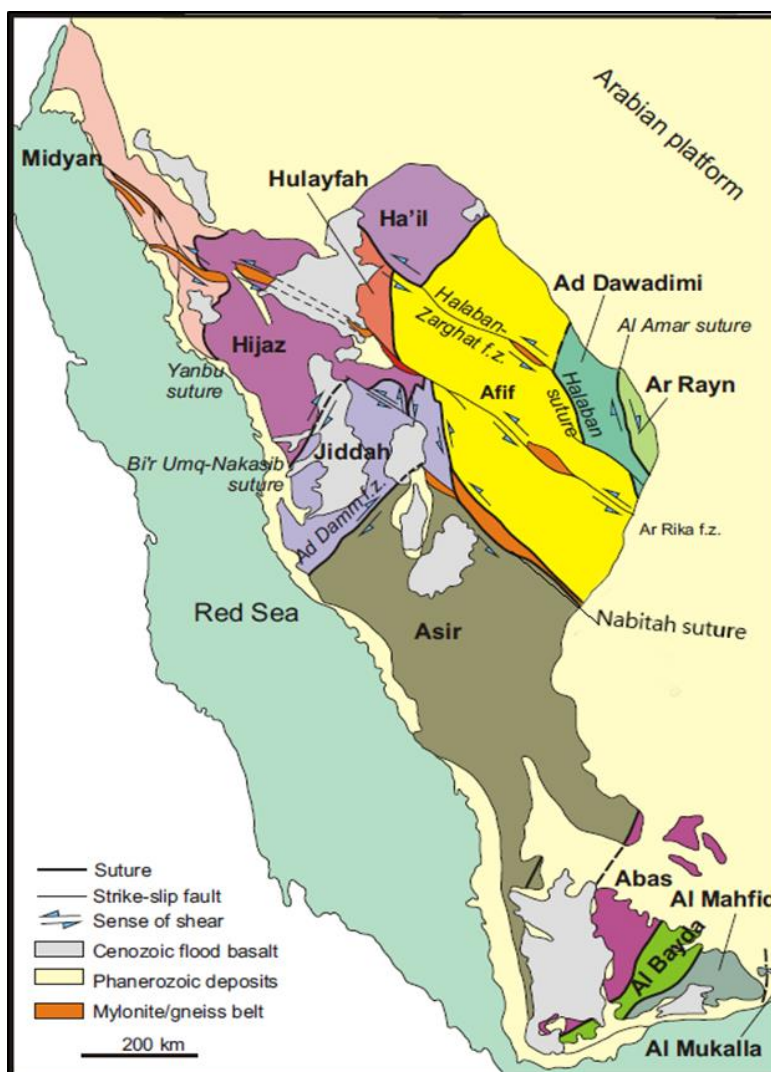


Figure 2.4 Arabian shield's terranes and sutures (after Stoeser and Camp, 1985; Windley and others, 1996; and Johnson and Woldehaimanot, 2003).

The other groups were derived from mixed oceanic and evolved continental sources which include Afif, Hail, Ad Dwadimi, and Ar Rayn terrains. The suture zones are Umq, Yanbu, Nabitah, Halaban, and Al Amar sutures (Alshanti, 2009).

2.3. LOCATION OF THE WADI AL KHADRA Ni-Cu PROSPECT

The Wadi Al Khadra prospect has an area is approximately 375,000 m², which is located in the Al Baha region, in the Southwestern part of Saudi Arabia at latitude 20° 09'10'' N. and longitude 41° 27'10'' E. The average high of Wadi Al Khadra is 2, 130 m above sea level. It is on a high plateau characterized by a rugged terrain with medium steep-sided canyons and escarpment that is characteristic of the region (Figure 2.5).

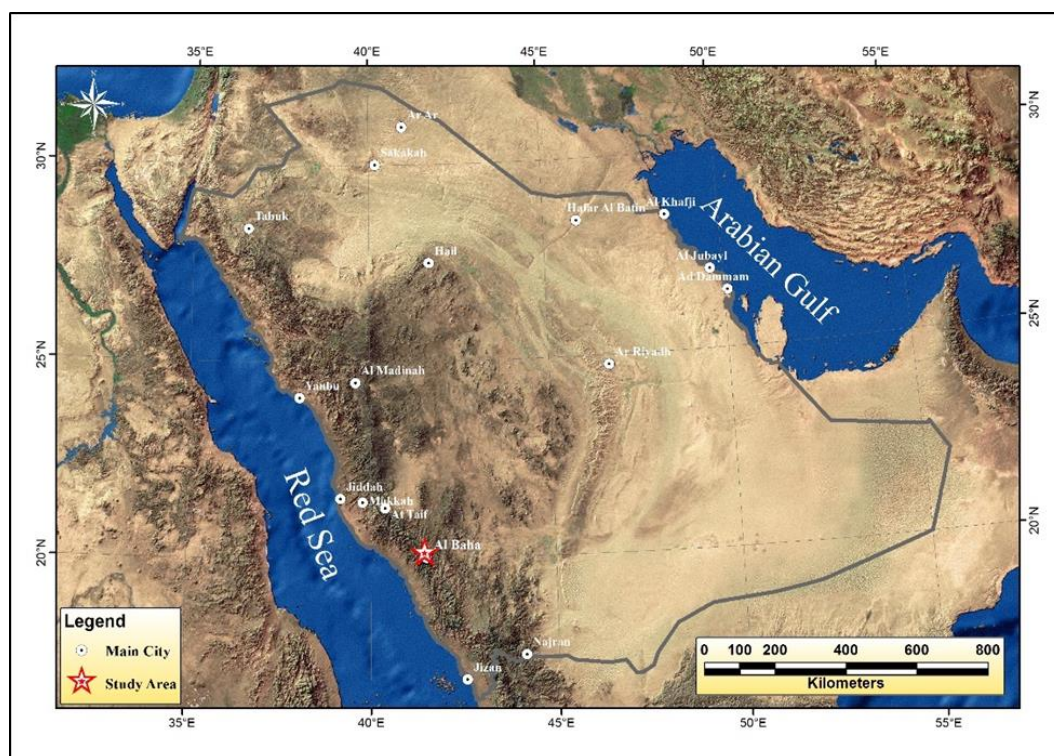


Figure 2.5 Location map of the study area in Saudi Arabia.

2.4. GEOLOGY OF THE WADI AL KHADRA PROSPECT

Regionally, the geology map of the Jabal Ibrahim quadrangle in the southern part of Arabian shield area described the Wadi Al Khadra prospect. Five principal units of Proterozoic rock are layered in the Jabal Ibrahim quadrangle. These layers are the Baish group, the Bahah group, the Qirshah formation, the Khutnah formation, and Ablah group. Carter and Johnson(1987) stated that the region is underlain by the meta volcanic Baish group (Bj) and Jof formation, which comprise a succession of volcanic, volcanoclastics, subordinate epiclastic rocks, portions of the metasedimentary Bahah group, and intruded by mafic and felsic sills and dikes that have a nearly north-south trend. They also noted that the intrusion of abundant, late-stage quartz veins with both directions 300° - 320° azimuth and 60° . On the regional scale, the formations of rock have been metamorphosed to green schist, whereas on the local scale, they are amphibolite-serpentinite facies. The age of all underlying rocks is Late Proterozoic (Figure 2.6). The mineral assemblage mainly consists of copper in oxidized and sulfide form, expressed by chalcopyrite, pyrite, niccolite, and arsenopyrite. Mineralization occurs in layered zones in mafic rocks of variable composition as veinlets, clusters, patches, and stringers along the foliation or fractures and mineralization. The shear zone strikes 300° - 305° azimuth and dips 85° to 90° NE.

The Bahah group and the Ras formation (br) is composed of fine to medium - grained elastic and volcanoclastics rocks interbedded with chert, marble, and locally basal conglomerates.

All of these units have been metamorphosed and structurally deformed to green schist facies. Geologists believe that these rocks overlie and are younger than those of the Jof Formation.

The sedimentary unit of the Rafa Formation of the Ablah Group appears only in the east of the study area, which uncomfortably overlies the older, layered rocks and diorite intrusion. According to Greenwood (1975a; 1975b) this unit consists mostly of medium- to coarse-grained arkose, but includes local, thick conglomerates at its base.

Locally, the study area is a part of the tectonic Asir terrane that is affected by sub-parallel and local faults that are involved in the main Nabitah fault zone in the east. There is a complex strike-slip fault divided into gabbro intrusion and metavolcanics. In general, all outcrops trend 330° azimuth in the study area. A volcanic rock consists of basalt, and a variety of lava flows intruded by mafic to felsic dikes faulted and folded with shear zones developing from east to west in a north-northwest trend.

Structure geology of an area is shown by fractures, folds and shear zones, along with microfolds; the Halaban and Ablah formations meet this general trend. A secondary set of structures, fractures, faults, and joints, are ranged between 290° - 335° azimuth and 30° - 60° azimuth, which could have occurred by a strain effect sustained by these rocks during different phases of tectonic movement (Figure 2.7). The Wadi has syngenetic copper and nickel minerals in a fairly disseminated style within thin-layered, ultramafic to mafic lava flows that range from normal flows to agglomerates. Due to different periods of structural deformation and intrusions, these rocks metamorphosed from mainly green schist up to local amphibolite-serpentinite facies.

Due to the complexity of the host rocks found in the study area, there are types of rocks classified into different geological units. The geological units consist of gabbro (Meta), Meta basalt, amphibolite, metavolcanics agglomerates, and Meta andesite-dacite:-

1. The Gabbro unit: This unit occurs along the eastern and northwestern boundary of an elongated, North - trending mafic intrusion that is approximately 2 km long and is as much as 2 km wide in the study area. Inherent textures suggest that the original lithology of the rocks was gabbro, which metamorphosed to green schist facies, whereas parts of the body are anorthosite (Greenwood, 1975a). Furthermore, a complex, intrusive body of the gabbro unit comprises coarse, medium, and fine - grained gabbro, dolerite, in addition to felsic and mafic dikes (SGS, 2009). Structurally, the local and regional faults have generated fractures, folds, and shear patterns orientated to this trend. The medium-grained gabbro unit is found primarily in the East and North part of the study area, whereas a few small outcrops appear in the Southeast zones.

2. A metamorphic unit: This unit is amphibolite. Geologist describe the rock texture as a fine-grained gabbro, basaltic lava flows, and some other highly metamorphosed rocks with unidentifiable textures. This unit primarily consists of lava flows metamorphosed to amphibolite facies. The amphibolite unit with intense facies tends along SE - NW shear zone fault systems. Contacts between the gabbro unit and an amphibolite unit in the study area appear close to the mineralization zone, , where serpentine is the most common mineral and appears to reduce in intensity to green schist facies westward and away from the gabbro unit. Rocks have been metamorphosed from the Precambrian age to the present time.

3. The second - largest outcrop in the study area includes mafic metavolcanics, agglomerates, meta volcanic/meta sediments, chlorite schist, and tuffs, and has been classified as the volcanic unit. This unit covers almost half of the entire area and exists in the N - NW zones. Basaltic lava flows, which are mostly abundant, are fine-grained and possess textures oriented to the bedding and/or foliation because of later metamorphism. It is hard to identify the contact zones because of deformation by later metamorphism, which differs from green schist and is local to amphibolite facies in the eastern part. The mineralization is associated with the volcanic unit, as it is shown to be remobilized or undergoing to pressures by metamorphism (SGS, 2009). Shapes of coarse-grained agglomerates are irregular and flattened to rounded clasts that ranged between 3 and 15 cm in diameter. The composition of clasts in volcanic rock ranges between basalt to dacite, fine-grained, massive, and finely laminated tuff, and a small amount of fragmental quartz and feldspar. Zones of massive tuff, finely laminated ruff, and epidote-hornblende, volcanic/sedimentary rocks are interlayered with the agglomerate. Nearby the study area, agglomerates, volcanic rocks, vents, and conduits been occur.

4. The meta – intrusive andesite: This unit have been observed more clearly in drill holes. Despite the metamorphism that occurred, some textures of meta – intrusive andesites appear. The textures range from fine to medium-grained rock and consist of extrusive lava flows in wide, massive layers. The medium to coarse-grained rock is described as thin with a weak contact alteration zone. Some silicification and/or recrystallization within a 0.5 - to 2.0-m aureole occurred and extended easterly at depth.

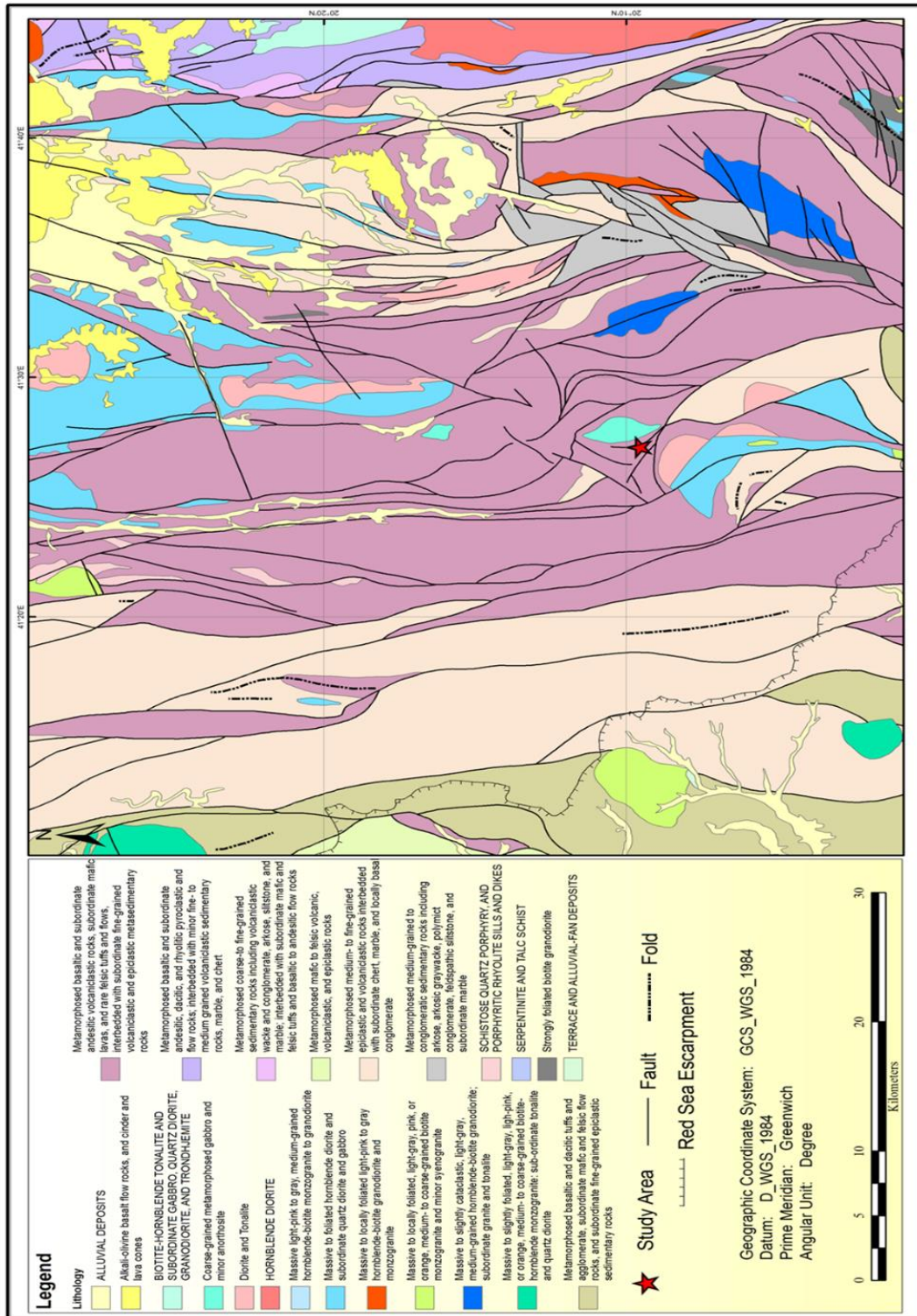


Figure 2.6 Geology map of Jabal Ibrahim quadrangle.

In general, the andesite is characterized as fine-grained and metamorphosed, with sericitized plagioclase, partially chloritized amphibole phenocrysts, minor quartz, biotite, and some carbonates.

5. The meta – intrusive unit: composed of felsic dikes and quartz veins intersect the metavolcanic layered rocks and the gabbro. Many irregular and fine-grained felsic dikes extend from 20 to 30 m. Felsic dikes and pods consists of, mostly aplite, dacite, and fine-grained granite, and could represent the latest intrusive event. Some of these dikes occur close to the Wadi Al Khadra mineralized area and along the Wadi. Geologists observed four quartz vein systems at the Wadi Al Khadra prospect. The vein systems are associated with the fault and shear zones, with three of the vein systems trended with fracture stages and foliation. The last vein system is affected more by faulting and less by metamorphism. All of four quartz vein systems are barren of Cu-Ni mineralization. However, some of the quartz veins include 2–3% fragments with chlorite, sericite, and epidote alteration. The textures of these veins are milky white, holocrystalline, fine– to medium–grained crystals. The veins and veinlets are composed of massive quartz that has been deformed (fold-fault), sheared, and fractured.

2.5. STRUCTURE TRENDS

The most prominent structural trends of the study area represented in:

2.5.1. The Northwest to Southeast Trends (Red Sea Trend). The correlation between the different rose diagrams revealed that the Northwest trend (the Eritrean or Arabian trend) represents the most predominant trend direction in the studied area. This trend cuts through the stable shelf in the most pronounced way and represents the most

significant manifestation. The trend occurred in the Mid-Tertiary time, as it appears related to the Red Sea and Gulf of Suez extent and direction as well as many other topographic features of the present day. Mesherf et al. (1980) stated that the Northwest trend has a local magnetic distribution along the Red Sea coast that fades away in areas at distances far from both sides of the Red Sea. He did not explain the cause responsible for this phenomenon. Mesherf (1990) also stated that the Eastern part of Saudi Arabia shows a series of strong positive magnetic anomalies of the Northwest trend as the result of the northward compressive force affecting the rocks west of the Arabian Peninsula. However, (Neev,1975) suggested that the Northwest–trending tensional features were developed in the Red Sea region contemporaneously with the Northeast trend fold system initiated due to the expansion of the central plate that runs parallel to the Pelusium line.

2.5.2. The Northeast to Southwest Trends (Aqaba Trends). The NE–SW trend appears as the first major trend on the magnetic anomaly maps. The correlation between the rose diagrams of the observed and residual magnetic anomaly maps indicates that this trend has the same azimuth and intensity significance. Moreover, the NE trend appears as of trivial order on maps, this confirms that this trend is of older age than the NW trends. In a similar manner, Said (1962) named this trend the Aualitic trend, which was developed and related to the Gulf of Aqaba rift tectonics. He also mentioned that it was less pronounced around the stable shelf and bound many of the fold systems located in the middle part of Egypt. Neev (1975) stated that the Jordan-Dead Sea-Aqaba rift, which has been active as a sinistral strike-slip fault since the Oligocene time, has developed into a graben since the late Pliocene time.

2.6. DRILL HOLES DATA OF WADI AL KHADRA PROSPECT

SGS bored four drill holes averaging 227.33m long with a total length of 905.95m and oriented at 200°-275° azimuth and with inclinations of 55°- 65°. These drill holes were located near the main oxidized outcrop on the large Southeast anomaly in the study area (Figure 2.8), and their samples were chemically analyzed. By studying the analysis results of the well samples, mineralization appeared as semi-hidden leaflets along the bed and / or foliage.

The southeastern part of the well - drilling area appears to be the most mineralized along the shear / fault area at an angle of 305 °, and this area is classified and depicted as having a secondary structure. This part of the mineral area is 0.8 to 1.5 m in thickness and decreases by 85 ° North to an almost vertical angle from the surface of the property. However, this structure is uncertainly linked to the local shear zone of error, due to the presence of a vein of white quartz with a thickness of 0.8 to 1.0 m, and the azimuth and amphibious layers are accurately dissected at 240 ° by this metal structure coupled with the surface.

2.6.1. Well (KAD-1). From the analysis of the rock samples of the well (KAD-1), it is clear that the intersects the well with the mineralization range near the surface from 0.0 m to 26.5 m. Surface sample tests also showed results from 0.10 to 1.65 percent of copper and 0.16 to 0.39 percent of nickel. Note that these samples were the closest to the sampling line with a protrusion outside the surface sampling line. The results of total separation gave results showing that an average of 26.5 m was 0.39 percent copper and 0.27 percent nickel (Fig 2.9a).

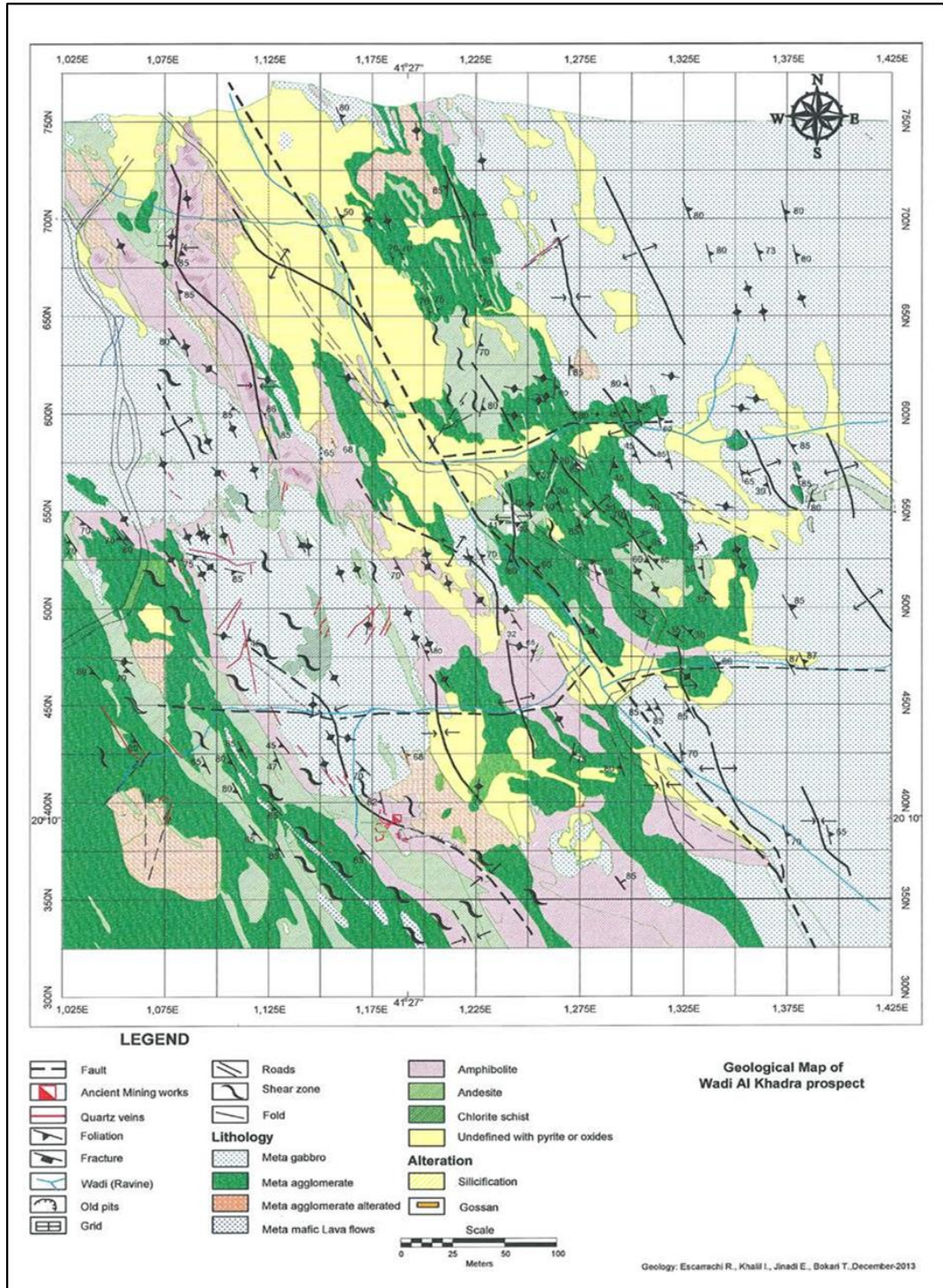


Figure 2.7 Geological map of Wadi Al Khadra prospect, SGS, 2013

2.6.2. Well (KAD-2). This well did not reach the same depth as the KAD-1 well, but the analysis shows that from the depth of 91.63 m to 102.57 m with an internal depth of 10.94m the proportion of copper concentration reaches 0.406 percent and 0.14 percent nickel (Fig 2.9b).

2.6.3. Well (KAD-3). This well contains in a thickness ranging from 21.29 m to 26.55 m of the vein with a metal separator of 5.55 m with an average of 0.33 percent copper and 0.32 percent nickel (Fig 2.9c).

2.6.4. Well (KAD-4). KAD-4 represents one of the most important wells; it shows the most substantial proportion of mineralization, also shows an intersection in the region for about 25 m. The well is located in the most prominent exploitative evaluation pillars (up to about 3m, 2m, and 3m) in the southwestern region of the Wadi Al Khadra. Surface sample assays at this site vary from 0.81 percent to 1.67 percent copper and 0.21 percent to 0.68 percent nickel (Fig 2.9 d). From this information, it is clear that there are two distinct concentrations of mineralization consistent with the geochemical anomalies of copper and nickel in the study area. The first concentration is located in the southern part of the area and the second concentration, which is located in the central part of the study area, is a long anomaly that may be a contact area. This anomaly partially dominates another area of minerals. These anomalies of copper and nickel permeate some of the geochemical abnormalities of silver and an extended, thin metal area northwestward. In the south, anomalies are distorted about 50 meters to 75 meters from the geochemical anomalies of copper and nickel.

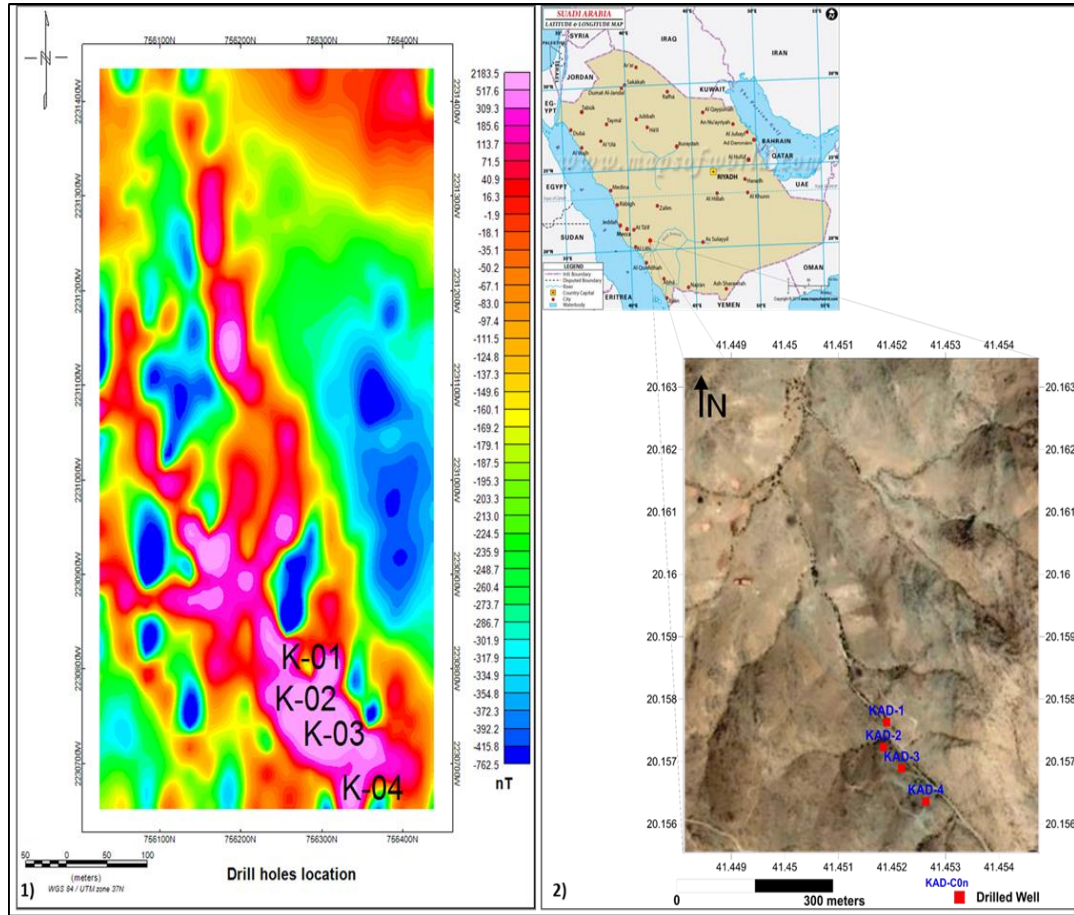


Figure 2.8 1) Location map of drilled well on RTP map of the study area, 2) Satellite map of location drill holes of the study area.

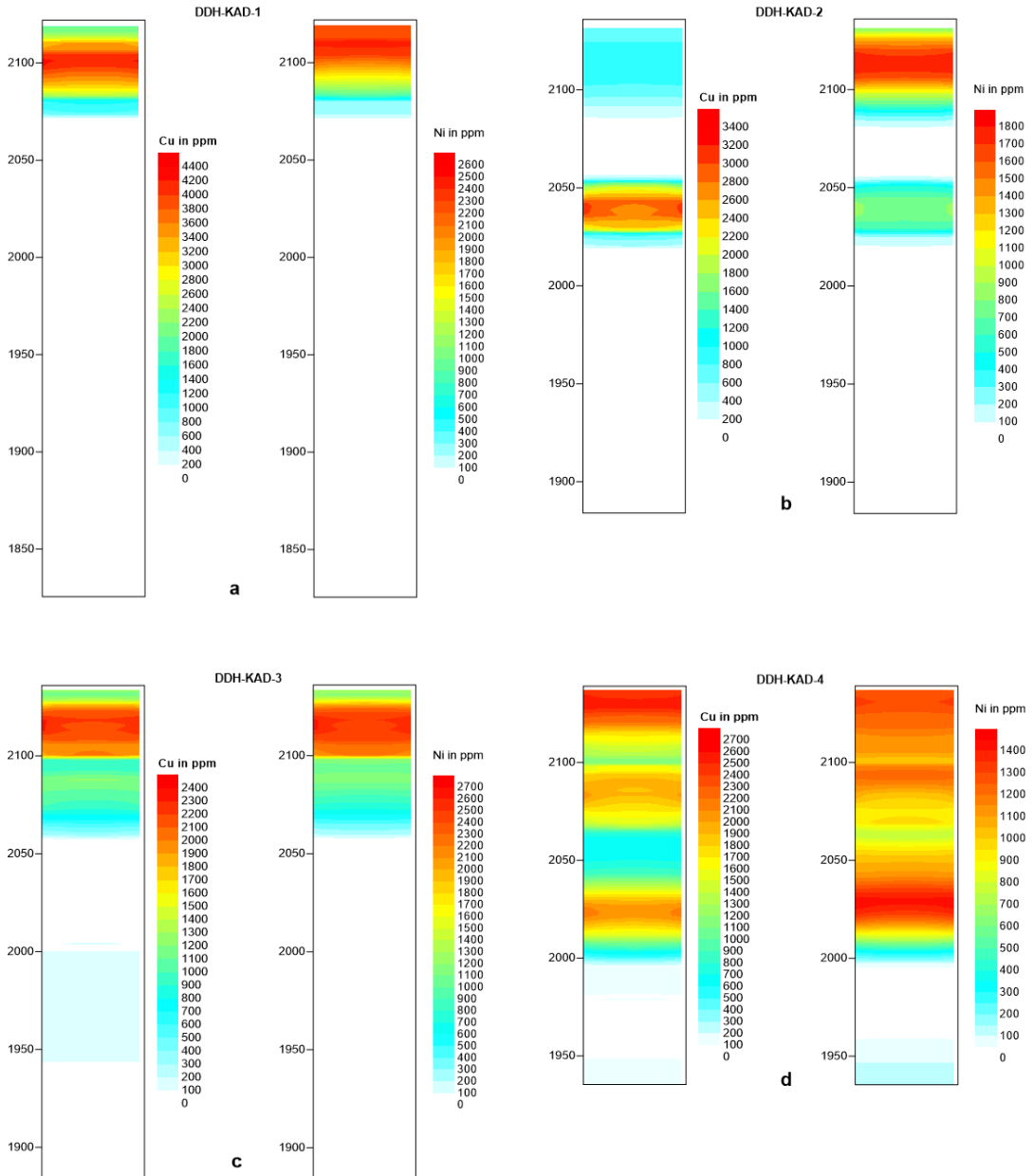


Figure 2.9 The distribution of the copper and nickel concentrations in the drilled holes.

3. DISTRIBUTION OF MINERAL DEPOSITS IN SAUDI ARABIA

3.1. BRIEFLY INTRODUCTION OF MINERAL DEPOSITS

Mineral deposits in nature are usually formed in many geological environments and found on the surface of earth or in between layers of rocks which make the crust of the earth. The mineral deposits of Saudi Arabia are different in form, formations, and ages. The metallic minerals resources (Figure 3.1) are contained in Precambrian rocks of the Arabian Shield, which is the major source of precious and basic minerals such as gold, silver, copper, nickel, zinc, chromium, manganese, tungsten, lead,

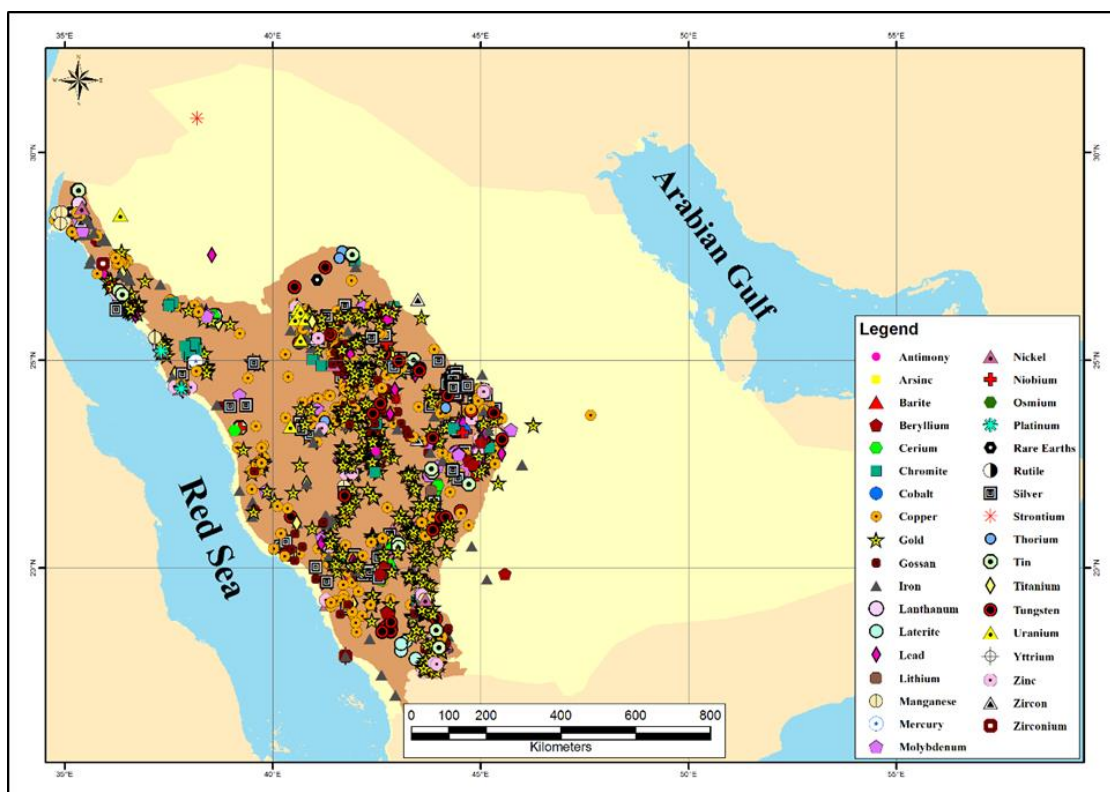


Figure 3.1 Map distribution of metallic minerals deposits in Saudi Arabia, Data sources by SGS.

tin, aluminum and iron as well as other minerals, and is exposed in the west part of the Saudi Arabia.

The industrial minerals and rocks commonly referred to as nonmetallic minerals (Figure 3.2) are contained in both Precambrian rocks and Phanerozoic rocks that overlie the Arabian shield extensive sedimentary formations containing industrial minerals such as gypsum, kaolin, bauxite, phosphates, feldspar, mica, Sulphur and salt, and are exposed in the central and northern part of Saudi Arabia. (Industrial cluster, 2019).

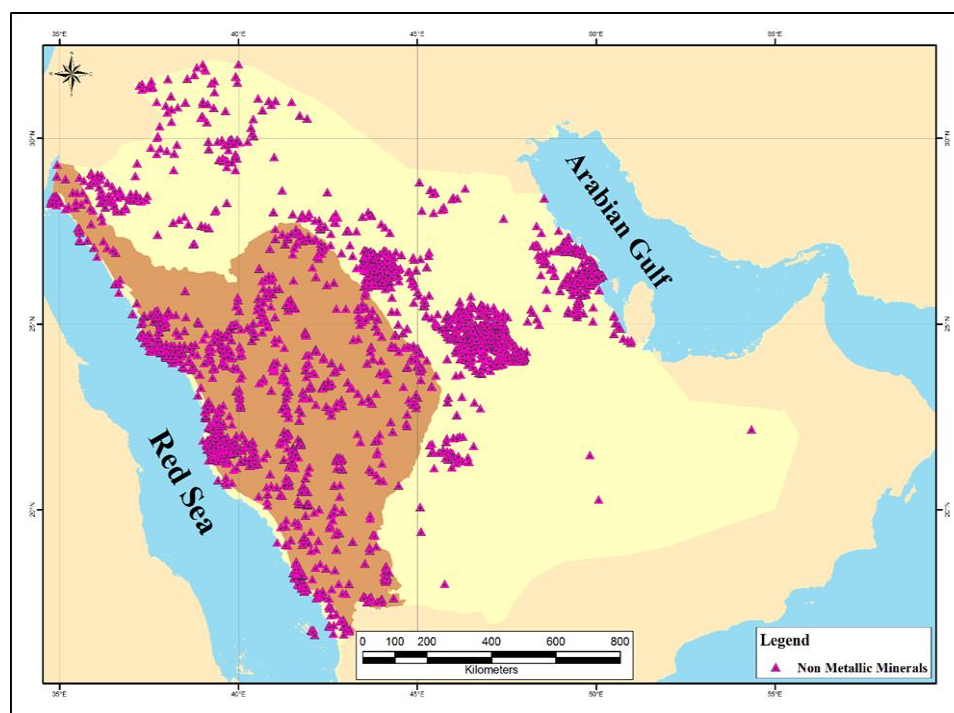


Figure 3.2 Map distribution of nonmetallic minerals deposits in Saudi Arabia, Data sources by SGS.

The government of Saudi Arabia has paid much attention to mineral prospecting and exploration for different mineral deposits, and huge sums of money have been spent

to search for many deposits. According to the recent statistics from the Ministry of Energy, Industry and Mineral Resources, the geologic storage of minerals in Saudi Arabia exceeds SAR4.9 trillion (1.3 trillion USD). Saudi's Vision 2030 aims at increasing the mining sector's economic contribution to 26 billion USD (SAR 97 billion), which is 18,000 times more than 2015 revenues of 140 million USD (SAR 520 million). (export.gov, 2018.Al-Awsat, 2018).

3.2. PROPERTIES OF NICKEL

Nickel is the fifth most common element in the crust of the earth and is concentrated in the core. It is a chemical element symbol (Ni), belongs to the transition metals, and has an atomic number 28 in the periodic table. Its characteristics are that is hard, ductile, and is silvery- white lustrous metal with a slight golden tinge (Chemistry, 2019). Nickel is used in many applications and follows manganese in importance for the industry of iron and alloys for making stainless steel. In addition, it has many other uses, such as in other alloys that are used in industries such as aircrafts, electrical machinery, equipment's, coinage, ceramics, magnets, and batteries (Chemistry,1952) (Anne, 2019).

3.2.1. Occurrences of Nickel. The most important minerals have an economic concentration of nickel such as Pentlandite, which occurs in the massive Cu-Ni Sulphides association with Chalcopyrite and Pyrrhotite, and the main minerals of nickel occur in laterites deposits such as Garnierite and nickeliferous limonite (Figure 3.3).

There are two types of ore nickel deposits which are:

- Magmatic sulfides deposits: the primary source of nickel at the present, e.g. Cu-Ni Sulphides deposits in association with layered basic ultrabasic intrusions or

in association with ultramafic volcanics (either massive bodies or disseminated) or may occur as a cement for the footwall breccia of some mafic – ultramafic intrusions.

- Laterites deposits: sometimes referred to residual deposits, which are a mixture of silicates of nickel that result after the weathering of ultramafic rocks and Serpentinites (Alshanti, 2009).



Figure 3.3 1) Nickel, and 2) Nickel-Copper-Platinum Ore Locality.
Sources by <http://www.geologypage.com/2014/06/nickel.html>

3.2.2. Occurrences of Nickel in Saudi Arabia. Nickel has been reported at more than 50 localities, all of which are in late Proterozoic rocks of the Arabian shield. Eight of the nickel localities have been drilled (Figure 3.4). These localities are in three types as follows: strati form massive sulfide mineralization in volcanoclastics rocks, disseminated massive sulfides in mafic and ultramafic rocks, and Gossans (Table 3.1) (Ministry of Energy, Industry, and Mineral Resources reprinted, 2016).

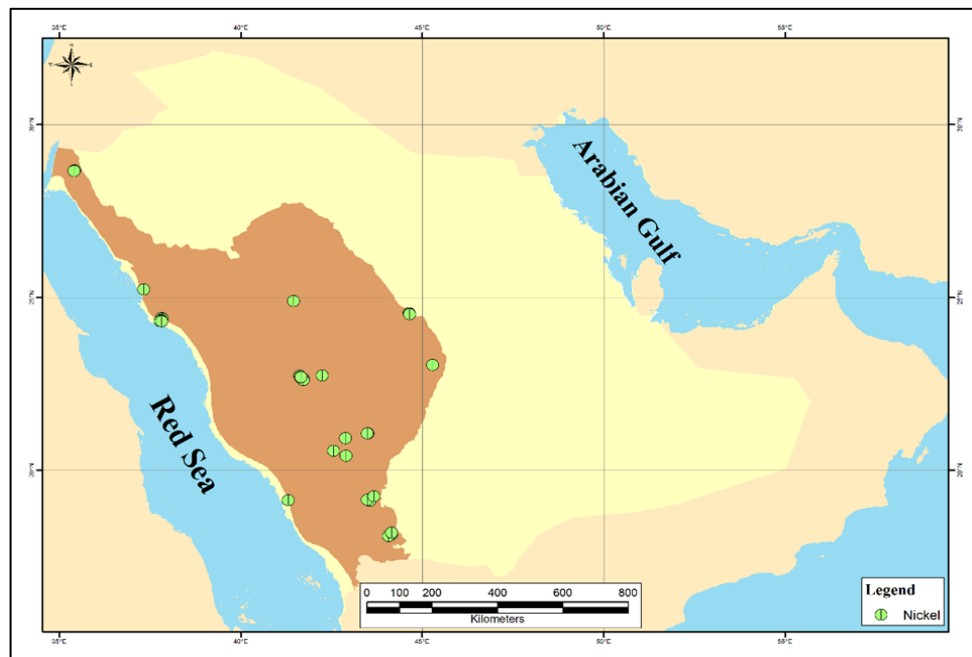


Figure 3.4 Map of nickel deposits and prospects drilled localities, sourced by SGS.

3.2.2.1. Stratiform massive sulfide mineralization in volcanoclastic rocks.

Hadbah and Jabal Mardah are two primary nickel occurrences in stratiform bodies in volcanoclastic rocks. The Hadbah nickel deposit in the Wadi Qatan area east of Abha in the southwestern part of the Arabian Shield is the largest and most extensively explored nickel in Saudi Arabia. It was explored between 1972 – 1977 by the Arabian Shield Development and National Mining Company. Nineteen holes were drilled into the deposit at that time. The deposit is estimated to contain 2.5 Mt with an average grade, based on analysis of a core from 15 holes with 0.92% Ni. In 1986-87, USGS drilled four holes in the Jabal Mardah prospect in the northeast part of the Arabian Shield to test the down dip extension of three of the larger gossans. Core from the holes showed the sulfide present to the chiefly pyrite. 39 m length of massive sulfides was obtained from one hole

Table 3.1 Nickel deposits and prospects tested by drill holes. (Ministry of Energy, Industry, and Mineral Resources Reprinted, 2016).

STRATIFORM BODIES IN VOLCANIC ROCKS	
Hadbah deposits	Stratiform, massive sulfide bodies in volcanoclastic rock. 19 drill holes indicates 2.5 Mt averaging 0.92% Ni.
Jabal Mardah	Stratiform sulfide bodies in volcanoclastic rocks. The best intercept from 4 drill holes was a 39 m interval averaging 0.97% Ni.
CONCENTRATIONS IN MAFIC AND ULTRAMAFIC ROCKS	
Jabal Judayr	2 holes drilled in serpentized gabbro and pyroxenite yields sulfide-bearing core that averaged 0.25% Ni.
Wadi Kamal	Sulfide-bearing core from 11 holes drilled beneath gossans in ultramafic and mafic rocks yield low values in nickel.
Umm ad Diba	15 percussion holes drilled in gabbroic rocks beneath a gossan anomalous in nickel and copper, indicate 60,000 tons averaging 1.3% Ni.
Jabal al Ghurabah	A hole drilled in layered mafic to ultramafic rocks yield core that assayed from 0.05 to 0.10% Ni.
Jabal Humayyan	A hole drilled in ophiolitic rocks to test a magnetic anomaly beneath a gossan anomalous in nickel, yield values that ranged from 0.01 to 0.16% Ni.
Jabal Rugaan	Three percussion holes drilled to test self – potential anomalies in troctolite yielded a maximum value of 0.07% Ni.

with an average of 0.97% Ni, of which 1 m contained 1.35% Ni. In 1988, exploration on the Jabal Mardah prospect was ceased and considered to be uneconomic (Carter & Tayeb, 1989).

3.2.2.2. Disseminated massive sulfides in mafic and ultramafic rocks. Most of the nickel occurrences in the study area are in mafic and ultramafic rocks. The Jabal Judayr, southeast of the Arabian shield, is the stock of the serpentinite gabbro and pyroxenite and is marked by well-developed gossans that are anomalous in nickel.

Strong magnetic and electromagnetic anomalies, coincident with the gossan, are indicative of a shallow conductive body. In 1974, USGS tested drilled two holes in the Jabal Judayr prospect to test the down dip extension of gossans and did the geophysical anomalies. Eighty-three samples of the sulfide core ranged from 0.03 – 0.43 % Ni and averaged 0.25% Ni which does not significantly change from the normal nickel content of ultramafic rocks. (Puffett et al, 1975).

The Wadi Kamal prospect west of the Arabian shield is underlain by an ultramafic layered complex, which is capped by gossans and contains up to 2.3% Ni and 2.5% Cu. In 1974, French Bureau de Recherches Geologiques et Minieres (BRGM) drilled 11 holes to test geophysical anomalies and the area beneath the gossans. The average nickel content was low and 17 m length of the core from one hole was averaging 0.53% Ni. (Chevremont & Johan, 1981).

3.2.2.3. Gossans. Gossans and underlying oxidizes zones cover all the previous deposits.

3.3. PROPERTIES OF COPPER

Copper is one of the oldest most abundant metals known and extracted by humans. It is a chemical element belonging to the transition metals, has the symbol (Cu), and has the atomic number 29 in the periodic table (Chemistry, 2019). It is a distinctive color reddish – salmon pink, soft, heavy, malleable, and ductile metal with very high thermal properties and is a good conductor of electricity. Copper is widely used in modern industries regarding electrical, and electronic products. Brass and bronze are two important copper alloys (Anne, 2019), (Massaro, 2002).



Figure 3.5 1) Copper from Bisbee, Arizona, and 2.Chalcopyrite, the most important ore of copper. Sources by <https://geology.com/minerals/copper.shtml>

3.3.1. Occurrences of Copper. In nature, copper occurs as metal in the native form and can be found with Sulphides or Oxidizes ores minerals. There are approximately 165 ore minerals that contain copper, and the most important are the Sulphides ore minerals, which have Chalcopyrite, Chalcocite, Bornite, and Enargite (Figure 3.5). The Oxidized ores minerals have Malachite, Azurite, Chrysocolla, and Cuprite. (Ministry of Energy). The copper occurs in many deposits, and most of these are magmatic deposits for Cu-Ni, contact metasomatic deposits, porphyry copper deposits, stratiform copper deposits, volcano – sedimentary massive Sulphides deposits, and vein deposits with precious and base metal deposits.

3.3.2. Occurrences of Copper in Saudi Arabia. Copper mineralization is prevalent in the Proterozoic rocks of the Arabian shield. Many ancient sites that provide evidence of an extensive small -scale copper mining industry date back several thousand years. Many localities have been investigated by DGMR (Figure 3.6). Most of the copper

deposits in Saudi Arabia are of the complex ores which are associated with some zinc, lead, gold, and silver.

3.3.2.1. Jabal Sayid copper – zinc deposit. In 1965, French Bureau de Recherches Geologiques et Minières (BRGM) discovered an ancient mine working at the Jabal Sayid deposit in the middle of the Arabian Shield. They started geologic mapping, geophysical surveys, bench-scale beneficiation, and diamond drilling. These activities concluded in 1979 (Bournant, 1981).

3.3.2.2. Kutam copper – zinc deposit. The Kutam deposit is located in the Asir Mountains in the southern area of the Arabian Shield and was discovered after the USGS found the ancient mines working in Kutam in 1973. (Smith et al, 1977).

3.3.2.3. Jabal Ash Shizm copper prospects. The Jabal Ash Shizm copper prospect, located in the northern part of the Arabian Shield, was studied by Charles Doughty in 1870. In 1930, the prospect was first examined as a potential source of copper by the Saudi Arabian Mining Syndicate (SAMS). In 1970, the prospect was subsequently explored by BRGM (Donzeau, 1980).

3.3.2.4. Umm Ad Damar copper prospect. The Umm Ad Damar prospect located in the middle of the Arabian shield and is 20 km southeast of the Jabal Sayid deposit. In 1935-36, the first references to the prospect and examination of the ancient mines by SAMS. In between 1954 – 1965, the geologic mapping, sampling, geophysical survey, and drilling were done by DGMR. BRGM was completed the previous stages for the prospect from 1966 – 1975 (Al-quorashi at el, 1989).

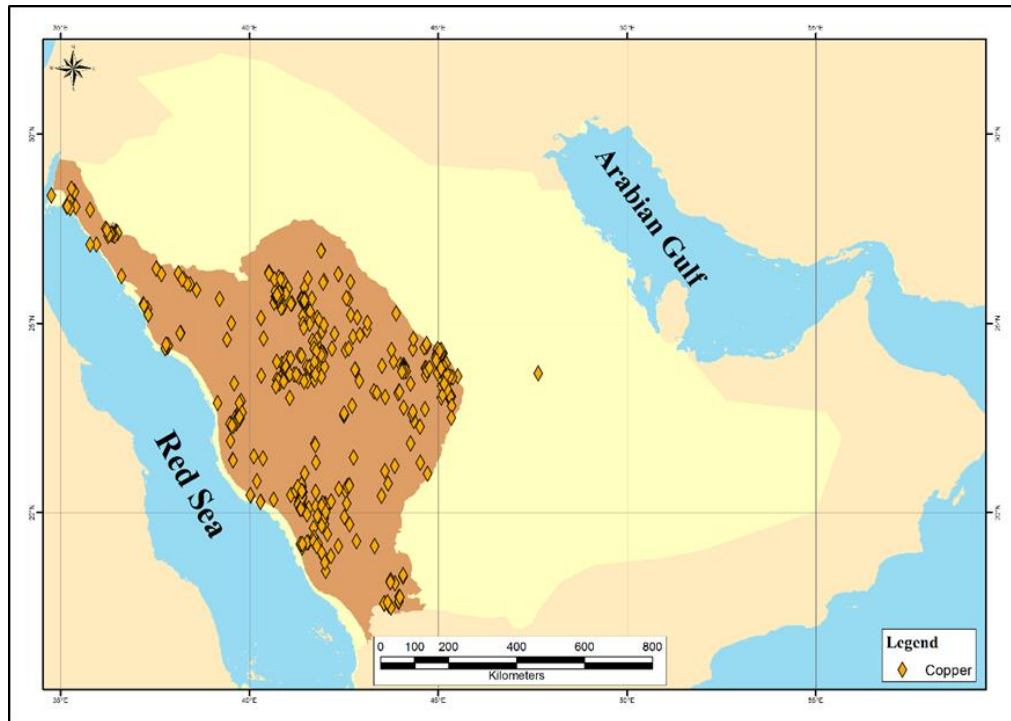


Figure 3.6 Map of Copper deposits and prospects drilled localities. Sourced by SGS.

4. GEOPHYSICAL METHODOLOGY

4.1. INTRODUCTION OF GEOPHYSICAL METHODS IN MINERAL EXPLORATION







Geophysical exploration is a branch of applied geophysics that measures the physical properties of rocks and minerals. Geophysical methods are grouped into two different groups; passive and active. The passive methods measure variations in natural fields, whereas the active methods measure the earth's response to temporary man-made fields. For example, the gravity method measures variations in the natural gravitational field of the earth, whereas the time domain electromagnetic method measures the earth's response to the emission of man-made electromagnetic radiation. In the case of mineral exploration, geophysical methods can be used for geological mapping to determine the extent of mineralization and in evaluating and delineating the ore (Dentith & Mudge, 2014).

4.2. SELF-POTENTIAL METHOD

Self-potential (SP) method is a passive electrical method that measures the natural potential difference between two locations on the ground surface of the earth. The SP method is non-intrusive, fast, relatively inexpensive, and requires a few voltmeter and non-polarizing electrodes (Nyquist & Corry, 2002). The physical property of the self-potential method is electrical conductivity. The potential difference measured can range from less than a millivolt (mV) to over a volt, and the sign of potential difference as positive or negative is an important diagnostic factor in the SP interpretation of anomalies. SP anomalies are generated by several natural sources (Table

4.1).The SP method is widely used in mineral and base metal exploration to detect massive ore bodies, metallic sulfides, and magnetite. Furthermore, it has been used in groundwater and geothermal investigations and applied to environmental problems (Essa & Munsch 2019).

Table 4.1 Types of SP anomalies and their respective geological sources (Reynolds, 1995).

Source	Type of anomaly
Mineral potentials	
<ul style="list-style-type: none"> - Sulphide ore bodies (pyrite, chalcopyrite, pyrrhotite, sphalerite, galena) - Graphite ore bodies - Magnetite + other electronically conducting minerals - Coal - Manganese 	 <p>Negative * hundreds of mV</p>
<ul style="list-style-type: none"> - Quartz veins - Pegmatites 	 <p>Positive * tens of mV</p>
Background potentials	
<ul style="list-style-type: none"> - Fluid streaming, geochemical reactions, etc. 	 <p>Positive + / - negative ≤ 100 mV</p>
<ul style="list-style-type: none"> - Bioelectric (plants, trees) 	 <p>Negative, ≤ 300 mV or so</p>
<ul style="list-style-type: none"> - Groundwater movement 	 <p>Positive or negative, up to hundreds of mV</p>
<ul style="list-style-type: none"> - Topography 	 <p>Negative, up to 2 V</p>

4.2.1. Occurrence of SP and Electrical Potentials. In the case of mineral exploration, the natural ground potential is assumed to consist primarily of two components: the mineralization (or electrolytic contact potential) potential and the background potential. (Note: electro kinetic, liquid-junction, and Nernst potential are assumed to be insignificant). The mineralization potential is effectively constant due to the electrochemical process associated with the mineralization. The background

potential is time variant and is generated by temporal variations in natural current flow in the subsurface - for example, an electrical storm.

4.2.2. Mechanism of Self-Potential. There are four principal mechanisms that produce SP potentials in the subsurface:

- Electrokinetic potential or streaming potential:

Caused by the flow of fluid electrolytes during a capillary or porous medium in different electrical properties to generate potentials along the flow path. The potentials are alternatively called electro filtration, electromechanical, or streaming potentials:

$$E_k = \frac{\varepsilon\mu C_E \delta P}{4\pi\eta} \quad (1)$$

where ε , μ , and η are the dielectric constant, resistivity, and dynamic viscosity of the electrolyte response, respectively. The pressure difference δP and C_E is the electro filtration coupling coefficient.

- Liquid-junction or diffusion potential:

Caused by the difference in motilities of anions and cations of dissimilar concentrations:

$$E_d = \frac{RT(I_a - I_c)}{nF} \ln(C_1/C_2) \quad (2)$$

where I_a and I_c are the motilities of the anions (+ ve) and cations (- ve) respectively, R is the universal gas constant, T is the absolute temperature, n is ionic valence, F is Faraday's Constant, and C_1 and C_2 are the solution concentrations.

- Nernst, or shale, potential:

Caused by two identical metal electrodes that engage in a homogeneous solution with the difference of the concentrations at those electrodes.

$$E_d = \frac{RT}{nF} \ln(C1/C2) \quad (3)$$

where $I_a = I_c$ in the diffusion potential equation.

- Mineralization, or electrolytic contact potential:

The potential associated with massive Sulphides ore bodies (Reynolds, 1995). The large negative potentials range from hundreds to more than thousands of millivolts, are frequently observed in association with bodies of disseminated and massive Sulphides, graphite, magnetite, and manganese mineralization.

These mineralization potentials are the signal of interest in mineral SP surveys. Sato and Mooney (1960) (Figure 4.1) provide an explanation of the electrochemical interactions between the mineralization and the groundwater.

In short summary, his SP anomalies are generated by the natural oxidization/reduction process associated with mineralized bodies that straddle the water table. The ions in the pore fluid below the water table are oxidized and release electrons, and the electrons flow vertically during the conductor to the point above the water table where they cause the reduction of electrolytes.

4.3. MAGNETIC METHOD

The magnetic (MAG) method is relatively inexpensive; it involves passive geophysical survey methods that measure spatial variation in the widely used for the direct detection of several different types of mineral deposits, for determining the location of subsurface geologic structures (e.g. faults, folds, dykes, and geologic contact)

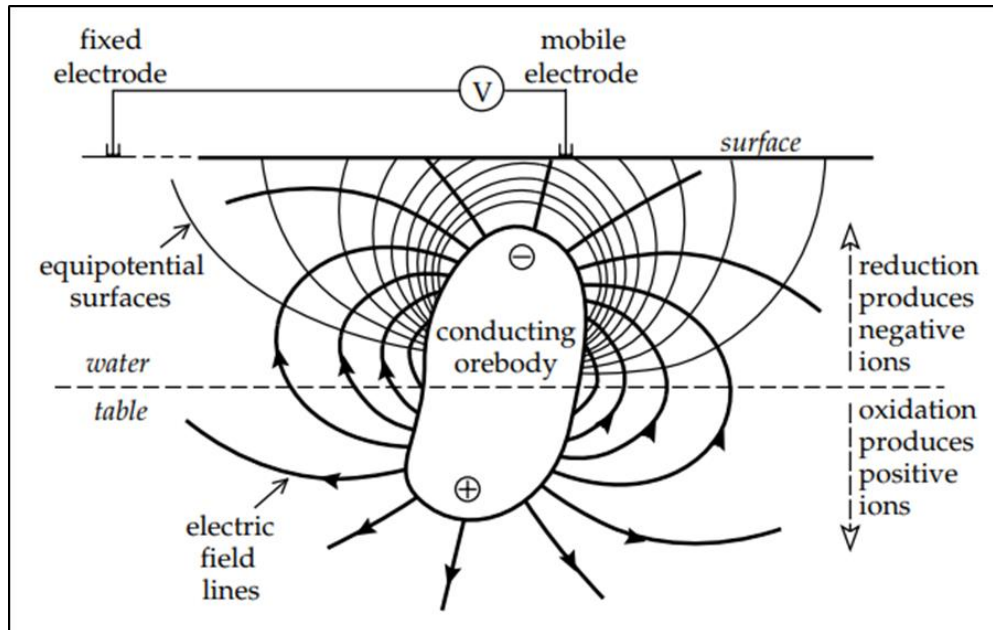


Figure 4.1 A schematic model of the origin of the self-potential anomaly of an orebody. The mechanism depends on differences in oxidation potential above and below the water table (LOWRIE, 2007).

, for archeological investigations, and for pseudo -geological mapping. The spatial variations in the earth's magnetic field of that are interest to those engaged in mineral exploration are caused in part by variations in the magnetic susceptibility of earthen materials and variations in the concentration of those materials (Dentith & Mudge, 2014) (Mickus,2014). The magnetic method, depending on the sophistication of the measuring instrumentation, typically involves the measurement of the relative or absolute earth's magnetic field as either a vector or a scalar. (Mabey et al., 1974). The instrument used for this study measured the relative intensity of the earth's magnetic field as a scalar.

The magnetic technique has relatively high depth penetration compared to other geophysical techniques such as ground penetrating radar, high frequency electromagnetics, and DC-resistivity. The main disadvantages are that anomalies are

generated only if ferromagnetic or ferrimagnetic materials are present. Also, the interpretation of magnetic anomalies is non-unique, which means the complementary data (e.g., other geophysical data or drill hole data) are often required to determine the cause of the magnetic anomalies (i.e. massive Sulphides as opposed to magnetite) (Mickus, 2014).

The bar magnetic consists of two poles (dipolar), a positive north-seeking pole and a negative south-seeking pole, and these poles always exist as pairs (Figure 4.2). These two poles produce a magnetic field called the magnetic field intensity (\mathbf{H}) (Mickus, 2014).

In geophysics, the most commonly used unit of magnetic intensity is the gamma (γ), which equals 10^{-9} T or Nano tesla (nT). The magnetic field intensity of the earth in Polar Regions is of the order of 60,000 γ or 60,000 nT at the equator; the magnetic field is about 30,000 γ .

The magnetic field intensity in Saudi Arabia is between 40,000 – 42,000 nT. The inclination angle of the magnetic field is between 20 - 40 degrees; the declination field angle of Saudi Arabia is between 2 and 3.2 degrees. As mentioned previously, the magnetic instrumentation used for this study measured the earth's magnetic field in a relative sense and also as a scalar.

4.3.1. Magnetic Field of the Earth. The magnetic field of the earth contains the three components: 1) the main field; 2) the external field; and 3) the field generated by magnetically susceptible material within the earth's crust. The main field contributes over 90% of the earth's total magnetic field and is caused by convection currents of conducting material (mainly iron and nickel) within the liquid outer core to a first order

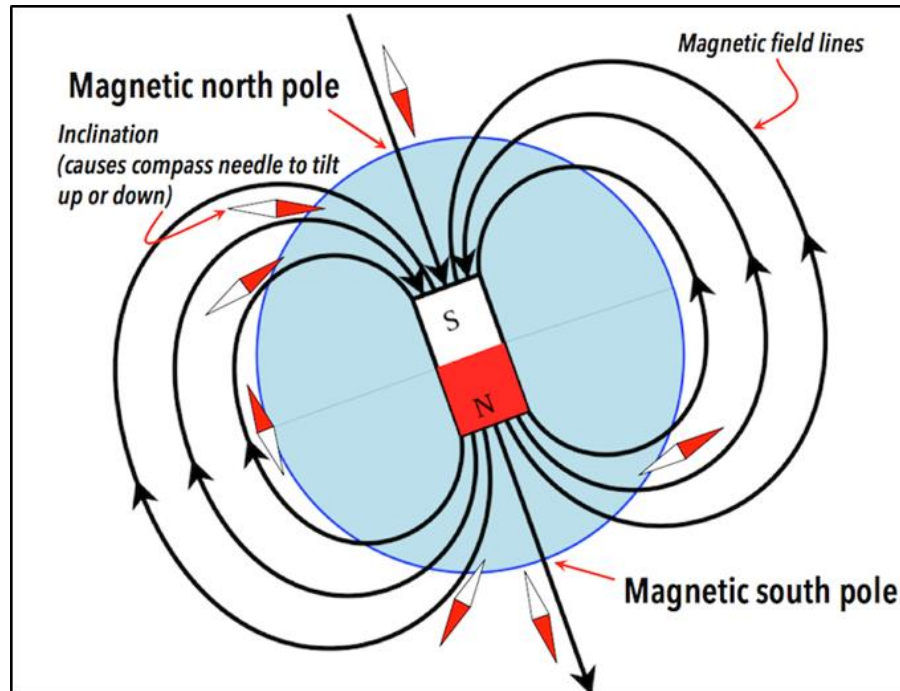


Figure 4.2 Earth's magnetic field depicted as the field of a bar magnet. The south pole of the magnet points to Earth's magnetic north pole. The red and white compass needles represent the orientation of the magnetic field at various locations on Earth's surface.

approximation. The earth's magnetic field can be modeled as though it was generated by an imbedded dipole oriented about 11.5° to true north (Mickus, 2014).

The external field is a small portion of the main magnetic field of the earth that represents about 10 % of the field, and it changes rapidly, randomly, and sometimes periodically. It is caused by the movement of charged particles within the differential flow of ions and electrons inside the magnetosphere and in the remove, italics form current systems in the ionosphere to the magnetic poles. These changes are called diurnal variation. The magnetic field of the earth is generated through the outer core within the convective movement of liquid iron. The earth's magnetic (geomagnetic) field, "F," at any point has few elements to represent its magnitude and direction.

The components are: 1) amplitude of the field (F); 2) magnetic inclination (I), which is the dip of a magnetic compass needle from the horizontal direction; and 3) magnetic declination (D) which is the angle between geographic and magnetic north. All these components are shown in Figure 4.3, and these values are collectively known as the International Geomagnetic Reference Field (IGRF) (Mickus, 2014).

Magnetic anomalies are caused by the superimposed presence of magnetic minerals and rocks on the normal geomagnetic field at that location. Anomalies are generally very complex and may be extremely difficult to interpret quantitatively (Haldar, 2013).

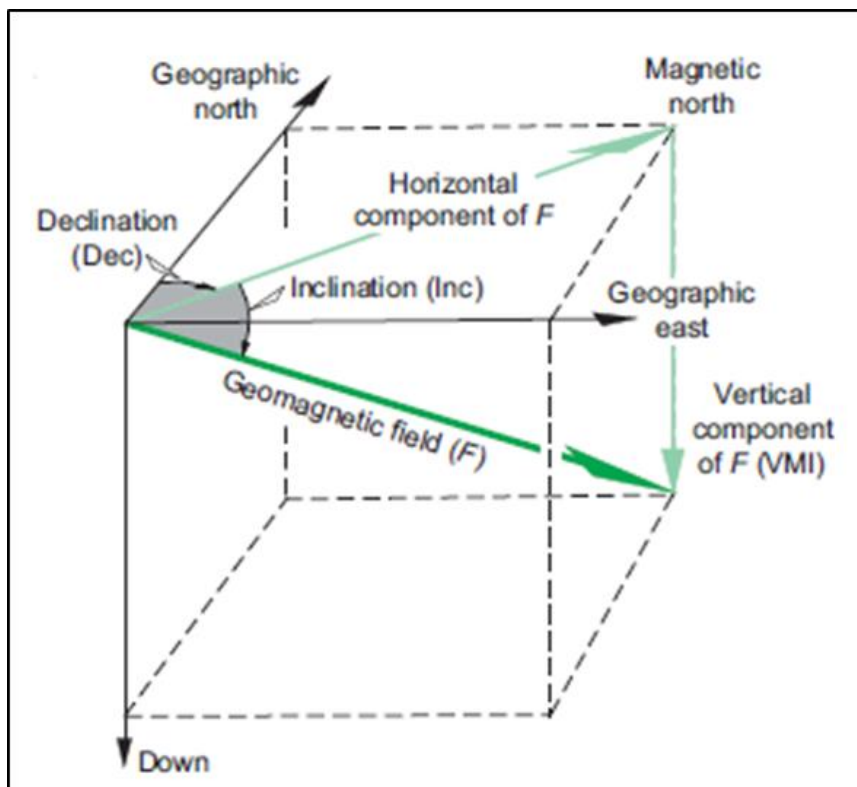


Figure 4.3 Schematic diagram of geomagnetic field elements, (Dentith and Mudge 2014).

4.3.2. Magnetic Susceptibility. Magnetic susceptibility is the ratio of magnetization M to the applied magnetizing field intensity H . Magnetization M refers to the magnetic moment per unit volume. Magnetic susceptibility is the most important variable in magnetics; it measures ability of a rock to acquire a magnetization in the presence of a magnetic field (Mabey et al., 1974), (Telford et al., 2004). Magnetic susceptibility is a no dimensional quantity and is the fundamental physical property used in the magnetic method. The measurement of the total magnetic field (which includes the external magnetic field and the magnetization) is called the magnetic induction (B) and is written as:

$$B = \mu_0(1 + K)H \quad (4)$$

where μ_0 is the magnetic permeability of free space.

The units of B are teslas, which is generally too large a number for applied magnetics work, so gammas (10^{-9} teslas) are more commonly used. Also, note that B is a vector quantity and in most magnetic work today, the amplitude of B is measured, and it is called the total magnetic field (Mickus, 2014).

Rocks can be studied using different physical properties among which are resistivity, radioactivity, magnetic susceptibility, and so on (Keary, 1991). The magnetic susceptibility of minerals makes it possible for magnetic surveying to be used for the mapping of magnetic rocks due to the uneven distribution of magnetically susceptible minerals in rocks. The presence of magnetically susceptible minerals in rocks causes small scale (but often measurable) distortions in the earth's magnetic field as observed on the earth's surface. The induced field may add constructively or destructively to the

earth's main field and generate a measurable anomaly. Magnetization is a function of location and varies from point to point (Blakely, 1995).

Basic igneous rocks usually contain more magnetic minerals than sedimentary rocks. Metamorphic rocks contain variable concentrations of magnetically susceptible minerals while sedimentary rocks, in general, contain relatively little magnetically susceptible mineralization.

Basic and ultrabasic dykes, sills, lava flows, and magnetically susceptible ore bodies are the most common sources of magnetic anomalies in igneous rock (Table 4.2). The amplitude of the magnetic field contribution generated by rock types varies from as low as 20 nT in limestone and 800 nT in basic igneous rocks to more than 6000 nT over sulfide orebodies (Figure 4.4). Magnetic fields are generated by the presence of magnetically susceptible material that is superimposed on the main field of the earth in that location (Haldar, 2013).

4.3.3. Types of Magnetic Materials. The materials in nature in terms of magnetic are divided into:

1. **Diamagnetic:** - composed of atoms that have no net magnetic moments. A negative magnetization is produced when the material is exposed to the external magnetic field, and thus the susceptibility is negative ($\chi < 0$) in the range of -10^{-6} to -10^{-5} . Examples of the diamagnetic materials are Cu, Ag, and Au (Figure 4.5).

2. **Paramagnetic:** - magnetic moments do not interact with each other, and they are randomly arranged in the absence of a magnetic field. The atomic magnetic moments are aligned in the direction of the field, and that will induce a net positive

magnetization and positive susceptibility ($\chi > 0$) in the range of 10^{-5} to 10^{-3} . Examples of the paramagnetic are Li, Na, and all platinum-group metals such as Ru and Pt.

3. Ferromagnetic: - magnetic dipolar moments aligned parallel to each other even without an external applied magnetic field. Magnetic susceptibility is large and positive. The examples of ferromagnetic materials are Ni, Fe.

4. Anti-ferromagnetic: - a special case of ferrimagnetism, where the alignment of the spin moment of the neighboring atoms is in opposite directions or iron in exactly opposite directions. Examples of the anti-ferromagnetic materials are MnO, FeO, and MnF₂.

5. Ferrimagnetic materials: a special case of antiferromagnetic materials; a phenomenon in which the magnetic interaction between any two dipoles align anti-parallel to each other, where they have no different magnitude. It consists of more states of different transition elements, and has very large susceptibility and +ve. The magnitude of dipoles is not equal; however, the cancellation of magnetic moments will be incomplete and result in a net magnetization in the material.

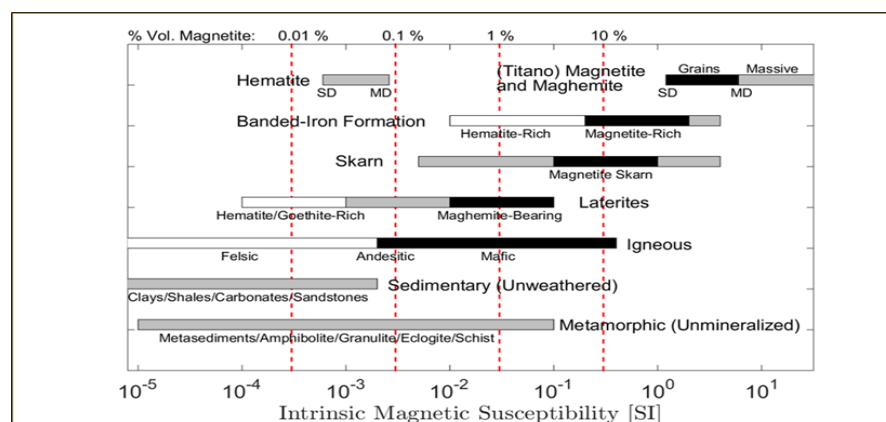


Figure 4.4 Magnetic susceptibility of common rocks, Exploration geophysics, Clark and Emerson (1991).

Table 4.2 Magnetic susceptibility of various rocks and minerals $\chi 10^3$ SI (Telford et al., 2004).

Type	Susceptibility X 10^3 (SI)	
	Range	Average
Rocks		
Schist	0.3 – 3	1.4
Granite	0 – 50	2.5
Rhyolite	0.2 – 35	
Porphyry	0.3 – 200	60
Gabbro	1 – 90	70
Basalts	0.2 – 175	70
Diorite	0.6 – 120	85
Andesite		160
Minerals		
Graphite		0.1
Chalcopyrite		0.4
Pyrite	0.05 – 5	1.5
Hematite	0.5 – 35	6.5
Pyrrhotite	1 – 6000	1500
Ilmenite	300 – 3500	1800
Magnetite	1200 – 19200	6000

Material	χ_m [cm ³ /g]	χ_v unitless	μ unitless	Type of magnetism
Bi	-1.34×10^{-6}	-13.13×10^{-6}	0.99983	
Be	-1.0×10^{-6}	-1.85×10^{-6}	0.99998	
Ag	-0.192×10^{-6}	-2.016×10^{-6}	0.99997	Diamagnetic
Au	-0.142×10^{-6}	-2.74×10^{-6}	0.99996	
Ge	-0.106×10^{-6}	-0.564×10^{-6}	0.99999	
Cu	-0.086×10^{-6}	-0.77×10^{-6}	0.99999	
Superconductors ^a		$\sim -8 \times 10^{-2}$		
Sn β	$+0.026 \times 10^{-6}$	$+0.19 \times 10^{-6}$	1	
W	$+0.32 \times 10^{-6}$	$+6.18 \times 10^{-6}$	1.00008	
Al	$+0.61 \times 10^{-6}$	$+1.65 \times 10^{-6}$	1.00002	Paramagnetic
Pt	$+0.983 \times 10^{-6}$	$+21.04 \times 10^{-6}$	1.00026	
Mn	$+8.9 \times 10^{-6}$	$+66.13 \times 10^{-6}$	1.00083	
Low carbon steel			5×10^3	
Fe-3% Si (grain oriented)			4×10^4	Ferromagnetic
Ni-Fe-Mo			10^6	

Figure 4.5 Magnetic properties of some materials

4.4. TIME-DOMAIN ELECTROMAGNETIC METHOD

One of the active geophysical methods is the time domain electromagnetic (TDEM method). In terms of mineral exploration, this tool is useful for locating and mapping subsurface metals, as it responds to the presence of electrical conductive materials such as metallic mineralization. On the downside, electrical conductivity is also a function of ground water salinity, percent saturation, and rock type, porosity, and permeability (McNeill, 1980 McNeill & Bosnar, 1986). One of the electromagnetic methods is the TDEM method. It was established in the early 1980 to image deeper structures.

The development of new instrumentation and interpretation methods has further redefined the concept of the TDEM method, and the redefinition enabled the application of the TDEM method to be incorporated in engineering, hydrogeological, geological,

and environmental studies. Today, TDEM forms a practical approach to assessing and analysing the electrical parameters of the subsurface medium.

The characteristics of the EM method are based on a wide range of applications. However, the applications depend on the equipment being utilized. These applications comprise groundwater surveys, mineral resources evaluation, mapping of contaminants plumes, mineral exploration, geological mapping, permafrost, landfill surveys, and geothermal resource investigation.

Electromagnetic (EM) methods provide powerful means to measure subsurface electrical resistivity. In this case, metallic mineralization, the composition of fluids that fill the pore space, porosity, and permeability, as well as rock type, affect the electrical conductivity of rocks (Figure 4.6).

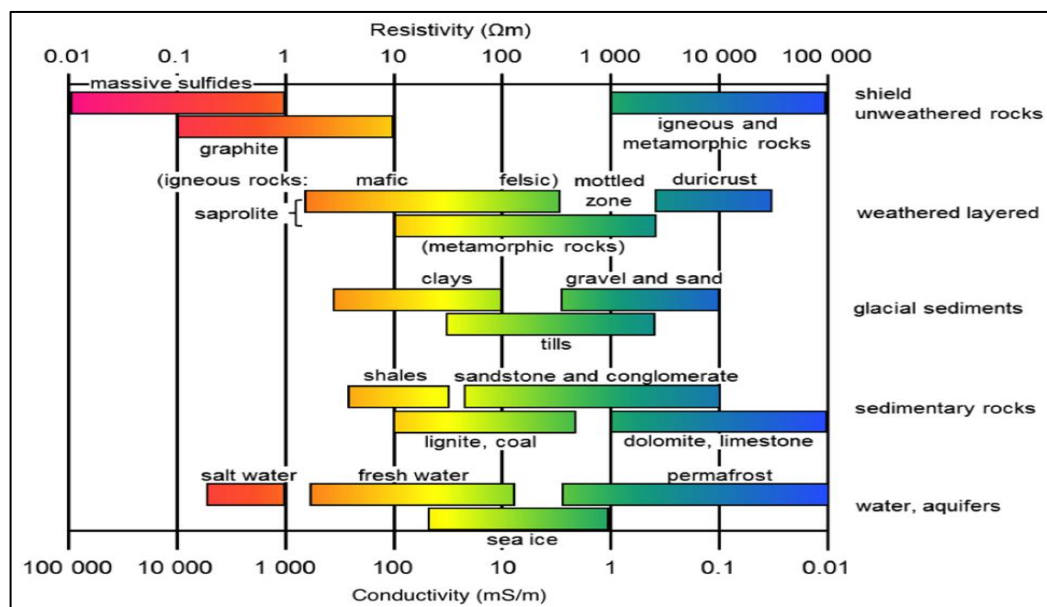


Figure 4.6 Illustrates generally the resistivities and electrical conductivities of most rock groups (adapted from Palacky, 1987).

One of the physical properties of the TDEM tool is that it is a transient technique. The method induces a strong direct current (DC), which is passed into the subsurface through a wire loop generally laid on the ground surface (but can be airborne). The DC current generates a stable magnetic field in the subsurface. This magnetic field will rapidly decay when the direct current is terminated abruptly (Figure 4.7). The TDEM tool measures the earth's response (eddy currents associated with rapid decay of the magnetic field) to the termination of the DC current.

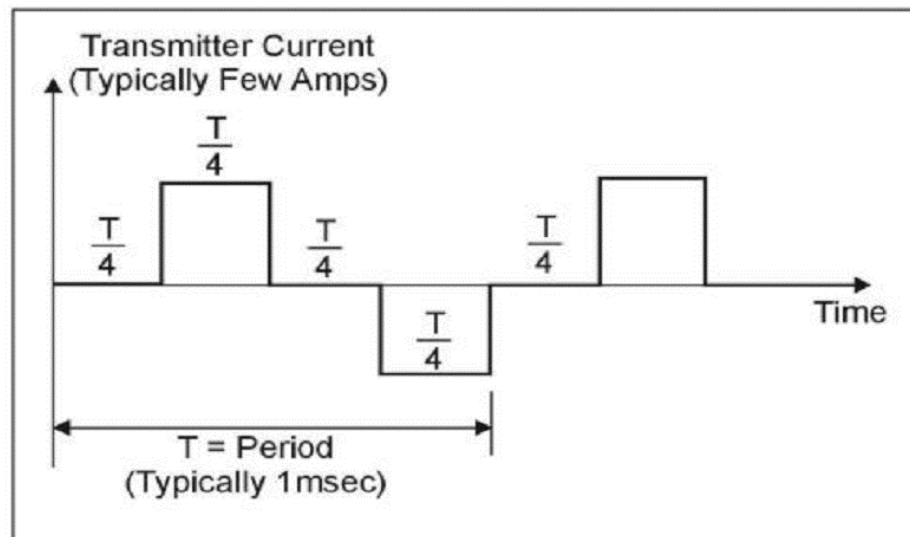


Figure 4.7 Transmitter current wave-form in TEM method, EPA, (Agency 2016).

Faraday's law states that the decay of the primary magnetic field will cause the eddy current to flow downward and outward with reducing velocity. The current will cause the amplitude to reduce with time, which can be observed in the smoke ring portrayed in Figure 4.8. Equation (5) shows the velocity (V_z) with which the ring expands away from the transmitter at a time (t).

$$VZ=2\sqrt{\pi\sigma\mu t} \quad (5)$$

where σ is the conductivity and μ is the magnetic permeability of the medium.

The rate of change of these currents and of their respective secondary magnetic field depends on the size, shape, and conductivity of the subsurface conductors.

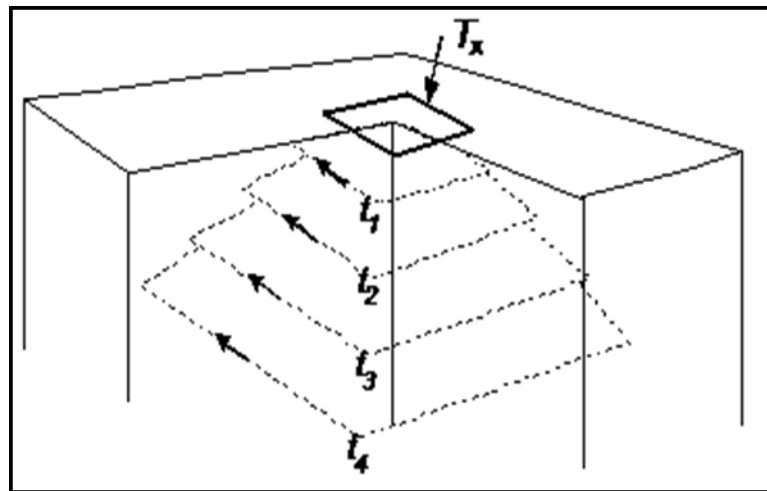


Figure 4.8 System of equivalent current filaments at various times after current interruption in the transmitter loop, showing their downward and outward movement. EPA, (Agency 2016).

The earth's response is recorded using a receiving unit, which is engaged with the transmitter in the same unit. As shown in Figure 4.9, the received voltage response can be divided into three stages:

1. The early-time stage, in which the response is constant with time where the eddy currents flow at the surface of the conductor.
2. The intermediate-time stage, in which the response shape continually varies with time. The surface currents start dissipating through Ohmic losses, and the magnetic field decreases due to the inward diffusion of the eddy currents.

3. The in late-time stage, in which the response is now a straight line on the log-log plot. Induced current distribution is invariant with time, and the only change observed is a decrease of the overall amplitude with time.

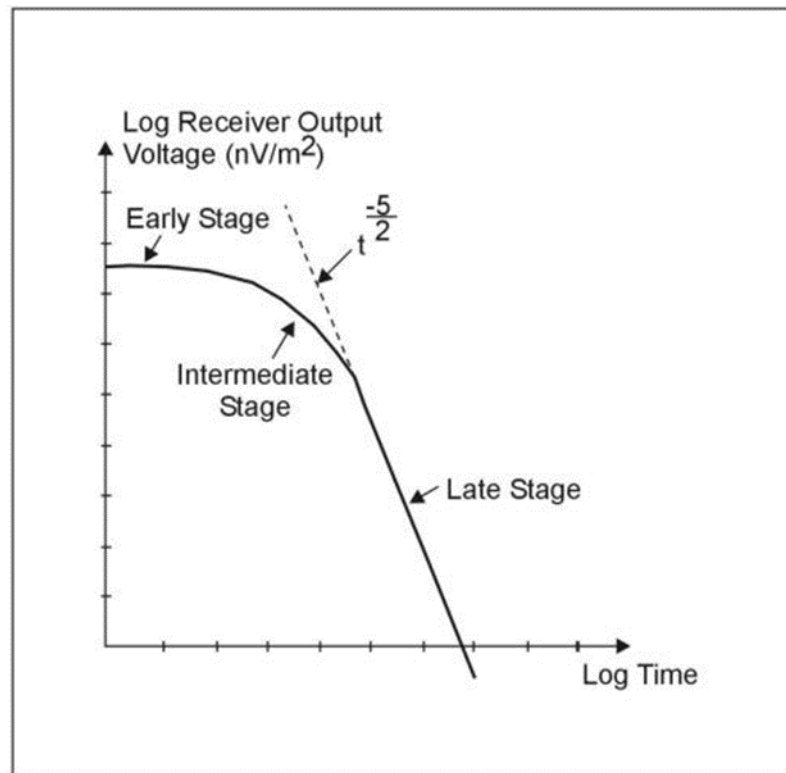


Figure 4.9 Log plot-receiver output voltage versus time (one transient) EPA, (Agency 2016).

The late-time response then varies quite simply with time and conductivity, and the apparent resistivity can be estimated at a later time from Equation (6).

$$\rho_{a(t)} = \frac{K_2 M^{2/3}}{V(t)^{2/3} t^{5/3}} \quad (6)$$

where, K_2 = constant, M = product of I current (amps) * area (m^2), t = time (seconds) and $V(t)$ = output voltage from a single turn receiver coil of $1 m^2$ area.

Note that unlike the conventional resistivity measurements where the measured voltage varies linearly with terrain resistivity, for TEM the measured voltage $V(t)$ varies as $\sigma^{2/3}$. Thus, the TEM is intrinsically more sensitive to small variations in conductivity than conventional resistivity soundings.

5. GEOPHYSICAL DATA ACQUISITION AND PROCESSING

5.1. INTRODUCTION OF DATA ACQUISITION

This section describes the field geophysical data acquisition and processing of three geophysical data sets: SP, Magnetic, and TDEM. These data were recently acquired by the Saudi Geological Survey (SGS) in the Wadi Al Khadra area to assess the Ni-Cu prospect. The surveys and the processing software and steps are described in this chapter.

5.2. SELF-POTENTIAL SURVEY DATA ACQUISITION

The SP survey covers an area about 800 m by 400 m. The SP data were acquired at 25 m intervals along 32 traverses profiles taken with lengths of 400 m. A total of 544 data points were acquired (Figure 5.1). An ELREC Lite instrument from IRIS, a French company, acquisition system were used to record the signature of the Wadi Al Khadra prospect. This instrument is handheld, has 2 channels, and is designed for mineral exploration (Figure 5.2).

To acquire SP data, the gradient method was employed. This method utilizes two mobile electrodes spaced at 25m intervals with one electric wire running from each electrode to the recording instrument. The potential difference between two observation locations is recorded. In a progressive manner, the potential differences are recorded between stations 2 and 3, 3 and 4, and 4 and 5, etc. When they take a reading, the instrument reads the potential difference between the two electrodes and stores the value in its memory.

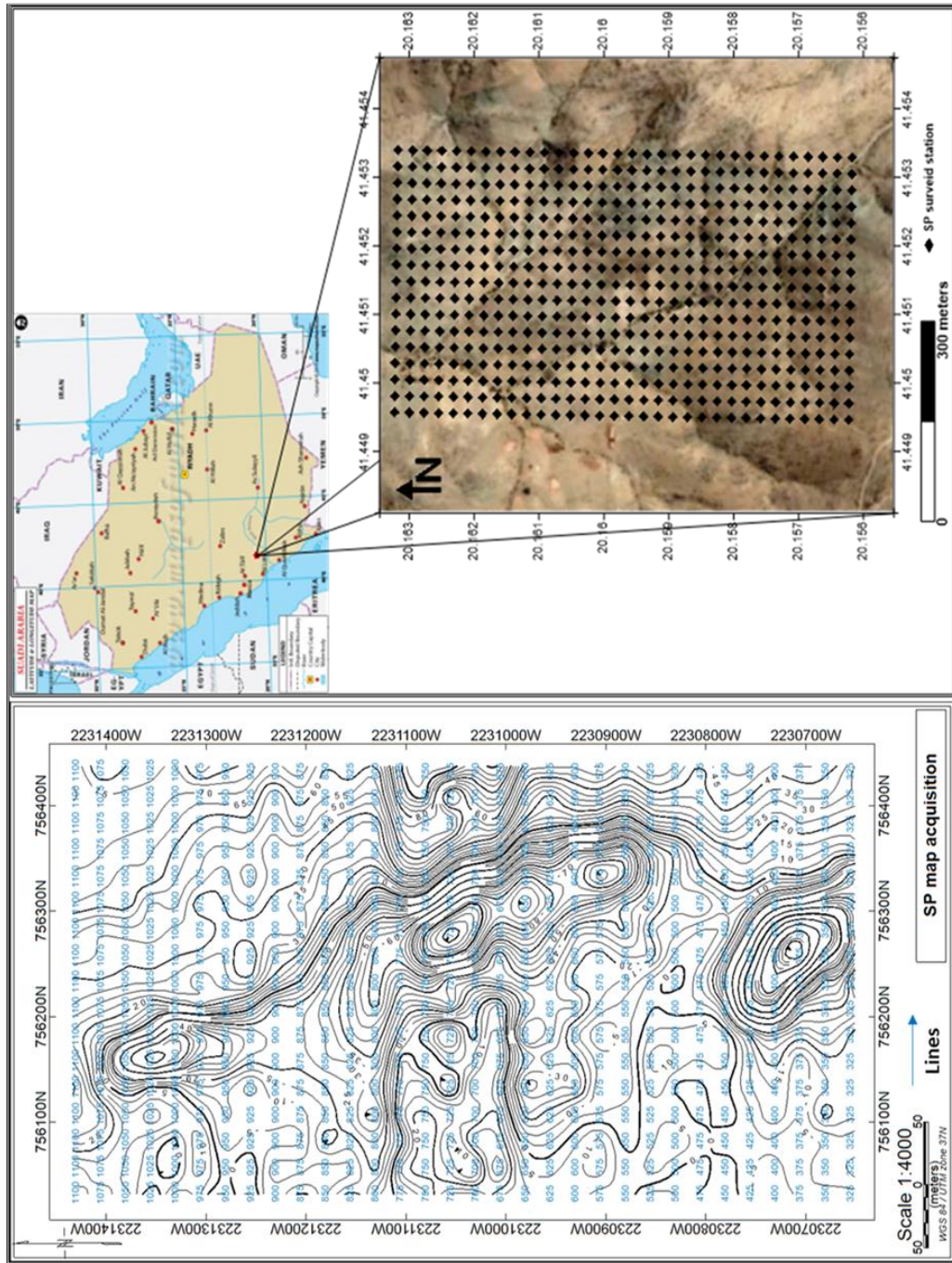


Figure 5.1 Map of SP data acquisition of Wadi Al Khadra Prospect.



Figure 5.2 Elrec Lite instruments were using of SP survey, IRIS Company, France.

5.3. SP DATA PROCESSING

The first processing step is to download the data and to calculate the potential difference between the base station (station 1) and all the other stations. The map of self-potential anomalies and values were plotted using Oasis Montaj™ Geosoft software version 7.0. The SP profiling data, in the form of electrical resistivity imaging, are processed by the ERT lab64, and each SP profile curve (1 per traverse) was generated by using Excel software.

5.4. MAGNETIC SURVEY DATA ACQUISITION

The ground magnetic survey covers an area about 800 m by 400 m (Figure 5.3) and was conducted by using a Geometrics G858 cesium magnetometer, a portable instrument designed to measure the magnitude of the magnetic field of the earth as a scalar (Figure 5.4). The magnetic data were acquired at 25 m intervals along thirty-two 400 m long east-west traverses that were spaced at 25m intervals .A total of 544 magnetic

intensity values were recorded. The diurnal variation in the total magnetic field was observed using a second proton magnetometer. After corrections for diurnal variations and drifts, the total magnetic field was gridded at a 25 m interval.

5.5. MAGNETIC DATA PROCESSING

It is important and useful to better understand the geology, subsurface structure, and tectonic setting in the study area, especially the major tectonic trends that are related to the distribution of metallic minerals in the study area. These objectives can be achieved, at least to a certain extent, by interpreting the available mainly magnetic data. Before starting to the process of magnetic data, the data was uploaded by Magmap which corrected the data for diurnal variations and drift (Figure 5.5).

In order to achieve the objectives, the processing of ground magnetic data has been done using multiple different approaches to enhance all interpretations. The software employed includes Oasis Montaj™ Geosoft software version 7.0 and Golden software Surfer. The processing approaches employed include: different kinds of separation and filtering, derivation of total magnetic intensity, reduction to the pole, vertical derivative, upward continuation, tilt derivative, high pass filtering, spectral analysis, analytical signal, 3-D Euler deconvolution, and 2D magnetic modeling. The multiple outputs of processing were interpreted with the primary goal of characterizing the igneous basement complex that has influenced the overlaying sedimentary section (i.e. sedimentary and structural basins/sub-basins), and also the major structural elements.

5.5.1. Reduction to the Pole (RTP). Reduction to the pole filtering was applied using by Geosoft Oasis Montaj™. Reduction to the pole modifies the data so that it appears the data were acquired at the north magnetic pole, where the earth's magnetic field is vertical (LUO et al., 2010). It is an accepted part of the magnetic data processing approach for large-scale mapping, since it simplifies the interpretations. Anomalies are essentially centred over the causative features. That is only made possible by removing the asymmetry which is introduced because of its influence by the inclined main field. The core field is only vertical at the south and north magnetic poles. Because of the declination and inclination of the induced magnetization vector from the magnetic poles, the determined magnetic field anomalies are changed from the centers of their magnetic sources (Figure 5.6). To reduce the polarity effect and align the peaks of magnetic anomalies directly over the source, RTP transformation is applied to the total magnetic data (Blakely, 1995) (Mendonca & Silvia, 1993).

RTP was calculated in the frequency domain using the following equation:

$$L(\theta) = \frac{1}{(\sin(I) + i \cos(I) \cos(D - \theta))} \quad (7)$$

where θ is the wave number direction, I the magnetic inclination, and D the magnetic declination.

5.5.2. First Vertical Derivative. Derivatives are used in total magnetic data to differentiate anomalies generated by deeper sources from anomalies generated by shallower sources (Ravat, 1996). The rate of change of the magnetic field in the vertical direction forms the first derivative filter of the magnet intensity. The first derivative filtering enhances anomalies generated by near-surface features. The impact of the derivative is that higher frequency (short wavelength) magnetic features are enhanced.

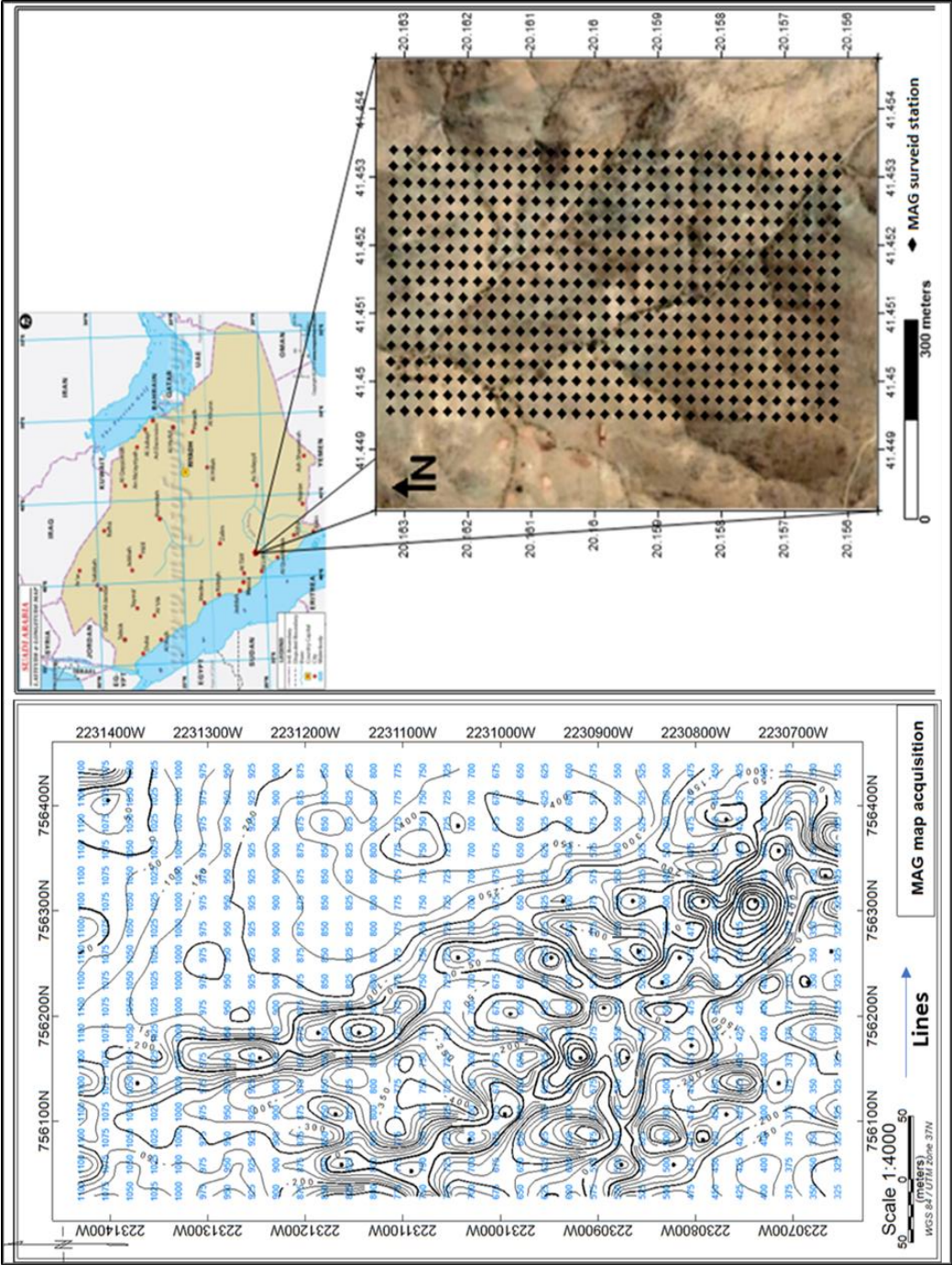


Figure 5.3 Map of Magnetic data acquisition of Wadi Al Khadra Prospect.

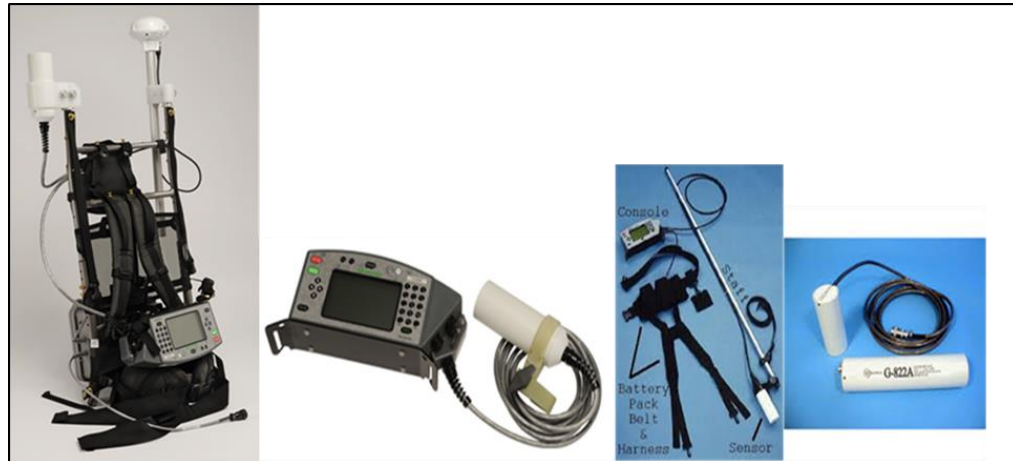


Figure 5.4 G-858 Portable Cesium Magnetometer was using of magnetic survey /Gradiometer, Geometrics.

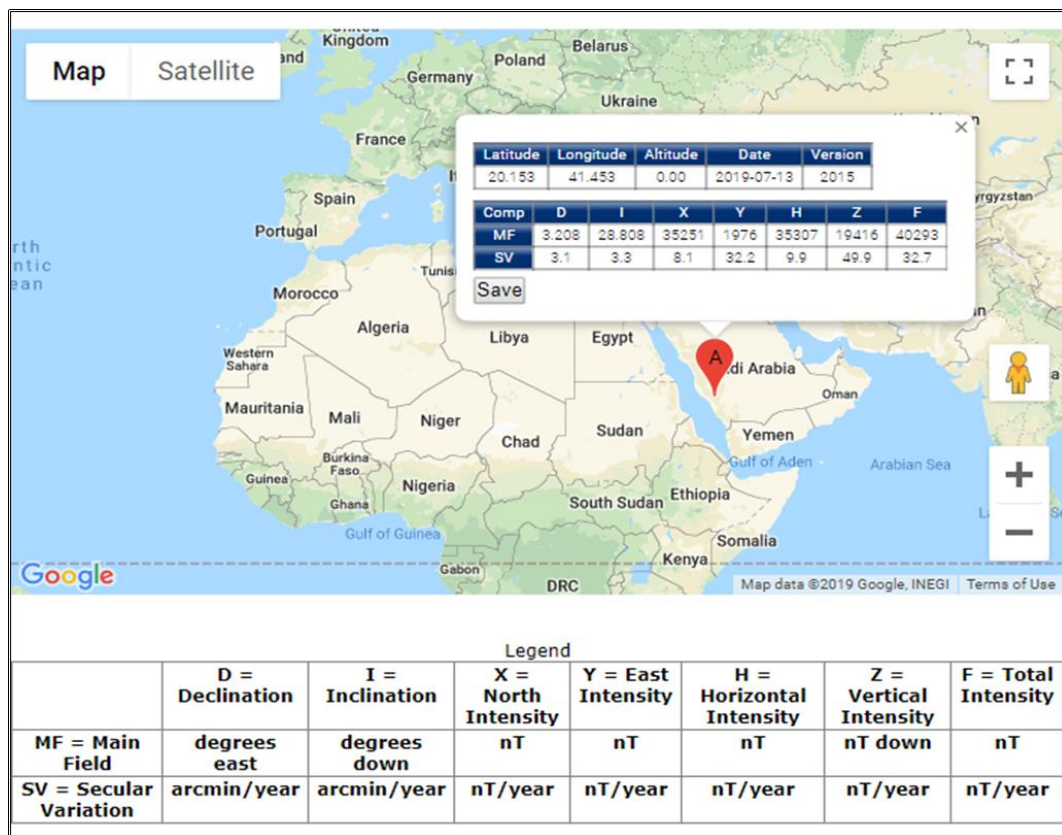


Figure 5.5 IGRF model of the study area, geomag.bgs.ac.uk/data

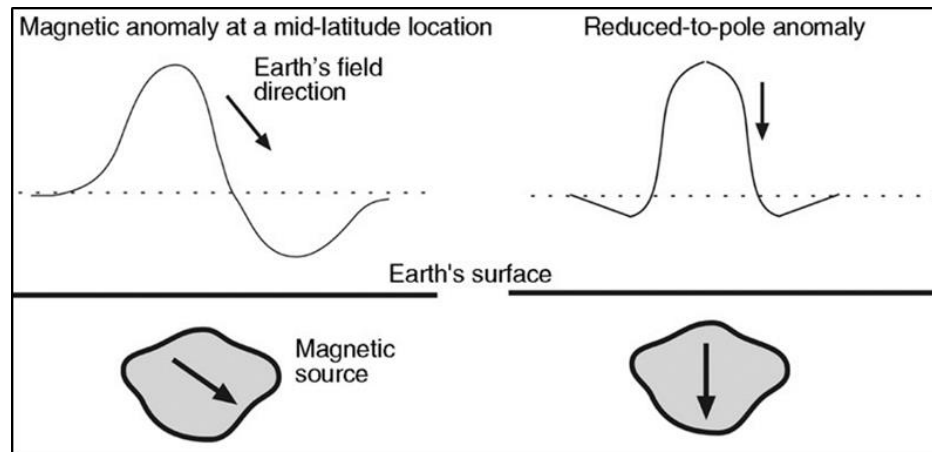


Figure 5.6 Effects of using the reduction-to-pole correction. Ravat (2007).

The computation enhances the resolution of the superposed anomalies and closely spaced anomalies. Therefore, the coincidence of the zero-value contour with vertical contacts at a high magnetic latitude forms the first property of vertical derivative maps (Hood, 1965). The first vertical derivation was calculated from the RTP magnetic data in the study area.

5.5.3. Tilt Derivative. To improve the shallow geological sources and to approximate the depth, another method, known as tilt derivative, can be used. This method adopts the idea that the structures of the source have buried 2D vertical contacts. Also, the method is based on the ratio of horizontal and vertical derivatives of the field (Salem et al., 2007). Therefore, the mineral exploration targets and shallow basement structures are mapped by total horizontal derivatives and tilt derivatives. According to Miller and Singh (1994) and verduzco et al. (2004) the tilt derivative is defined as:

$$TDR = \tan^{-1} \left(\frac{VDR}{THDR} \right) \quad (8)$$

where VDR is first vertical derivative and THDR is the total horizontal derivative of the total magnetic intensity T.

The tilt derivative is changing with an inclination within an amplitude range of $\pm\pi/2$. The zero crossing is near to the edges of the model structures according to inclinations of 0 and 90°. The edges of source bodies of the RTP and RTE fields are delineated by the zero contours of the tilt derivative map. The negative values of the zero contour are outside of the source (Miller & Singh, 1994). Also, the depth to the top of the contact, which is half the physical distance between $\pm 45^\circ$ contours, is equal to the horizontal distance from 45° to 0° location of the tilt derivative.

5.5.4. Upward Continuation Filtering. In order to project the observed anomaly field to higher and lower elevations, the continuation method is used. Higher and lower elevations are referred to as upward and downward continuation (Yarger, 1985). The method is important in that if the continuation does not extend into the sources, the character of the geo-potential field anomaly is retained. Therefore, the effect of the impact of near-surface bodies is reduced by upward and downward continuations.

The upward continuation filter reduces the impact of higher wave number components associated with more local near surface anomalies (Lidiak et al, 1985). This means that, the continuation projects the observed anomaly field to higher elevations. Also, because of its ability to produce almost no side effects, which may require the application of other filters to correct, it is considered a clean filter. This ability enables the filter to minimize the impact of noise in the grid and shallow sources. In the study area, RTP magnetic data continued upward to 20 meters.

5.5.5. Analytical Signal Derivative (AS). The analytical signal (AS) is determined by finding the square root of the sum of the squares of the x, y, and z-direction derivatives. The significant linear magnetic anomalies, such as steps and fault zones, are used to approximate the depth that is caused by applying the analytical signal derivative to examine the buried structures. Also, the steps and fault are used to locate the edges of the source anomaly and approximate its geometry by applying the same method. To get the amount of depth in the two dimensional of the digitized magnetic data, the method is directly applied based on the gradients of x, y, and z (dt/dx , dt/dy , and dT/dz). Besides, the method assumes that causative sources are two dimensions geological structures such as horizontal cylinder, dikes, and contacts.

5.5.6. Regional and Residual Magnetic Maps. The regional (low-pass) map is a filter that is used for smoothing and shows deep-seated structures of high amplitude positive and negative magnetic anomalies, while the residual (high-pass) filter is a filter that is used for sharpening and shows the sudden changes in the magnetic relief. It always accompanies the shallow-seated geological features and/or bodies of low amplitude positive and negative magnetic anomalies.

5.5.7. 3-D Euler Deconvolution. The Euler deconvolution is a technique used in the interpretation of magnetic and gravity data to create the mapping. This technique is showing the locations and depth of the geologic sources of the gravity or magnetic anomalies observed in the two-dimension grid. Therefore, the method approximates the outline and depth of boundaries of the source bodies. The depth estimate is utilized in defining the depth and location of the source that produces gravity or magnetic anomaly in mineral exploration. Euler's homogeneity is the core determinant of three-dimensional

Euler deconvolution. Euler's homogeneity is an equation that connects the gradient component and potential field to the source location with homogeneity. The homogeneity may be interpreted as a structural index. Based on the structure index (SI) choice, the depth approximation results in Euler deconvolution. The SI parameter is based on the potential field and source body type, and magnetic field of narrow 2-D Dyke. The 2-D Dyke has a structural index of $SI=1$. On the other hand, a vertical pipe or cylinder gives $SI=2$, while a sphere gives $SI=3$. Lastly, contact and steps have $SI=0$ (Whitehead, 2010). The depth of this research was estimated using $SI = 0$, which corresponded to the contact, as well as a window size of 10×10 km.

5.5.8. Radially Average Power Spectrum. To determine the average depth analysis levels for the magnetic source for the location of the study area, the two dimensional radially averaged power spectrum techniques are used based on fast Fourier transform (FFT). This technique is important since it provides the interpreter with insights and general information about the hidden structures that have a geographic extension. The curves of the power spectrum consist of two parts of linear segments. The first part is linked with deeper sources, and it is where the rate of power decay is linear and can be estimated by a straight line. On the other hand, the second part is connected to shallower sources, and it is a high-frequency end (Spector & Grant, 1970; Reeves, 2005).

5.5.9. 2D Modeling. The 2-D modeling approach to interpretation incorporates the fitting of geophysical parameters to potential data; thus, the potential problem that is carried out unambiguously could inversely be solved by potential modelling. From the theoretical view, the two reversed operations are completed sequentially. The first

operation involves a direct modelling process, while the second operation involves an inverse modelling process. The direct modelling process changes the alterations reflected by potential field data in the location of the study. The residual potential anomaly maps show the process of an expedient subsurface geological setting. On the other hand, inverse modeling pairs the calculated potential impacts with observed impacts, where the calculated impacts are produced from the inferred assumed potential models.

5.6. TIME-DOMAIN ELECTROMAGNETIC SURVEY DATA ACQUISITION

The time-domain electromagnetic (TDEM) survey was designed after the acquisition of magnetic and self-potential surveys in order to deeply investigate detected anomalies on the magnetic and self-potential data. The TDEM survey (Figure 5.7) was carried out along 7 profiles (TDEM soundings, 2268 stations) from east to west, and readings were taken every 25 m in order to gain some idea of the structure below the surface.

The survey was done by using a Zonge Nano TEM system with receiver GDP-32 (Figure 5.8) and the maximum transmitter loop size that could be used was 20m with a receiver loop size of 5m. Therefore, the maximum depth which could be observed was about 50 m below the survey area, and the delay times were used in the range of 20 m/s to 40 m/s.

The arrangement of a common survey incorporates a square single-turn loop with a horizontal receiver coil placed at the centre (Figure 5.9). Also, at each secession of gate time, a series of values of the receiver output voltage is included in the data from a resistivity sounding. The gates are in time.

The time can be between a few microseconds and hundreds of milliseconds. Afterwards, depending on the preferred depth of exploration, the location of the transmitter current is turned off. As a function of time, the receiver coil is used to determine the time rate of change of the magnetic field which is given by $e(t) = dB/dt$. The units of $e(t)$ are V/m² of the receiver coil area when properly calibrated.

Nevertheless, it is common to use measured decay and nV/m², since the signals determined are extremely small. Basically, they range from many thousands of nV/m² at early times to less than 0.1 nV/m² at late times. The calibration of the modern receivers has nV/m² or V/m². The calibration is checked by Q-coil, which is laid on the ground at an exact distance from the receiver coil. Q-coil is a small short-circuited multi-turn coil, which is used to give a transient signal of a renowned amplitude.

5.7. TDEM DATA PROCESSING

The processing and modeling of TDEM data was carried out using by Zond EM 2D software. At the respective site, each of the collections of the model described the geo-electrical parameters of the subsurface section. These sections show the varieties acquired both vertically and along the side in the electrical resistivities and their relating geographical units.

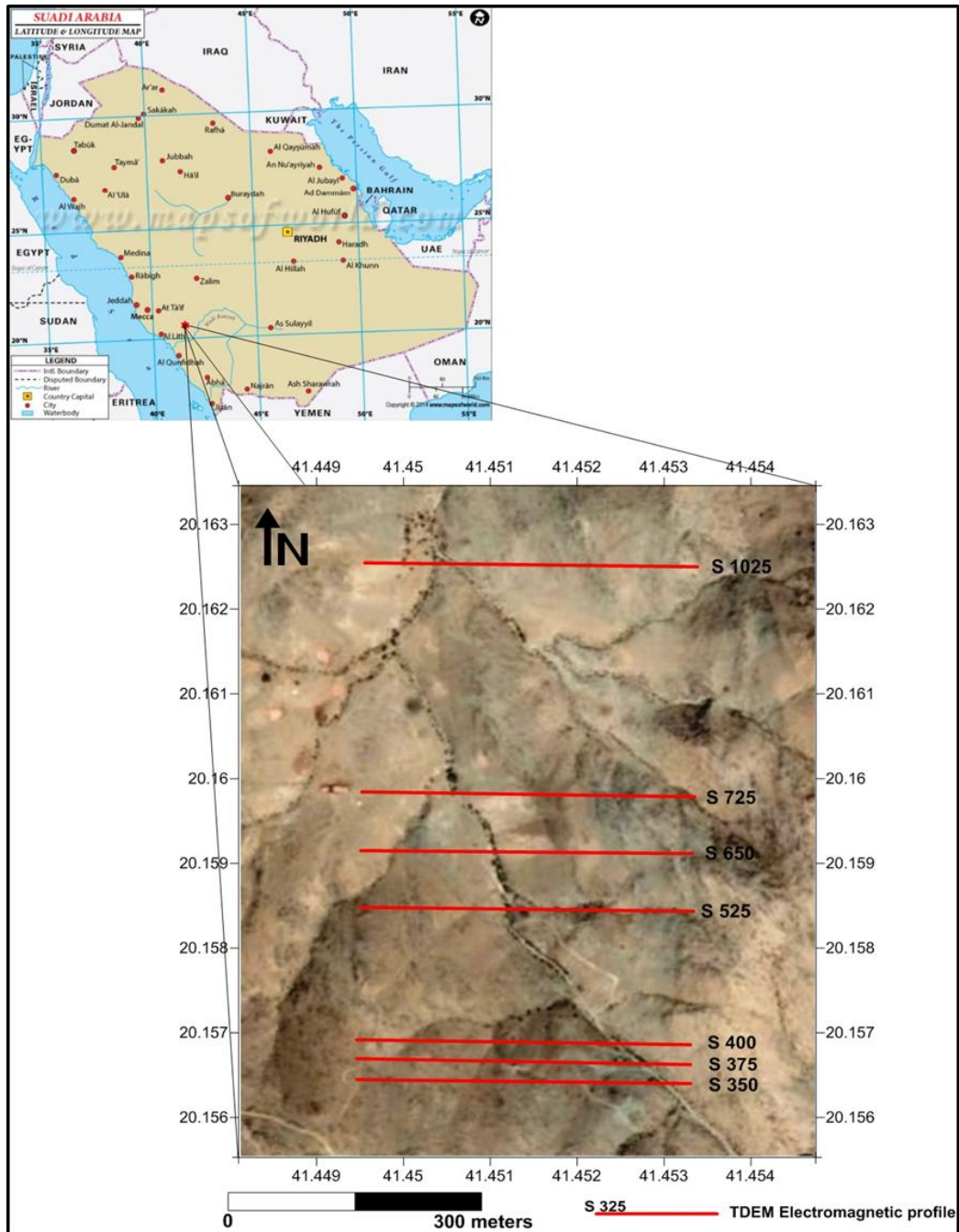


Figure 5.7 Map of TDEM acquisition data of Wadi Al Khadra Prospect



Figure 5.8 GDP-32 receiver used for TDEM survey, A Zonge.

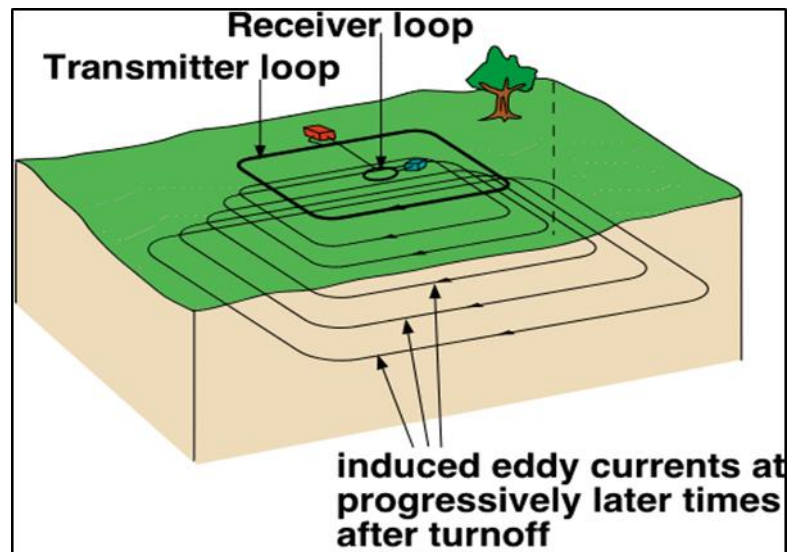


Figure 5.9 Layout of TEM survey, adapted from Zonge International.

6. GEOPHYSICAL DATA RESULTS AND INTERPRETATIONS

6.1. SELF-POTENTIAL RESULTS

The self - potential results will be showing as map and profiles to better interpretation of data:

6.1.1. Self-Potential Mapping. The interpretation of SP data shows that the values range from +109.7 mV to -189 mV. It is clear that there are relatively high negative values (negative anomalies) in three locations (1, 2, and 3) in the study area (Figure 6.1). The problem of distinguishing between possible anomalies (SP) of different origins in basement rocks was addressed using the SP / height gradient. Traditionally, area surveys have exhibited negative-positive / elevation gradients, usually between 0 and -120 mV (Figures 6.2 – 6.10), while positive gradients vary over a wider range between 10 and 50 mV. Simple models show how these gradients are disturbed in the presence of basaltic rock catchments, or lateral variations of physical properties (e.g. resistance) or by positive deformations associated with higher mineral concentrations.

The SP / Alt color gamut is more sensitive to disturbances than the SP, and therefore, the color gamut was used to detect anomalies, using digital SP and topographic networks, the gradient can be calculated in 2D to illustrate this method. Anomalies are easily identified in the active central area, but they are difficult to distinguish in other areas. By contrast, anomalies are clearly displayed on the gradient map along with different types of terrain (different SP / height gradient values). In the rest area, where data coverage is dense, gradient information is compared as a function of SP map resolution to illustrate the sensitivity of the detection method for small-scale structures.

As a method, the gradual gradient appears to match the qualitative interpretation of SP surveys in non-sedimentary or basement areas and other environments.

6.1.2. Self-Potential Profiling. SP data were acquired along thirty-two measurement traverses in the Wadi Al Khadra prospect area. Data acquired along nine of the traverses are presented as profiles in Figures 6.2 - 6.10 it is clear from these profiles, given the significant variations in surface topography, indicated by the SP results, that the values change from place to place, with positive and negative values that could result from variations in rock types. The extent of the changes in SP values with location is also explained.

When looking at profiles, it is easy to observe the places, depths, and values of anomalies that form isolated objects with negative values. The strong gradient in redox potential within the upper 20 cm implies an abrupt change in the rock structure.

The three locations characterized by negative SP anomalies (in Figure 6.1 - 1, 2 and 3) are indicative of zones where subsurface metals are present (vertical transition from oxidizing to reducing conditions).

Thus, the SP tool is suitable for determining the location of metals, (copper, nickel, and associated mineralization in this case). The amplitude of the negative anomalies is related to the concentration of metallic mineralization, the depth of that mineralization and the rate at which oxidization/reduction is occurring locally.

The size of the anomalies is presumed to be indicative of the areal extent of relatively high concentrations of metallic mineralization.

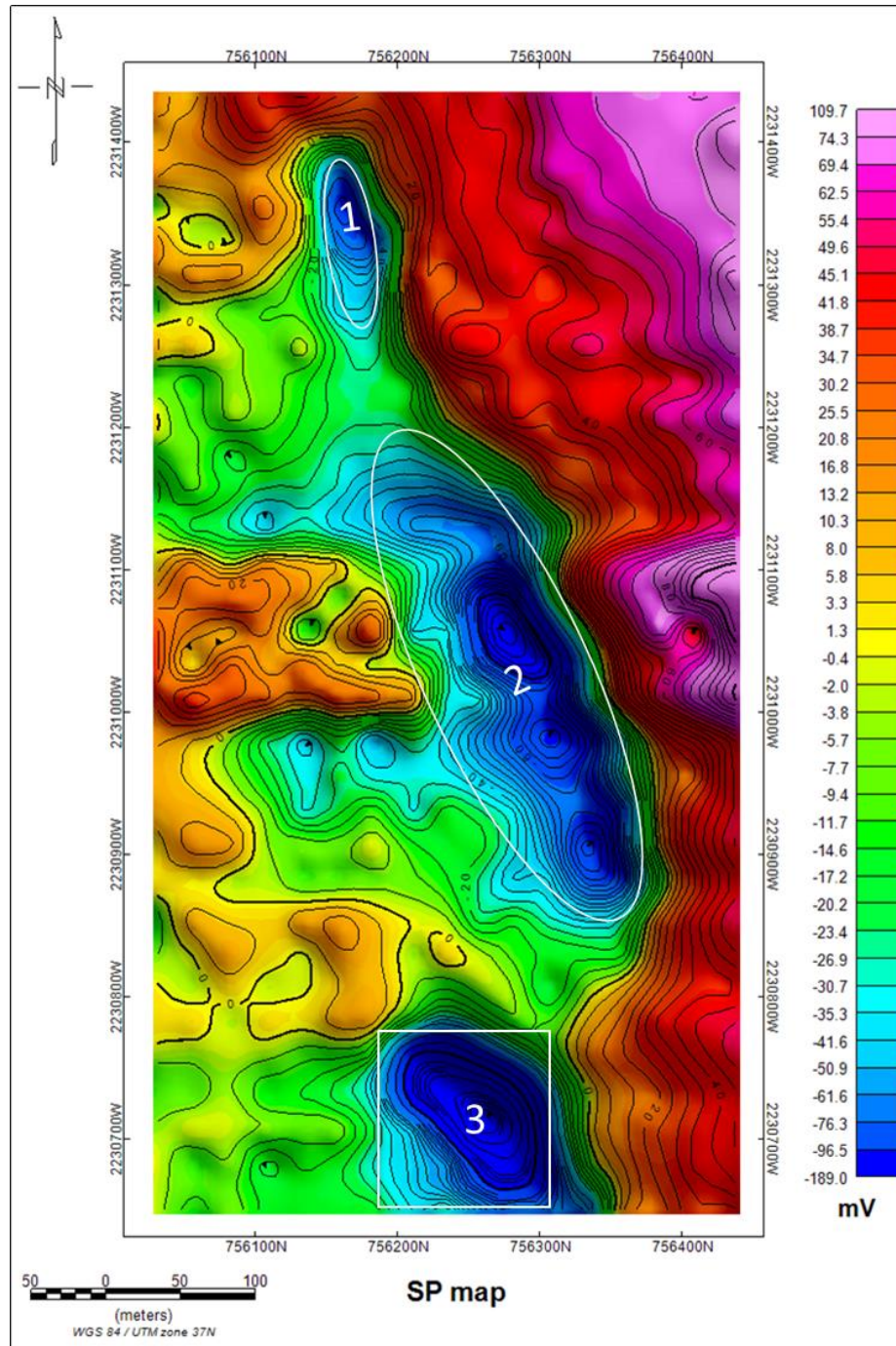


Figure 6.1 SP contour map of Wadi Al Khadra Prospect.

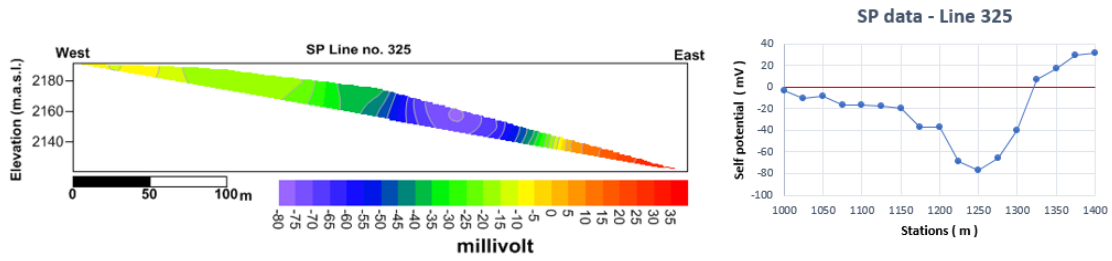


Figure 6.2 Self-potential anomaly in line 325 associated with grounded monitoring instruments.

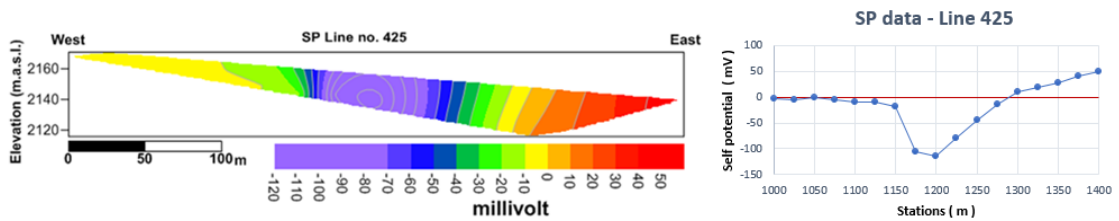


Figure 6.3 Self-potential anomaly in line 425 associated with grounded monitoring instruments.

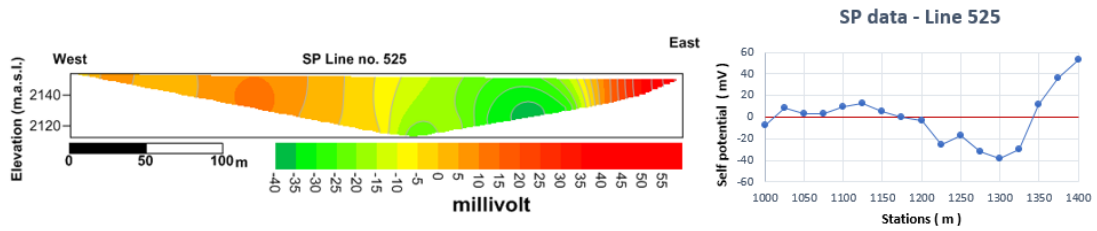


Figure 6.4 Self-potential anomaly in line 525 associated with grounded monitoring instruments.

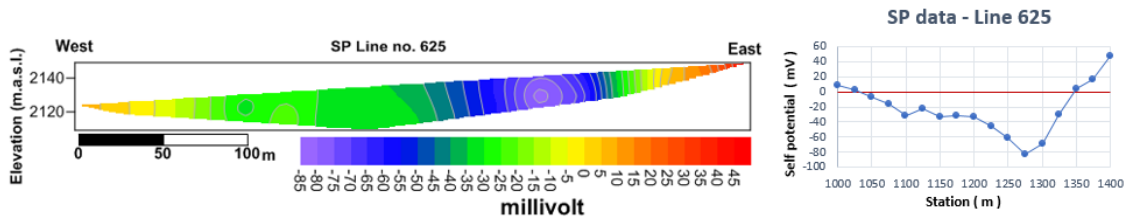


Figure 6.5 Self-potential anomaly in line 625 associated with grounded monitoring instruments.

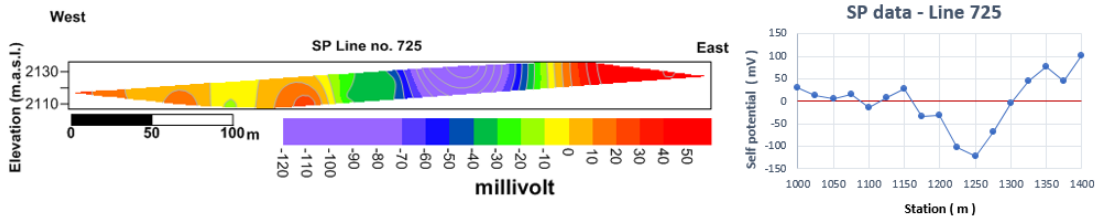


Figure 6.6 Self-potential anomaly in line 725 associated with grounded monitoring instruments.

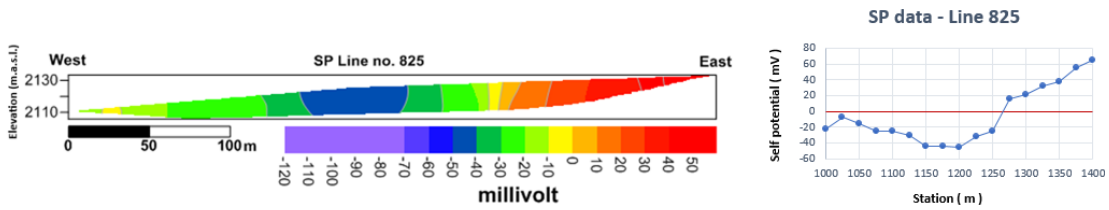


Figure 6.7 Self-potential anomaly in line 825 associated with grounded monitoring instruments.

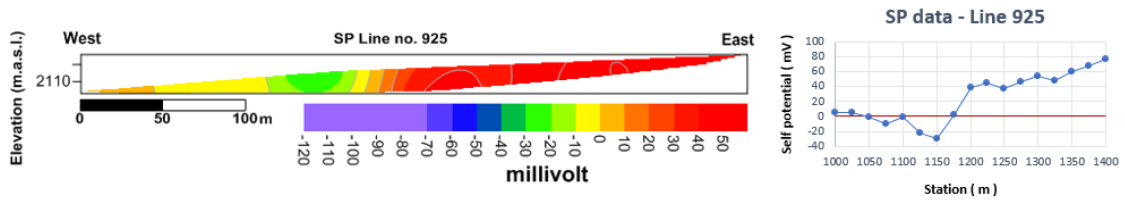


Figure 6.8 Self-potential anomaly in line 925 associated with grounded monitoring instruments.

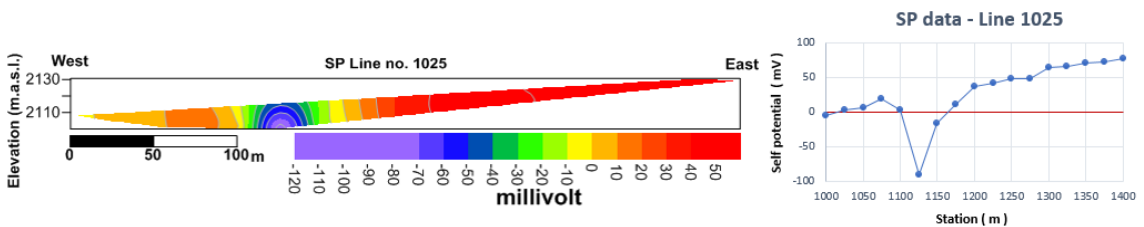


Figure 6.9 Self-potential anomaly in line 1025 associated with grounded monitoring instruments.

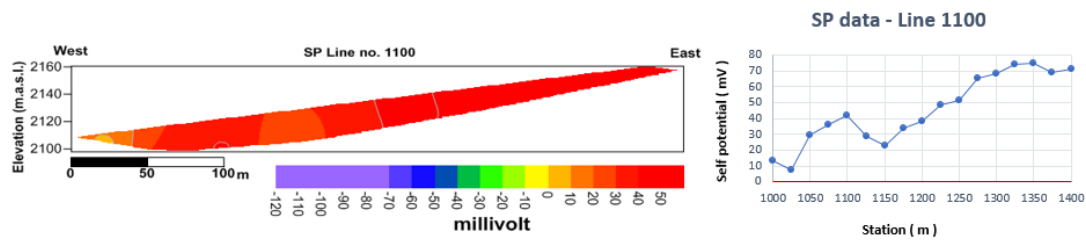


Figure 6.10 Self-potential anomaly in line 1100 associated with grounded monitoring instruments.

6.2. MAGNETIC DATA RESULTS

The magnetic results consist of qualitative and quantitative interpretations of the potential field as follow:

6.2.1. Overview of Magnetic Results. It is important and useful to understand the geology, subsurface structure and tectonic setting in the study area better, especially the major tectonic trends that are related to the distribution of metallic minerals in the study area. These objectives can be achieved, at least to a certain extent, by interpreting the available mainly magnetic data. To achieve the objectives, the magnetic data were processed and interpreted using multiple approaches. The processing approaches included; different kinds of separation and filtering, total magnetic intensity, reduction to the pole, vertical derivative, upward / downward continuation, tilt derivative, high pass, spectral analysis, analytical signal, 3-D Euler deconvolution, and 2D magnetic modeling.

The multiple outputs of processing were used to characterize the igneous basement complex that has influenced the overlaying sedimentary section, i.e. sedimentary and structural basins/sub-basins, and, the major structural elements.

6.2.2. Qualitative Interpretation of the Potential Field. A qualitative assessment of magnetic data maps was used to infer the subsurface geology, subsurface structure, and subsurface lithology. Magnetic anomalies are generated most typically by the presence of magnetically susceptible minerals in the subsurface, where areas of high magnetic susceptibility (the presence of nickel in this case) are characterized by positive magnetic anomalies on RTP map. Areas of low magnetic susceptibility are characterized by lower magnitude anomalies. To complicate matters further, areas where the igneous bedrock is shallower are also characterized by higher amplitude positive magnetic values. In the absence of magnetically susceptible minerals, positive anomalies are often generated by structures such as anticlines, horsts, domes, or up-thrown sides of fault block. Negative magnetic anomalies are often attributable to structures such as synclines, grabens, basins, or down-thrown sides of fault blocks. In spite of the limitations of magnetic interpretation, useful qualitative analysis (in terms of estimated depth to igneous rock) is often possible. The relative positions of anomaly maxima, minima, and inflection points are functions of multiple factors including depth.

The nature of the magnetic anomaly of a given magnetized body as mapped on the earth's surface is complicated. This is because several factors affect the magnetic signature of a causative body, including:

- ◆ Direction (inclination and deviation) of the earth's magnetic field at the study location.
- ◆ Presence and concentration of magnetically susceptible minerals.
- ◆ Magnetic susceptibility of the body causing the anomalies.
- ◆ Direction of polarization of the magnetically susceptible minerals.

- ◆ Orientation of the causative body with respect to the Earth's magnetic field.
- ◆ Locations where magnetic data are acquired.

The purpose of the qualitative analysis is to infer the geological character of the subsurface structures based on the assessment of the suite of processed magnetic maps.

6.2.2.1. Nature of the observed magnetic anomalies. The description of observed magnetic anomalies can involve the size, shape, sharpness, gradients, and positions of the anomalies. In the absence of magnetically susceptible minerals in the sedimentary section, these features can be used to infer the nature and dimensions of the igneous basement. The variables describing potential field anomalies are arranged in decreasing order according to (Rombering, 1958) as follows:

i) Size: This gives an indication about the magnitude of the anomaly. The size (volume) of a certain anomaly is directly proportional to the size of its causative body or structure and it can be computed if the depth to the source is known.

ii) Sharpness: Sharp anomalies are easy to identify, whereas diffuse ones tend to merge with the general background, and they may not be overly visible or interpretable.

iii) Perceptibility: This variable depends on the size, sharpness, and level of the background. If an anomaly generated by variable depth to igneous rock is masked by other anomalies (perhaps generated by the presence of magnetically susceptible minerals), it can be difficult to isolate and identify.

iv) Resolution: Resolution depends on the separation between structures that generate the anomalies. The greater the separation, the clearer and more distinct the resolution will be.

v) Eccentricity: is an interesting aspect of resolution. A long irregular or eccentric geologic structure close to the surface gives an eccentric or elongated anomaly.

vi) Elongation of contours: The direction of iso-anomaly contours at any map suggests the direction and length of the structures causing them. The length is to be understood in relation to the depth.

vii) Shape: This is not a quantitative variable in an engineering sense, it is a criterion for the shape of the structure producing it. Many variables are involved in studying the relation between anomalies and structures. All these concepts of description are useful in defining the nature of causative features that generate observable magnetic anomalies.

6.2.2.2. Description of the detailed ground magnetic data. The ground magnetic survey covered the study area. The magnetic data acquired in the study area was presented in the form of a total intensity contour map, which depicts two high-amplitude positive anomalies (labelled 1, and 2) in the southeastern and northeastern portions of the study area (Figure 6.11). The maximum total magnetic intensity value was 40,751.7 nT and the minimum was 38,795.7 nT . As the following text explains, the total magnetic intensity map was not used for interpretational purposes.

To interpret ground magnetic survey data , it is preferable to use the RTP map (Figure 6.12), to overcome the problems associated with the inclination and declination of the earth's magnetic field (inclination is 28.808° and declination is 3.20°). The RTP magnetic map shows negative and positive magnetic anomalies as well as sharp gradients representing the shallow and / or near surface structural features affecting this. The main trends of the contour lines are aligned generally in the NW-SE directions. Negative

anomalies reflect relatively deeper basement. Positive magnetic anomalies may reflect a shallow basement and / or the basic nature of the composition of the underlying basement, but in this case, it could be the magnetic data reflecting presence of nickel and/or magnetite.

Different types of rock usually have a connection with local magnetic anomalies or features. In this case, anomalies are created when different magnetic characteristics are added to the overall regional magnetic pattern. Areas of magnetism that are either lower or higher than the average magnetic field of the location are referred to as magnetic anomalies.

In this case, a magnetic reading that is greater than the average magnetic field strength and is connected to more strongly magnetic rocks is referred to as positive magnetic anomaly. On the other hand, a reading that is below the average magnetic field is referred to as a negative magnetic anomaly. Irregularities in the bedrock surface beneath sedimentary cover can create positive anomalies. However, the development of a trough on the bedrock surface can also create negative anomalies.

In this case, the negative anomalies are represented by the concentration of minerals such as nickel and copper that have higher magnetic susceptibility than the surrounding rocks, which reflect positive anomalies. Using the results of the drilled and analyzed wells in section 3 (Geology of the Study Area), the phenomena of magnetic values and their relationships to the strength, signal and form of anomalies can be explained. The western part of the surveyed area is characterized by a closed negative short - wavelength magnetic anomaly (A1). However, a low magnetic relief reflecting relatively deeper basement characterizes the northeastern part (A 2). In the eastern part

(A3), there are three small circular negative anomalies that are interpreted as small basic intrusions with negative polarization i.e. reversed polarization (Wassif, 1989-1991 & Ghazala, 2000).

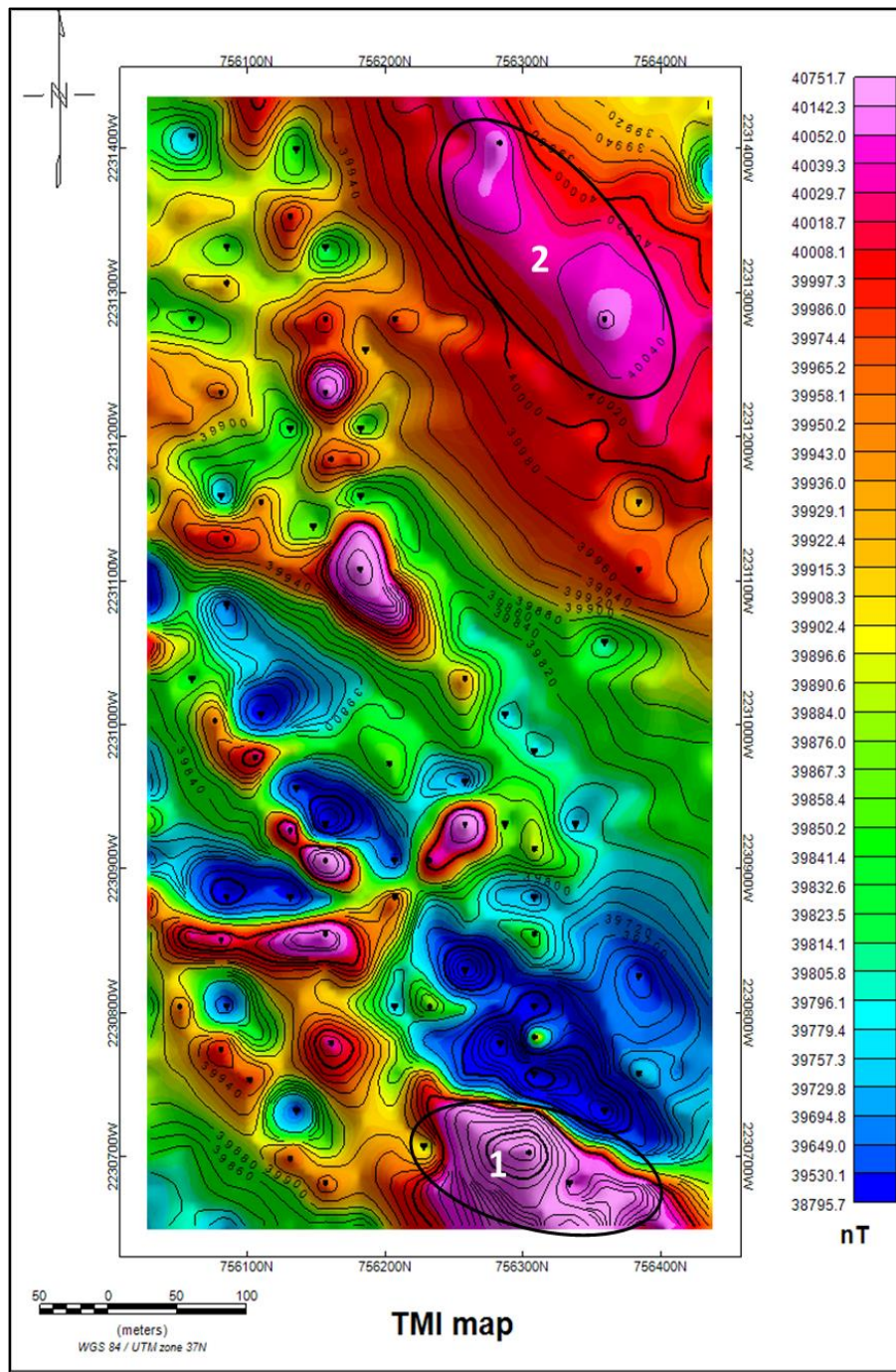


Figure 6.11 Map of total magnetic intensity (TMI) of Wadi Al Khadra Prospect.

In the southern part (A4), there is a high positive short – wavelength magnetic anomaly. Figure 6.13 presents tilt derivatives data. The tilt derivatives vary markedly with inclination within an amplitude range of $\pm\pi/2$. For inclinations of 0 and 90°, the zero crossing is close to the edges of the model structures. The tilt derivative has its zero values close to the edges of the body for RTP and RTE fields. This contribution shows that it is relatively simple with existing potential field data to construct images of the study area by using the tilt derivative of RTP, which provides an effective alternative to the vertical derivative to map the continuity of structures and to enhance the magnetic fabric. The advantages of the tilt derivative are its abilities to normalize a magnetic field image and to discriminate between signal and noise. Since the zero crossing of the tilt derivative is close to the edge of the structure for RTP, then applying a threshold cutoff of 0.0 isolates all bodies with positive susceptibility contrast.

Figure 6.14 presents the first vertical derivative data. The first vertical derivative was calculated from the RTP magnetic data of Wadi Al Khadra, and it is the rate of change of the magnetic field in the vertical direction. Computation of the first vertical derivative removed long-wavelength. Features of the magnetic field and significantly improved the resolution of closely spaced and superposed anomalies. A property of the first vertical derivative maps is the coincidence of the zero-value contour with vertical contacts at high magnetic latitudes (Hood, 1965).

6.2.2.3. Regional and residual maps of the ground magnetic data. A least square polynomial fitting was applied to the RTP magnetic data of the study area. Upward continuation and high filters were used to deduce deep and shallow structure in this area. Figure 6.15, showed that this was a large area with a high magnetic anomaly

in the southeastern and northeastern parts and a low magnetic anomaly in the eastern parts.

However, Figures 6.16-6.17 present high- and low-pass magnetic anomaly maps derived from different techniques, which contain the largest positive anomalies in the Middle Eastern and southern part of the study area. There is another moderately negative anomaly in the eastern and some places on the western parts of the study area.

6.2.2.4. Structural trend analysis. Geological interpretation of the potential field data is based mainly on deducing any relationships between the available data and the prevailing subsurface structural conditions in the studied area. Structural trend analysis techniques have frequently been used in various fields of geology and geophysics to define structural problems. Affleck (1963) discussed the possible relationship between crust forces and the strength expression of the magnetic anomaly trends, as the tectonic history of the rocks is reflected in both the magnitude and the pattern of the anomalies. Hall (1964) stated that there is a significant relation between the direction, pattern, and intensity of the magnetic anomaly trends.

This is because the distinctness with which faults appear on the magnetic map depends principally on the existence and the strength of magnetic contrast in the relevant body of rocks. Hall discussed the significance of the anomaly peaks affecting the basement rocks as follows:

- a. a sharp peak with small standard deviation may indicate a trend caused by fracturing of uniform medium in response to stress of constant direction;
- b. a broad peak with large standard deviation may be expected to be formed by successive renewals of shifting stress direction; and

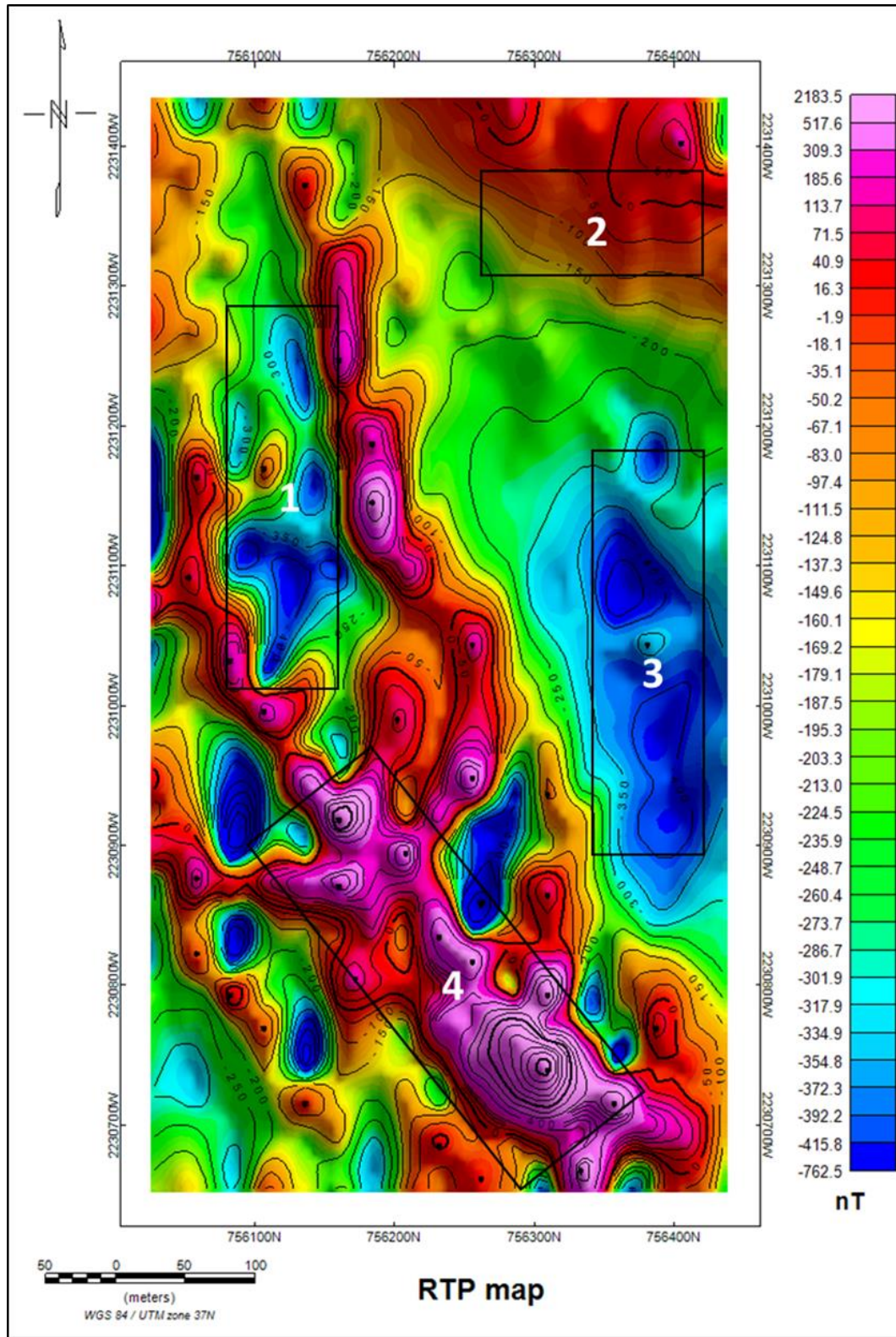


Figure 6.12 Reduce to the pole (RTP) map of the Wadi AL Khadra Prospect.

- c. a peak with moderate symmetry may be formed by larger and smaller stresses in different directions.

The RTP magnetic anomaly and the residual anomaly maps were interpreted to determine the common structural trends affecting the area of study. The azimuth and length of each detected lineament on the different maps probably represent the faults and/or contacts of varied length and directions (Figures 6.15-6.17).

Rose diagrams are used to plot and to analyze the structure system statistically (Figure 6.18). The rose diagrams revealed a predominant structural trend, which has variable length and intensities.

Therefore, from the magnetic point of view, the NW-SE trend represents the most dominant tectonic trend affecting the examined location. The rose diagram also portrays another minor NE-SW structural trend; however, the trends are less significant in this location. All the major trend categories are described briefly in decreasing order, as shown in Figure 6.18.

Because the basement rocks generally have much more magnetic susceptibility than the overlying sediments, the potential field anomalies can be used to compute the depth to the basement causing these anomalies.

In all cases, the following criteria must be taken into consideration in magnetic data interpretation as a measure of the quality for the characteristics and depth estimators:

- The profile must be taken normal to the anomaly strike.
- The length taken from the profile must be readily identifiable for the anomaly.

- The profile must not extend too much outside the anomaly to avoid interference from neighboring anomalies.

6.2.3. Quantitative Interpretation of the Potential Field Data. Quantitative interpretation of magnetic data includes applying different techniques to delineate analytical parameters for the anomaly sources. Computation of the depth of the anomaly sources plays an important part in such an interpretation; however, this subject includes numerous limitations and assumptions, in the sense that one should not consider the process as clear cut.

6.2.3.1. Spectral analysis methods. 2D radially averaged power spectrum techniques were applied to determine the average depths of the magnetic sources in the area of study. This gave the interpreter general information about hidden structures with geographic extension in the area. In the present work, this technique was applied to the RTP magnetic data using Geosoft Oasis Montaj™ V.7. The resulting diagram of the radially averaged power spectrum illustrates the estimated average depth levels to the deep, intermediate, and/or shallow depth segments in the study area (Figure 6.20).

The 2D power spectrum diagram of the magnetic source bodies indicates that the deeper sources have an average height above sea level of about 2,097 m, the intermediate sources are about 2,100 m above sea level, and the shallow or near surface sources are about 2,191 m above sea level. Moreover, the average heights in the selected area of ground ranged from 2,097 m to 2,191 m. These levels in the area of study were taken into consideration during the application of the different types of filter, as mentioned previously.

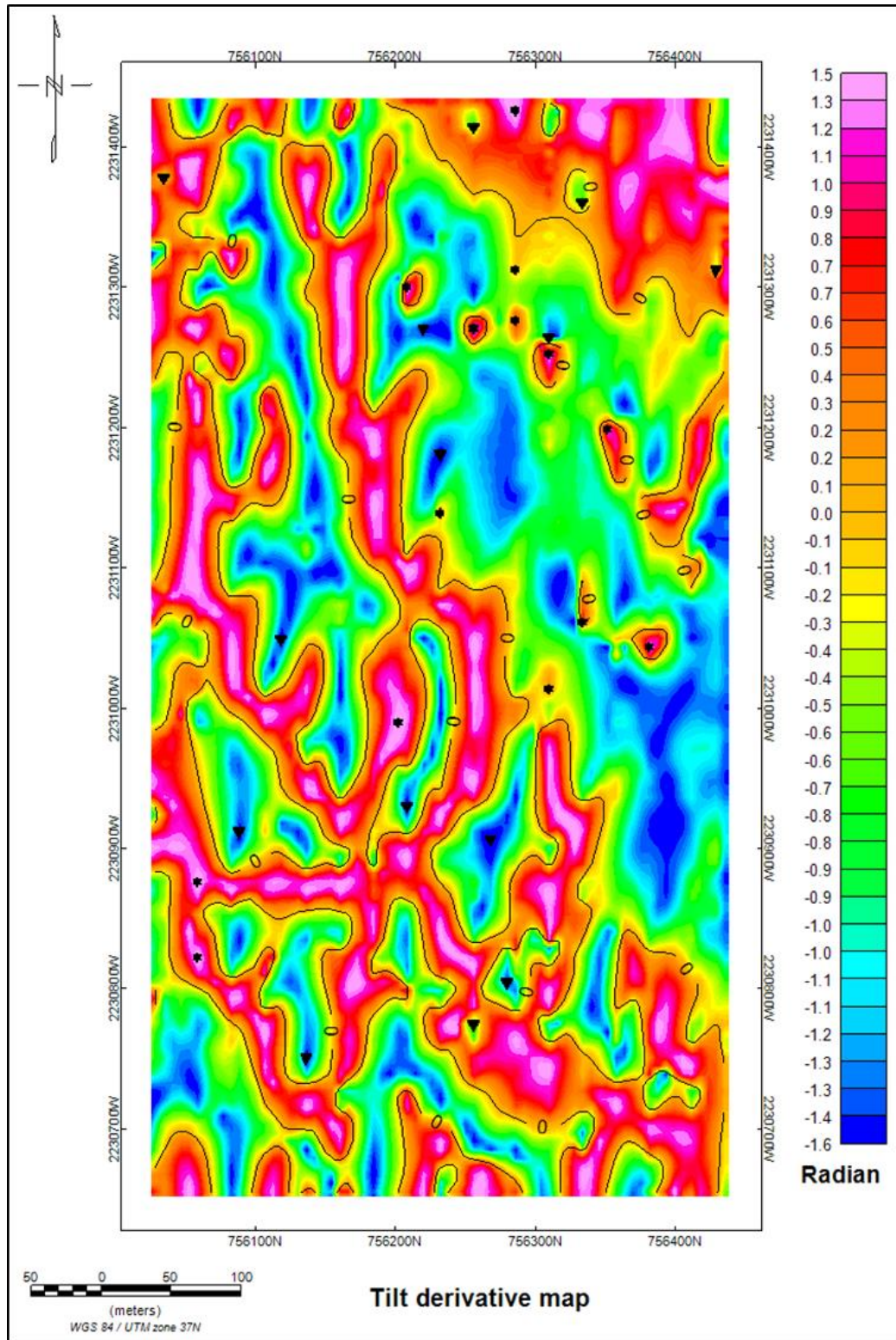


Figure 6.13 Tilt derivative (contour at zero level) map of the Wadi Al Khadra Prospect.

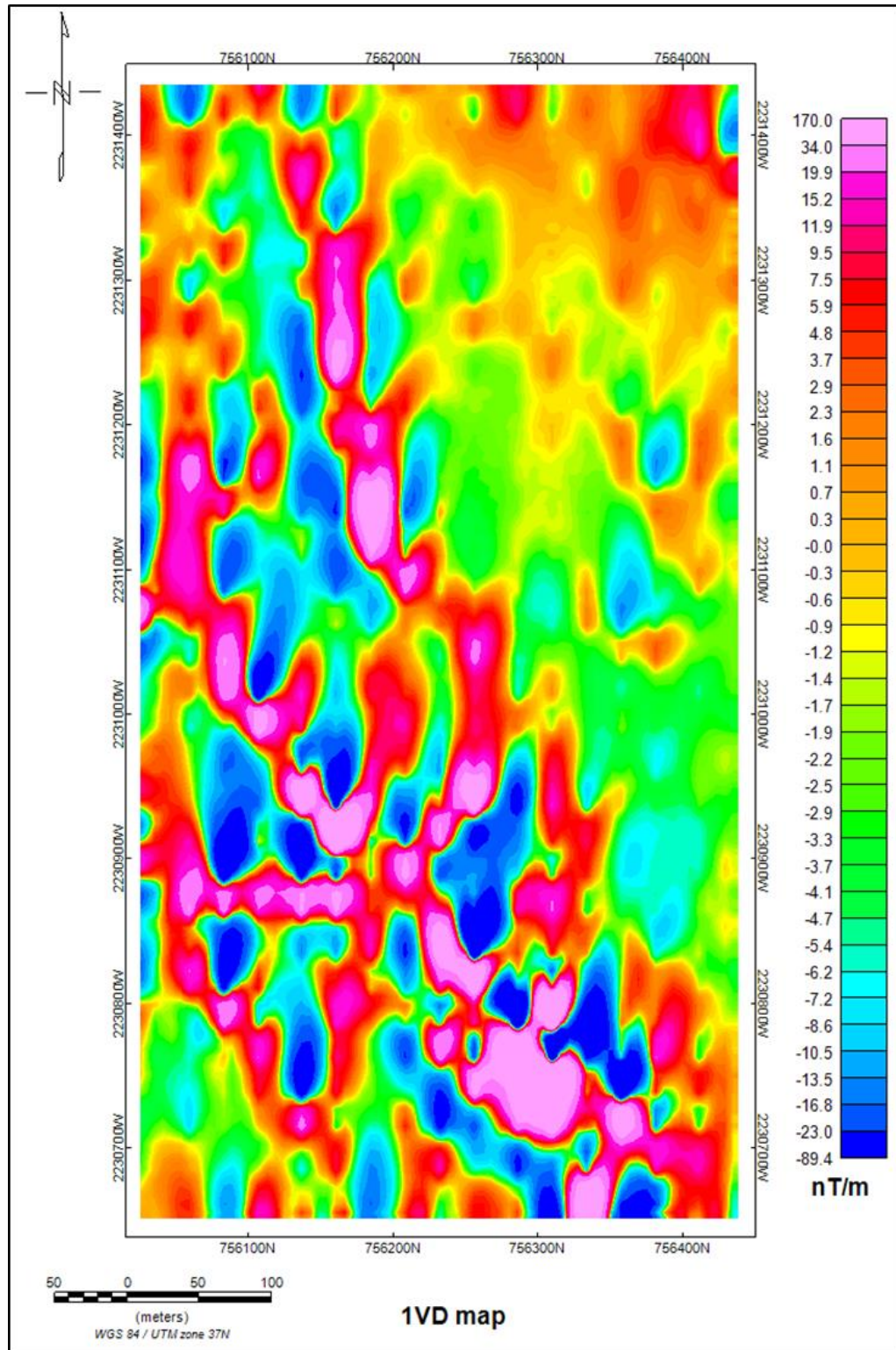


Figure 6.14 First vertical derivative map of Wadi Al Khadra Prospect.

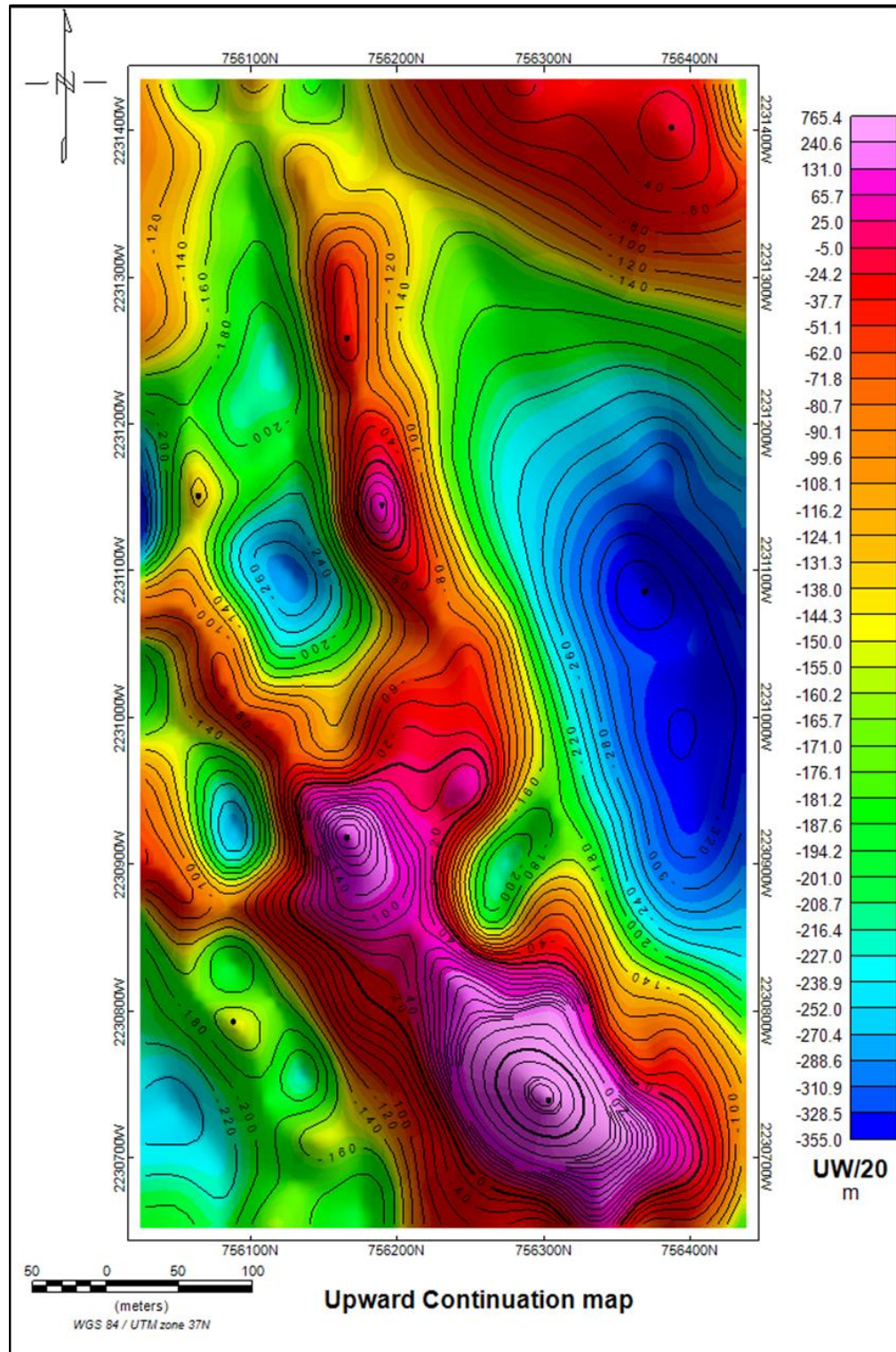


Figure 6.15 Residual anomaly map from Upward continuation.

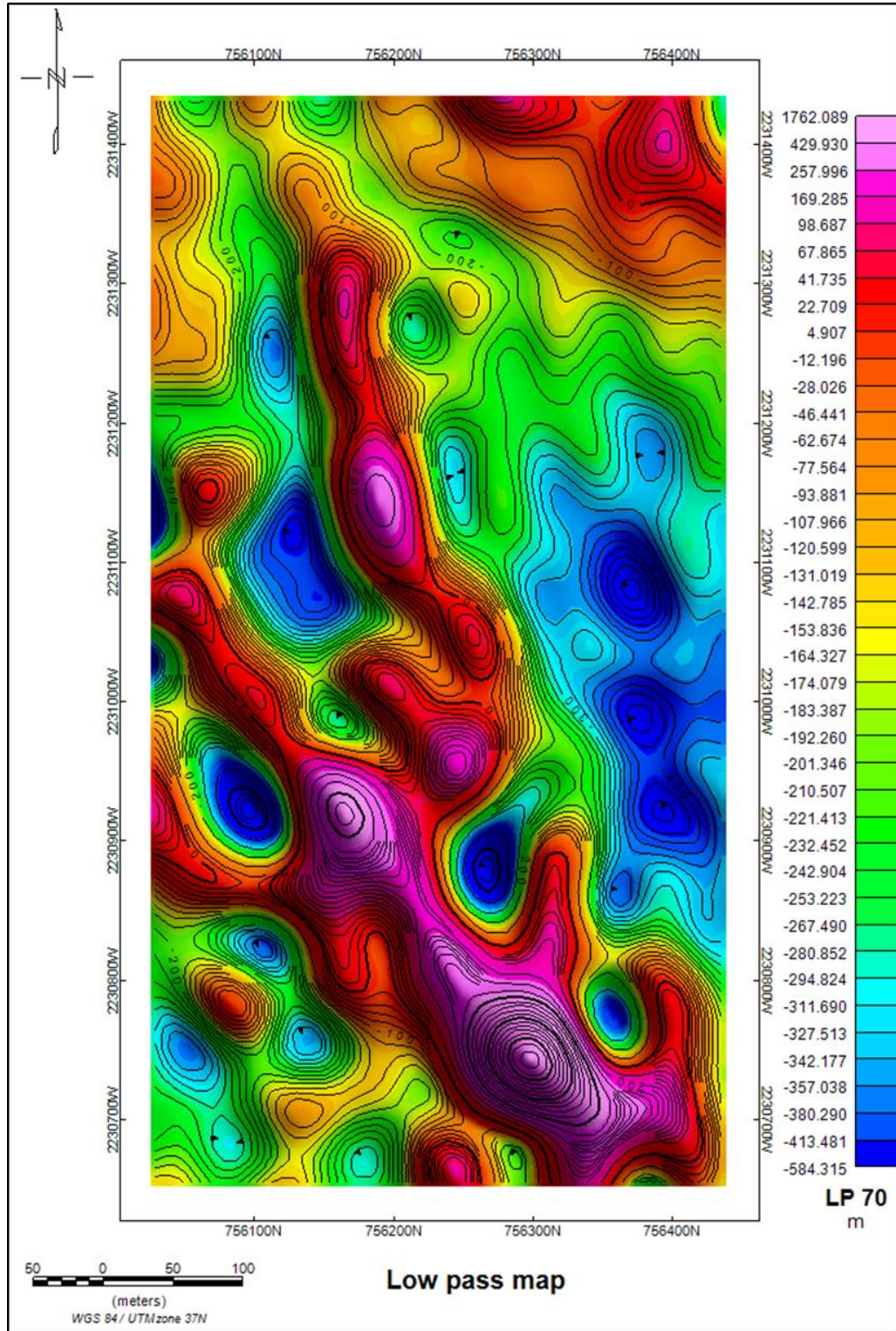


Figure 6.16 Regional anomaly (low pas map).

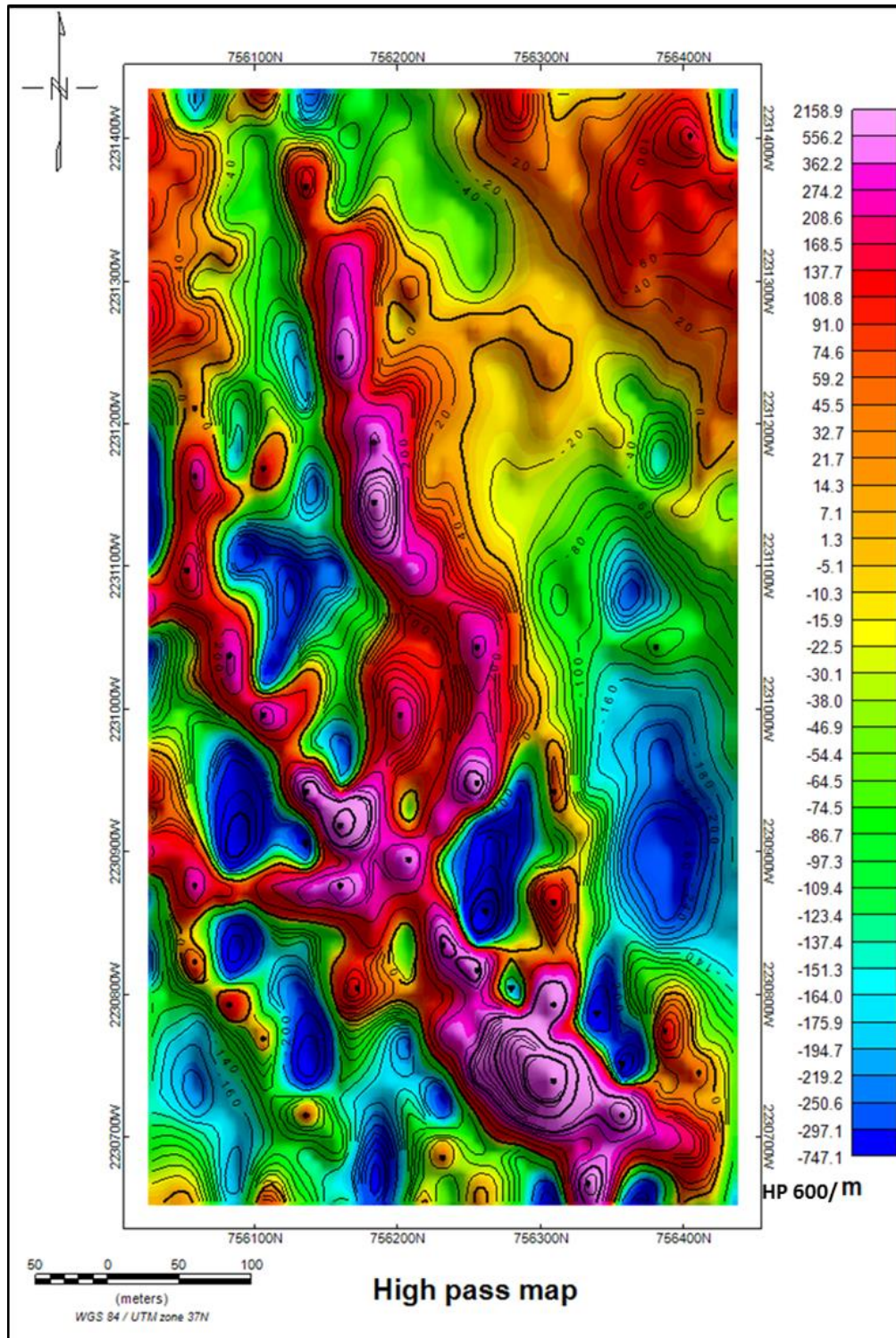


Figure 6.17 Residual anomaly (High pass map).

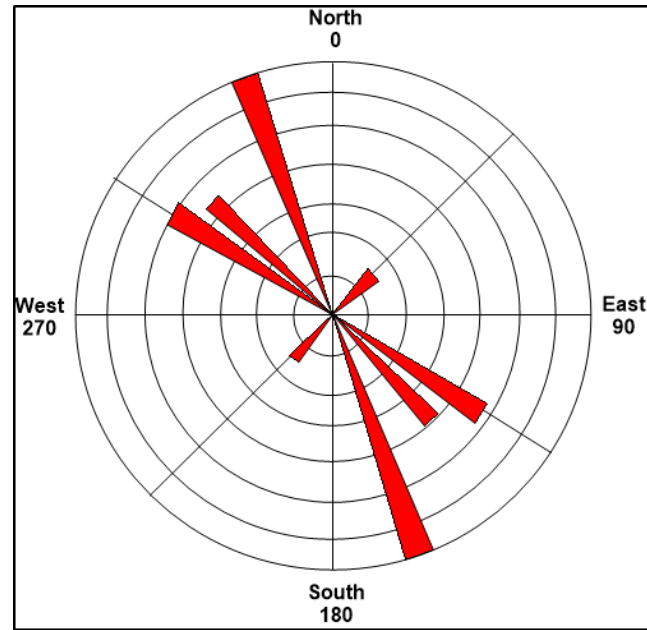


Figure 6.18 Rose diagram shows analyzed and plotted structure trends systems in the study area.

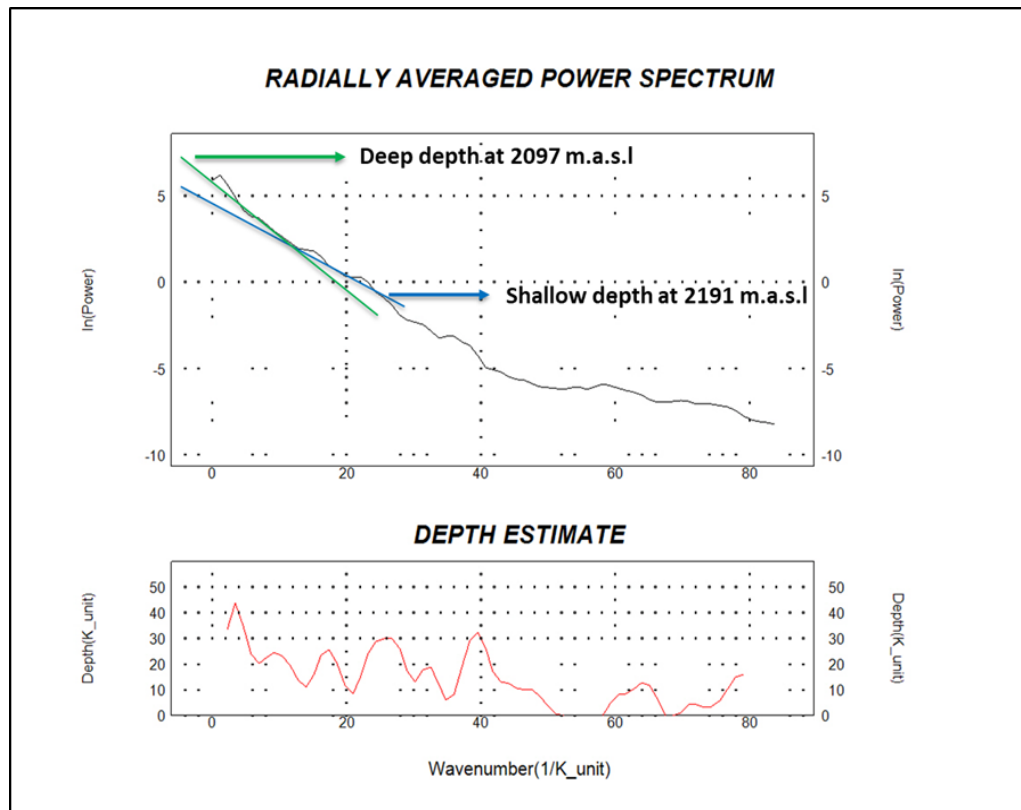


Figure 6.19 2D radially averaged power spectrum for magnetic survey.

6.2.3.2. Analytical signal derivative. The analytical signal derivative map (Figure 6.20) was calculated from the RTP magnetic data of the Wadi Al Khadra using by Geosoft Oasis Montaj™ V.7. The application of the analytical signal derivative is a powerful technique to evaluate buried structures causing significant linear magnetic anomalies, such fault zone and steps. This method was directly applied to get the depth in the two dimensions of the digitized magnetic data for the gradients of x, y, and z (dT/dx , dT/dy and dT/dz).

This map displays several circular and linear maxima closures, which are just over the subsurface magnetic source bodies in the study area. Furthermore, this analytical signal map can be directly used to yield the corresponding depth value for the expected source bodies with respect to the level of observation. Figure 6.21 illustrates the basement relief map for the study area using analytical signal results. It may represent the best-fit subsurface basement configuration. The terrain elevation of the study area ranges between 2,098 and 2,192 m above sea level.

Obviously, there is a noticeable gradient in heights. The lowest portion is in the north and northern west part, whereas the highest portion is in the southern and northern east part of the study area. This gradient in elevation may indicate that there is a gradient in the rock transition stages, perhaps due to the sedimentation of relatively heavy weight metals such as copper. Therefore, there may be a mating or twinning of both minerals in the metagabbro rocks that transformed from gabbro.

6.2.3.3. 3D euler deconvolution method. The Euler deconvolution for the area of study using Geosoft Oasis Montaj™ V.7. was calculated by applying a structural index equal to zero and a window size of 10x10 km. The Euler plots are in Figure 6.22.

They show more or less linear, accurate sigmoid Euler anomalies representing the location, trend, and depth of the sources. The Euler anomalies ranged from 5 to 50 m in depth. The linear clusters of the Euler plot showed that the extension of the expected linear step of distinct magnetic susceptibility has contrasts due to faulting at different depths. These linear Euler anomalies have varied lengths and extensions. A close inspection of the Euler anomaly cluster indicates that the shallower trends are in the central part of the study area extending in the NE and SW directions. On the other hand, the deepest Euler anomaly trends predominated in the remaining parts of the study area. Furthermore, most of the Euler anomaly trends are in the same position, confirming that these normal features have depth extent due rejuvenation along these features that is associated with the eastward and northwestward compression stresses affecting the western parts of the Arabian Peninsula.

6.2.3.4. 2D modeling. 2D modeling techniques of interpretation usually involve fitting geophysical parameters to potential data. Strictly speaking, potential molding could be the inverse solution to a potential problem that cannot be resolved unambiguously. Theoretically, two reversed operations are performed sequentially; the first is a direct modeling process and the second is an inverse modeling process.

The direct modeling process transforms the variations reflected by potential field data in an area of study, as shown by the residual potential anomaly maps, into a convenient subsurface geological setting. However, the inverse modeling process matches the calculated potential effects resulting from the inferred assumed potential models with the observed effects. With more geological control and better data, we can get information about the surface and subsurface magnetic susceptibility variations,

established geological contacts, and structural knowledge; the modeling can be performed with a higher degree of confidence.

The 2D magnetic modeling technique was applied along two long extended magnetic anomaly profiles passing through the major magnetic anomalies in the area of study, running in the north-south and east-west directions. The location of these anomaly profiles is in Figure 6.23. Moreover, two magnetic anomaly profiles were also interpreted for the selected area of ground magnetic survey. Figures 6.24 and 6.25 show the interpreted geologic cross-sections of the individual magnetic anomaly profiles in the area.

A close inspection and correlation between the constructed interpreted cross sections indicated that the minimum and maximum depths of the basement surface were 2,097 and 2,191m, respectively. These results are consistent with the previously constructed terrain elevation map (Figure 6.21). Moreover, the major horst and graben structures are clearly visible along these cross sections.

These structural features are delimited with high angle dipping basement due to normal faulting. On the other hand, the subsurface configuration in the area of ground magnetic survey was established along the interpreted cross sections. The location of these anomaly profiles is shown in Figure 6.23.

It can be seen that the interpreted cross-section along the magnetic anomaly profile A-A', extends for about 856.5m from the north to the south of the study area. It shows the shape and dimension of the northern basin, which show the general eastward dipping of the basement surface (Figure 6.24). The geologic cross section B-B' extends for about 696m in the west to east direction. It shows structurally controlled rock with a

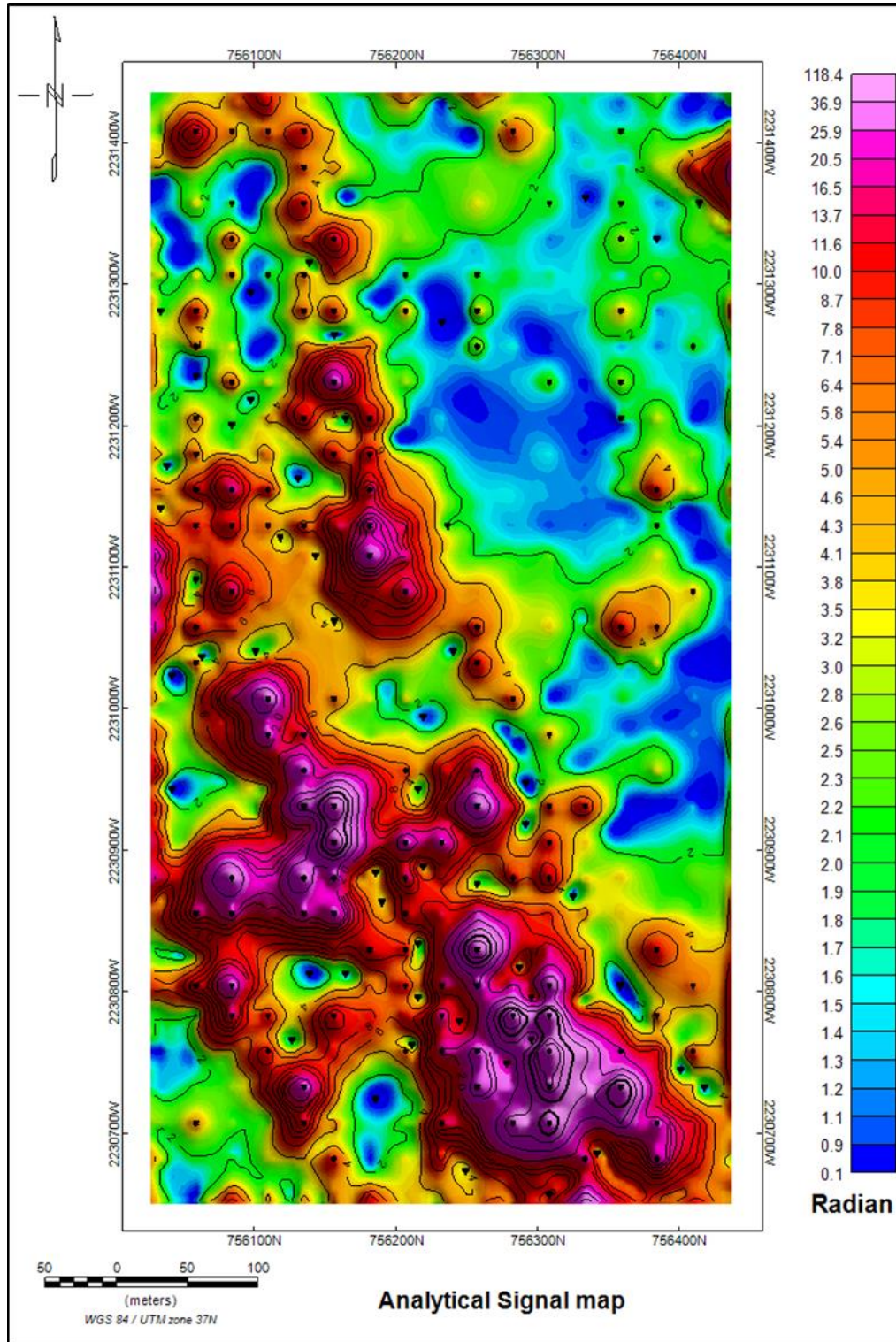


Figure 6.20 Analytical signal map of magnetic survey.

high angle normal faults. Some local structural highs and lows of small dimensions represent the horst and graben structures. These sections indicated that the basement surface has a maximum depth of about 2,097m in the Middle Western part of the study area (6.25).

6.2.3.5. Magnetic susceptibility. First, based on alignment against the field, if $\chi < 0$, this is known as diamagnetism, while the second category is based on an alignment with the magnetic field, $\chi > 0$, known as para-magnetism. The assumed magnetic susceptibility of the underlying basement rocks is taken to range from 0.358 to 0.377 in CGS units; however, it is assumed to be zero for the nonmagnetic sedimentary cover (Figure 6.26). The higher values of magnetic susceptibility are located in the southeastern parts of the study area, elongated to the west and in the middle, whereas the lowest values are located in the middle.

6.3. TIME-DOMAIN ELECTROMAGNETIC RESULTS

A qualitative and quantitative interpretations have been used of TDEM results to better understand for the subsurface structures.

6.3.1. Overview of TDEM Results. A qualitative interpretation of the TEM sounding data from Wadi Al Khadra prospect was carried out to illustrate the general mineralization picture. It also demarcated the resistivity change behavior within the probed formations. This complemented the analysis of the results through the construction and description of several conductivity contour maps for several specified loop values. The interpreted resistivity data are represented as maps. The processed data included response profiles. The profiles included graphs of measured voltage at preferred

decay times at all the stations in the decay. Also, the processed data included transient decay, which can be displayed on a graph of voltage (in mV) vs. time of decay (in m.s.).

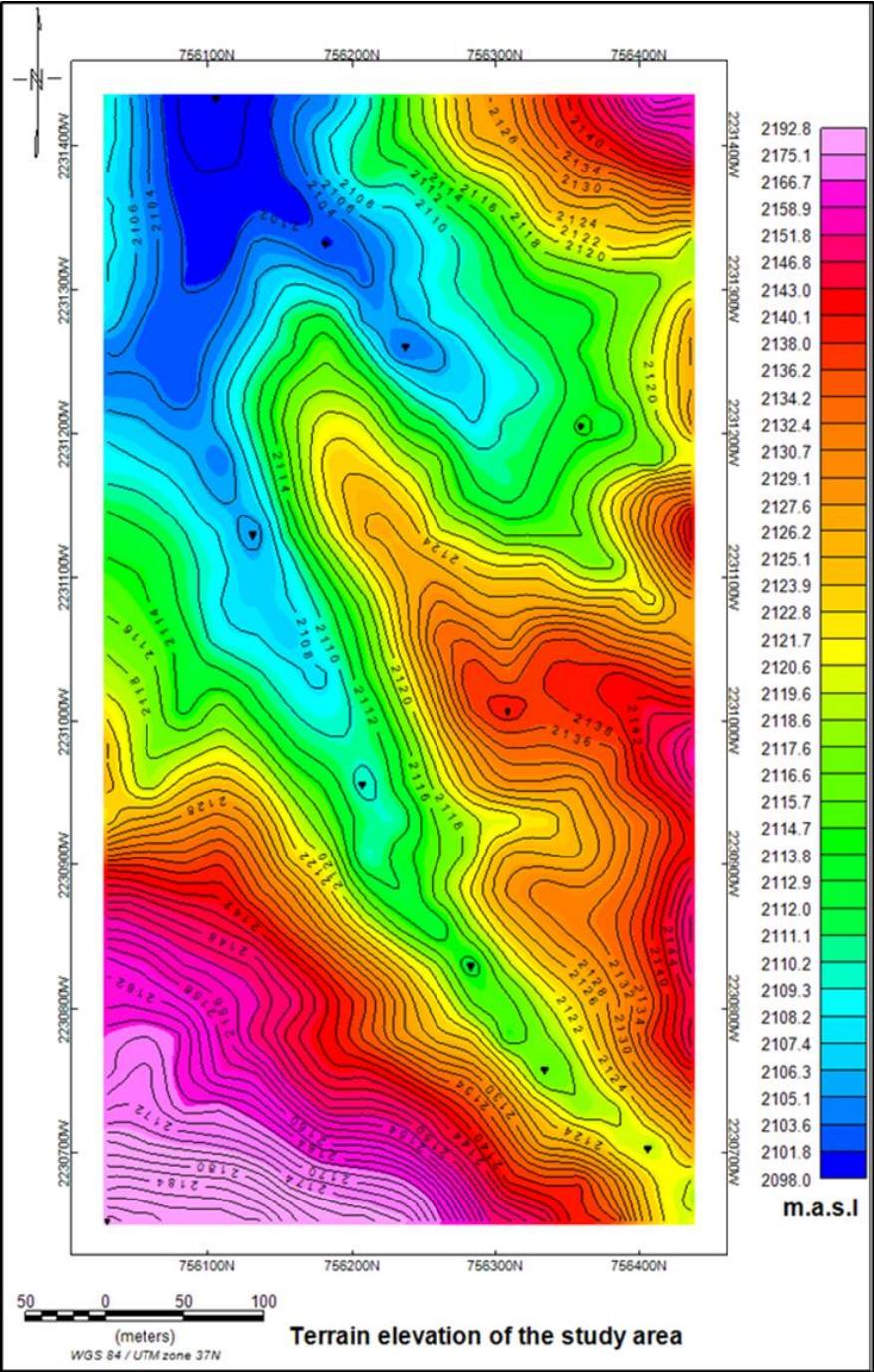


Figure 6.21 The elevation map of the study area.

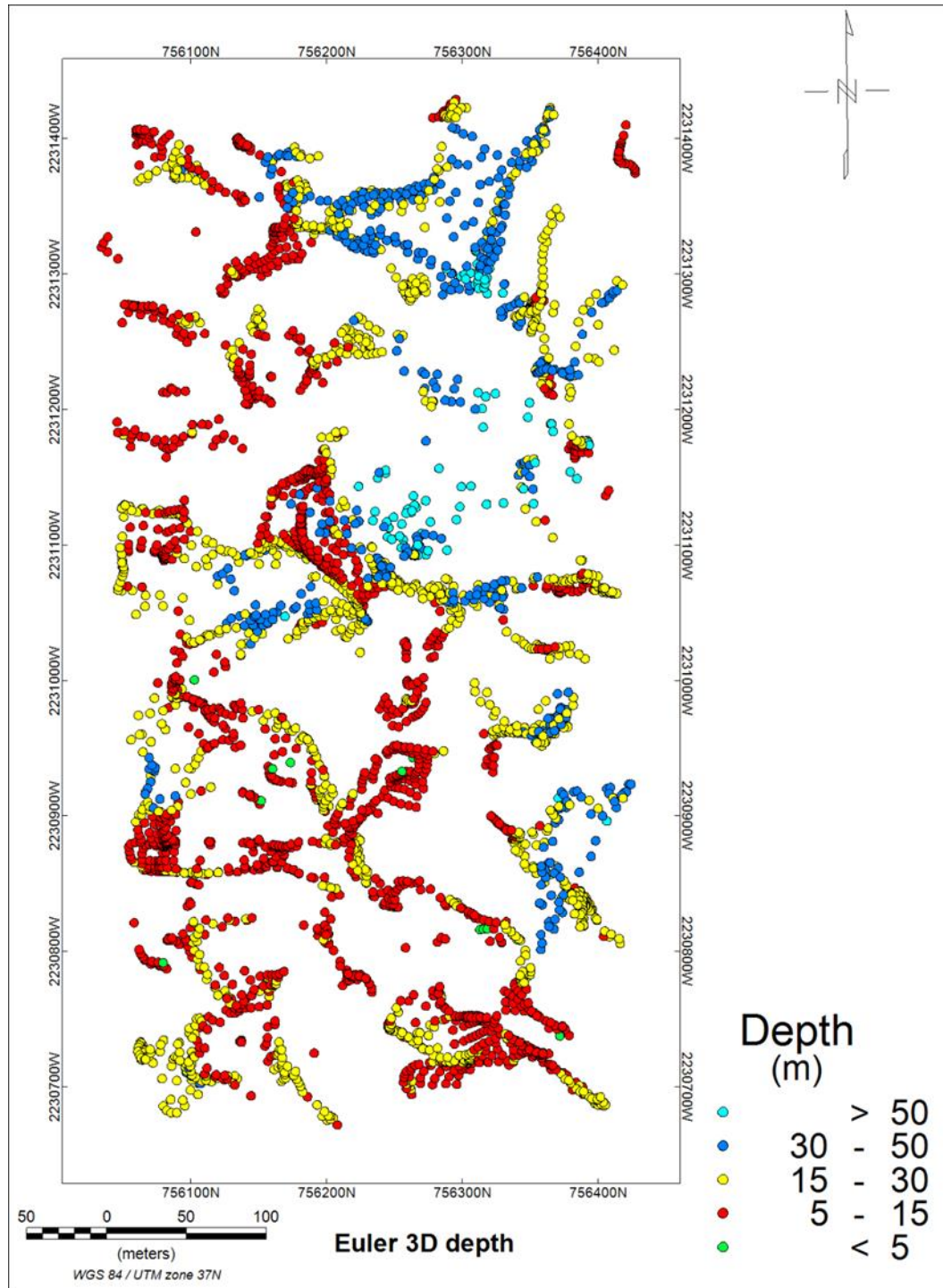


Figure 6.22 Map of Euler Deconvolution.

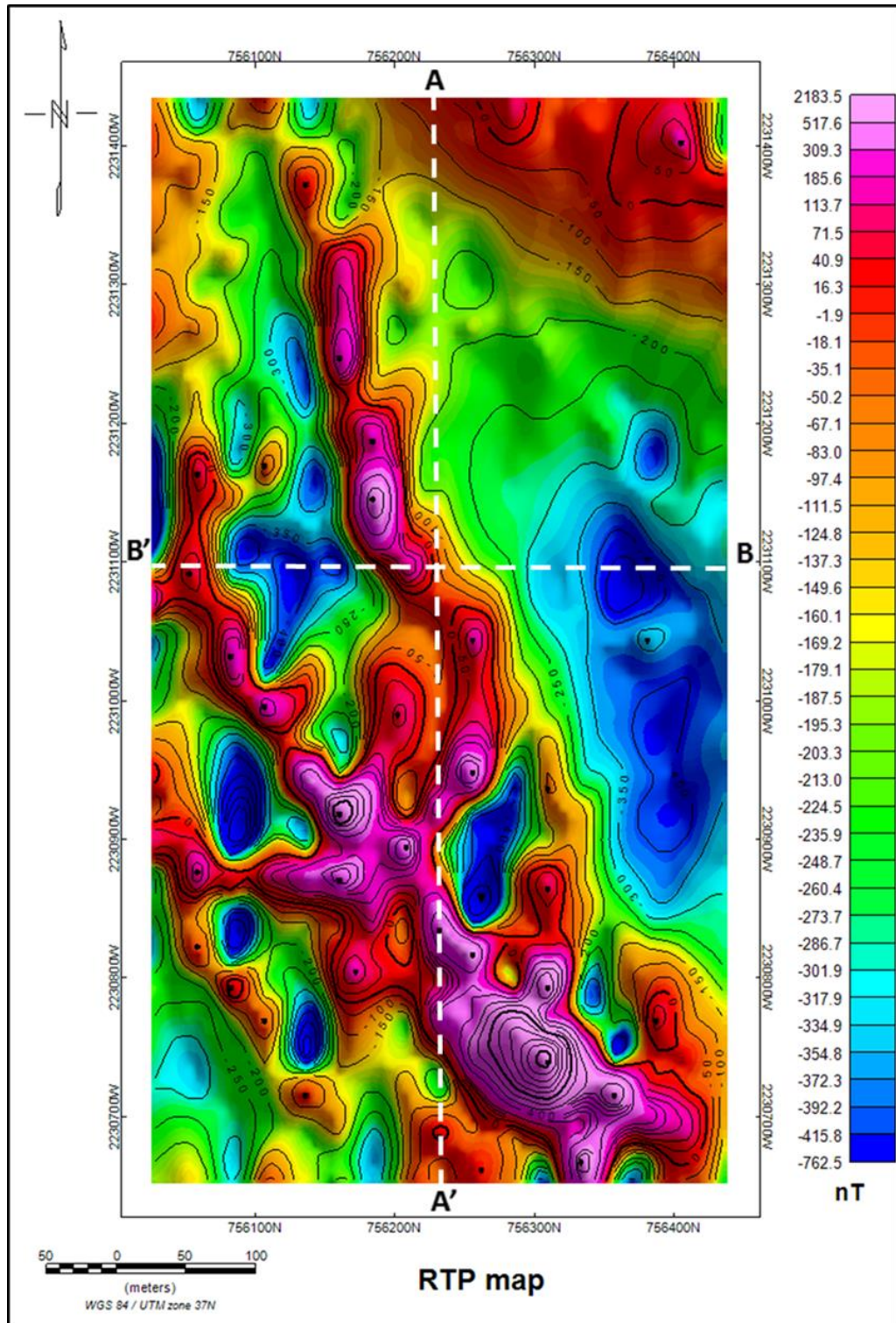


Figure 6.23 RTP of magnetic anomaly map, showing location of the selected profiles for 2D modeling.

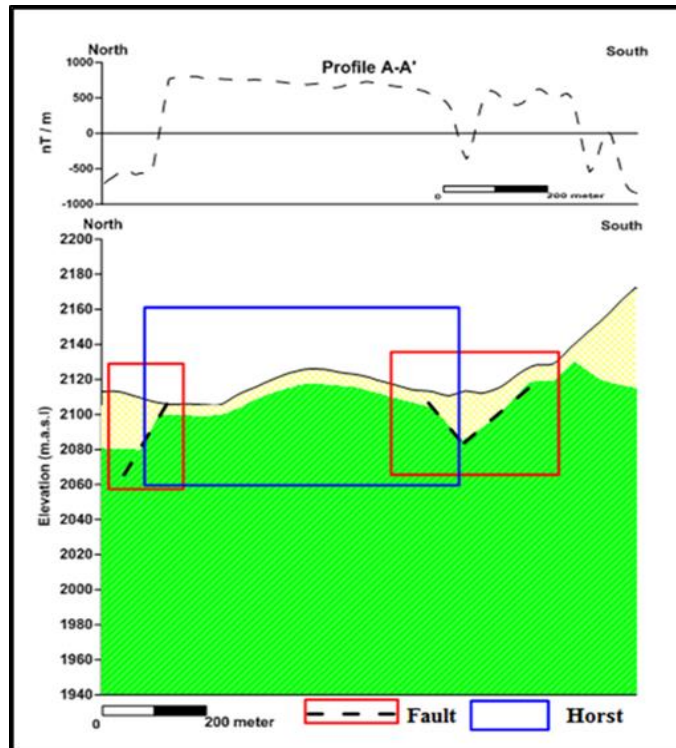


Figure 6.24 Two-dimension magnetic model along the profile A-A'

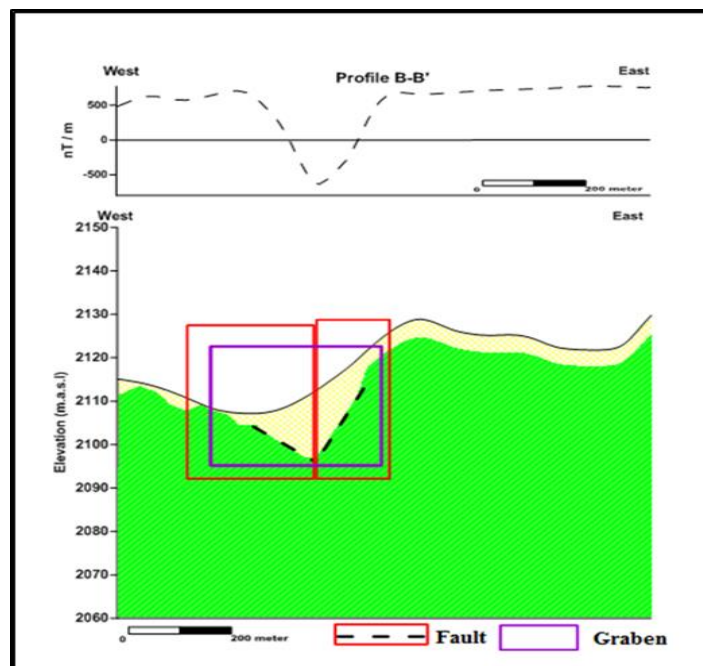


Figure 6.25 Two-dimension magnetic model along the profile B-B'

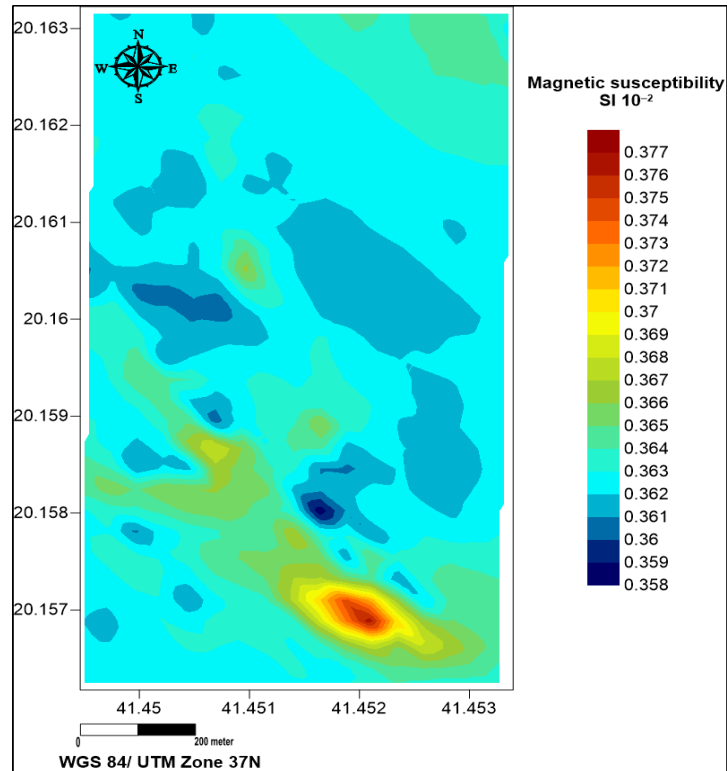


Figure 6.26 Map of Magnetic Susceptibility in the study area.

Last, the processed data included response contours, which were the result of plotting response profile data in map form. Ideally, there are different stages of interpretations, just like the types of data systems and data plots. There were two stages of interpretation:

1. The first stage involved designating the possible subsurface target. The designation was based on the size, shape, and location of any deviation evident on maps and profiles of pertinent parameters.
2. The second stage was based on the quantitative approach. It was used to ascertain the quality of the conductor by focusing on the time constants, which are obtained from decay plots of the field intensity.

Different applications are important to various types of display parameters. The final step of the interpretation process is quantitative interpretation. In this case, quantitative interpretation of TDEM sounding involved determining the thickness and actual resistivity of varied formations. The quantitative interpretation of the resistivity and the TEM data for the present study included:

- Automatic interpretation of the electromagnetic sounding curves with Zond EM software (2017);
- Illustration and analysis of the geoelectrical cross-section, which reflects the lithological implications of the studied sections; and
- Preparing isopach maps of the layers and their depths.

6.3.2. Two Dimension Sounding (Resistivity Profiles). If the location of each sounding is known, it is possible to draw profiles to illustrate the distribution of resistivity values in the study area. Due to the large and uneven resistance values, a standard logarithm was used to express them. Three measurements were carried out at each station with voltages of 0.1, 1 and 10 volts, and the measurements were repeated 1,000 times to obtain high-quality data representing different depths. The average of these measurements was taken and processed to develop a one-dimensional model showing the distribution of electrical resistance with depth at each station. Finally, connecting these stations to obtain a 2D sector shows the change of electrical resistance in the horizontal direction along the profile (Figures 6.27-6.33).

With observation of electrical values, it is possible to locate low resistivity values, which are concentrated in some surface areas and some deep places. The shallow parts appear in soundings 575, 650, and 725, with horizontal extent of about 100 m, while the

deeper body starts to appear in the other profiles. This body looks like a tube starting from the east in the southern sounding (350) at heights from 2,080 to 2,060 m above sea level with a width of about 9 m, and it extends whenever it goes north in sounding 375; the diameter of this body and its width increase. The range in height is between 2,090 and 2045 m above sea level, and it reaches a maximum in Profile 400, with height ranges from 2,040 to 2,100 m above sea level. It disappears in the next two soundings (575, 650) to appear again in sounding 750 with a little bend to the west in the last sounding (1025).

The depth of this body starts from 75 m in sounding No. 350 and reaches to 25 m in sounding No. 725. Both shallow and deep bodies have resistivity values ranging from 0.01 to $1.2 \log^{10} \Omega\text{m}$; there may be a mineral concentration of copper and nickel here. The high values may refer to the hostel basement rock.

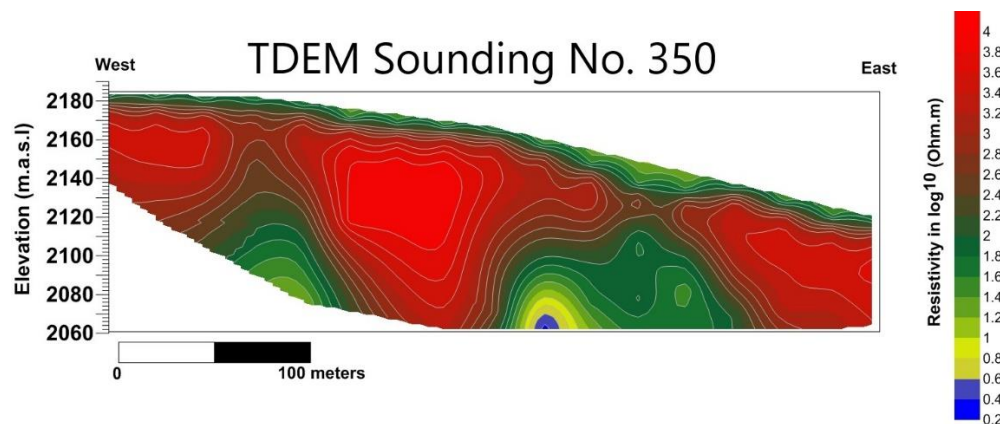


Figure 6.27 TDEM sounding No. 350 in the Wadi Al Khadra prospect survey.

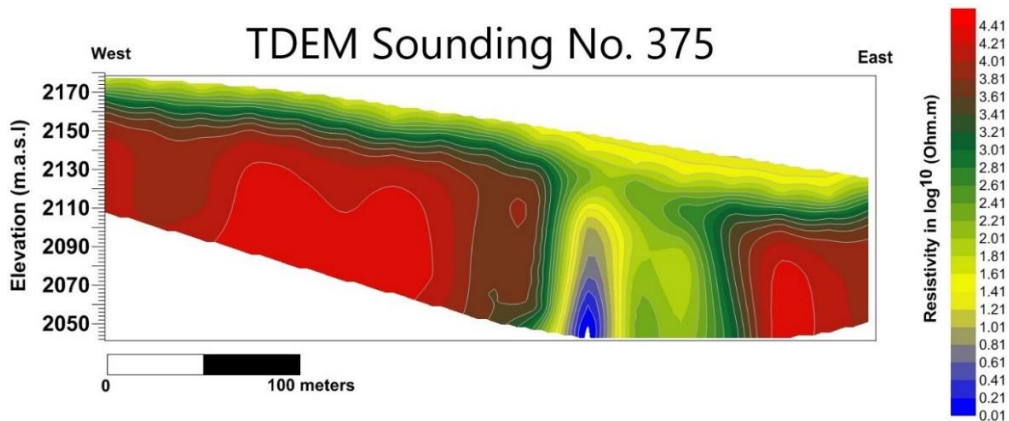


Figure 6.28 TDEM sounding No. 375 in the Wadi Al Khadra prospect survey.

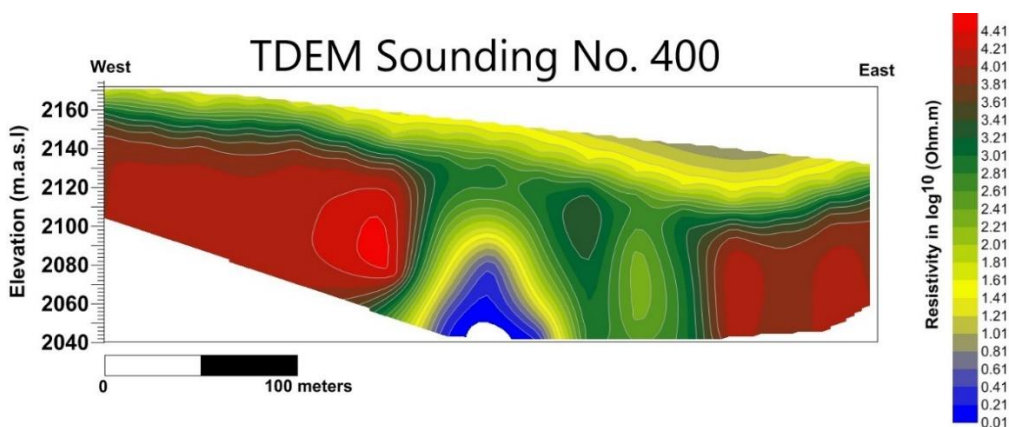


Figure 6.29 TDEM sounding No. 400 in the Wadi Al Khadra prospect survey.

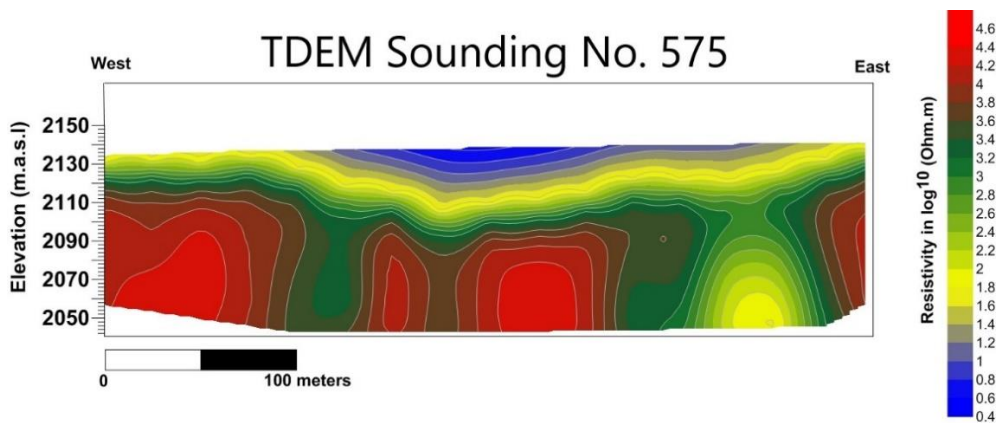


Figure 6.30 TDEM sounding No. 575 in the Wadi Al Khadra prospect survey.

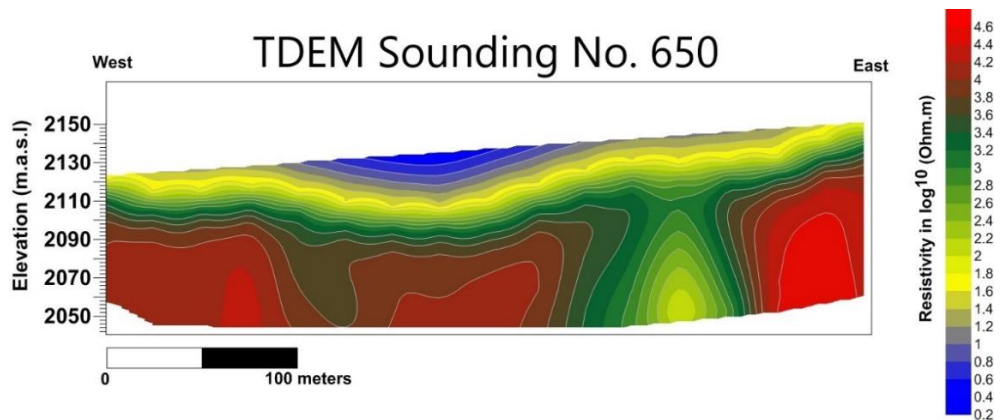


Figure 6.31 TDEM sounding No. 650 in the Wadi Al Khadra prospect survey.

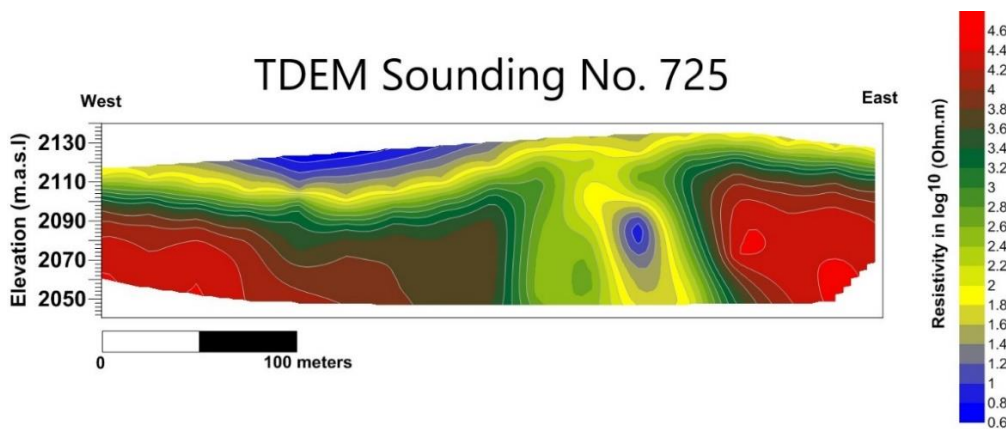


Figure 6.32 TDEM sounding No. 725 in the Wadi Al Khadra prospect survey.

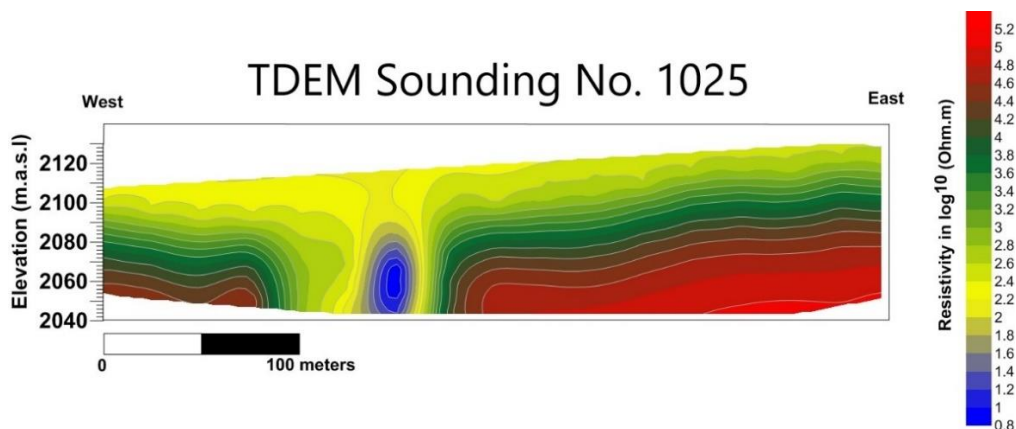


Figure 6.33 TDEM sounding No. 1025 in the Wadi Al Khadra prospect survey.

6.3.3. Two Dimension of Electrical Resistivities Change with the Depth. To illustrate the distribution of electrical resistivity values with the change in the depth, five maps were created in different depths. It turns out that there is a body with a noticeably low electrical resistivity value. This body clearly appears in the three top maps at different heights from 2,040 to 2,115 m above sea level; it then disappears and starts to come into view again at 2,140 m above sea level (Figure 6.34).

The surface layers in the study area exhibited high to middle resistivity values that may be attributable to the nature of the weathered basement rocks in such arid regions covered with transported sediments; such high values may reflect mixed gravel and sand lithology (Figure 6.34a).

There was very low resistivity in two parts: the first was in the surface layers with an extended width of about 100 m in the middle to western middle parts. The second was in the deepest part: this part appears as a connected body, it appears at a depth of about 25 m in the north, it disappears in the middle part, and it reappears in the south. Both parts could be accumulations of copper and nickel.

6.3.4. 3D Dimension. Five 3D maps were created to facilitate the identification of bodies with similar electrical resistivity values (Figure 6.35). Every map shows the distribution of electrical resistivity ranges (0-1 Ωm , 1-2 Ωm , 2-3 Ωm , 3-4 Ωm , and 4-5 Ωm).

The maps show a general increase in resistivity towards the west, which may be due to an increase in the thickness of the probed formations, since the eastern part is localized in a topographic high area.

These maps were prepared by contouring the apparent resistivity values for a certain frequency of all TEM stations, which are distributed throughout the study area.

Construction of these maps assisted the interpretation as follows:

- It showed the different resistivity layers affected by the artificial electromagnetic waves traveling through the ground.
- It detected the basement layers and the locations of mineral concentrations.
- It illustrated the lateral variations along certain horizontal planes.
- It explained the probable regions of the mineral accumulations in the study area.
- It gave an exact geological and mineralogical picture of the study area.

There was a noticeable gradient in the distribution of resistance values in the study area, despite the convergence of some values. This convergence shows the homogeneity of the layers in terms of origin.

The resemblances between anomalies and the drifts of the contour lines for most of the TDEM maps gave an image of the electrical homogeneity of the area. Abnormal changes in resistivity values are probably due to concentrations of copper and nickel, especially since the resistivity values of these anomalies are very small compared to the surrounding values.

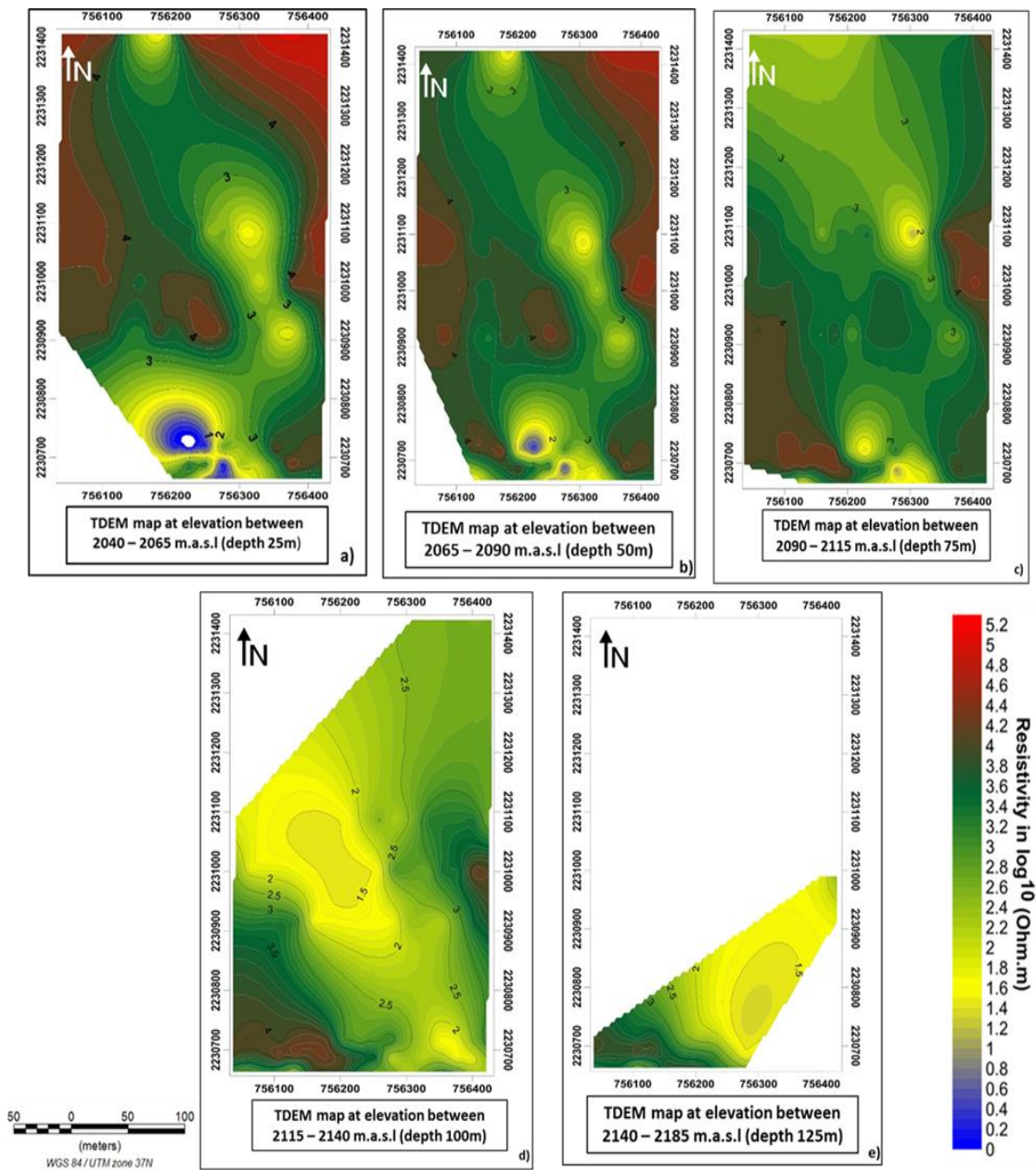


Figure 6.34 2D TDEM sounding maps in different depth level shows the distribution of resistivity values.

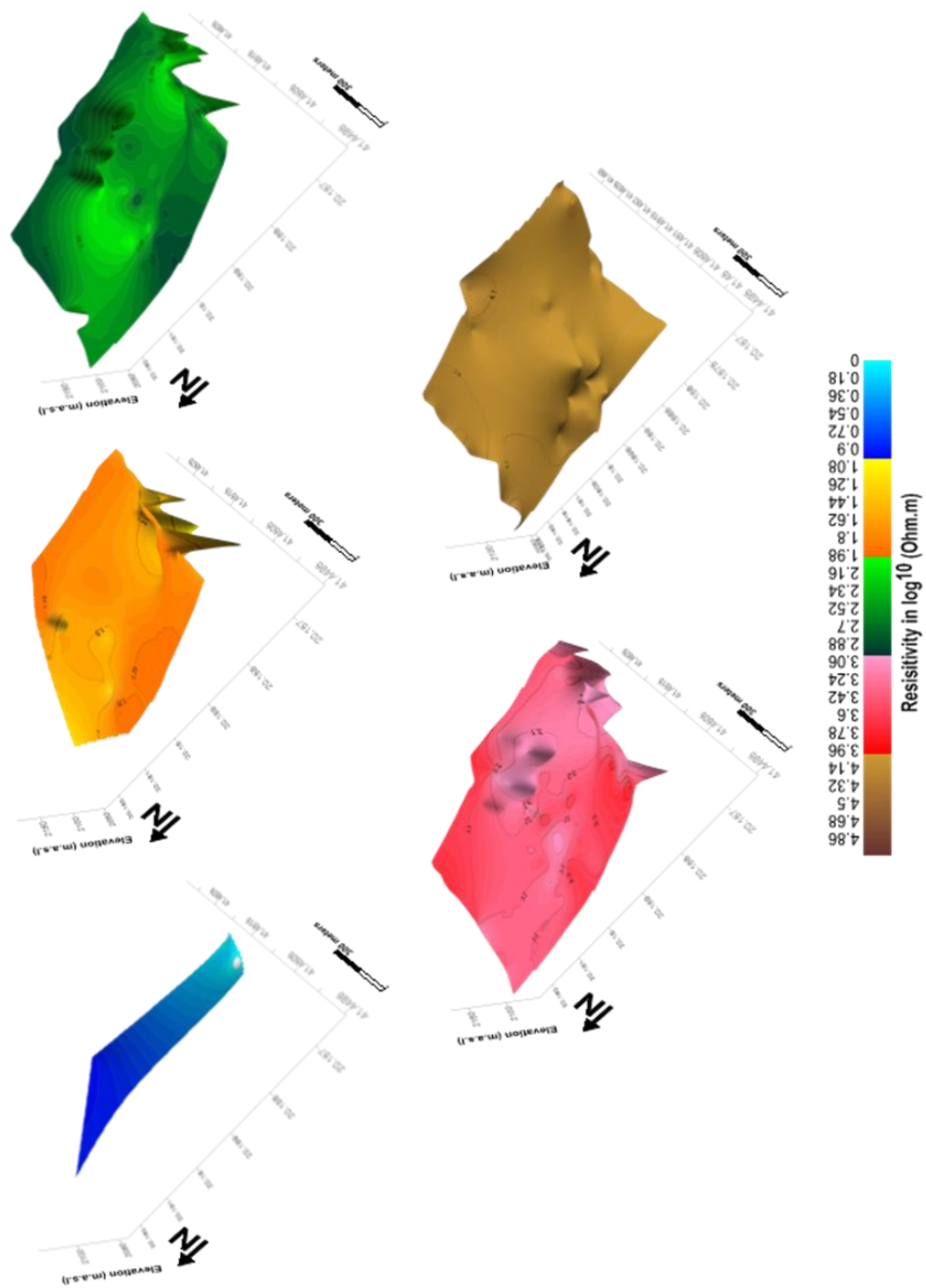


Figure 6.35 3D TDEM sounding maps in different depth shows the distribution of resistivity values.

7. DISCUSSION, CONCLUSION, AND RECOMMENDATIONS

This section focuses on the interpretation of the integrated data set as it pertains to the nine specific objectives presented in the introductory section.

7.1. GEOPHYSICAL METHODS CAN BE USED TO MAP THE DISTRIBUTION OF METALLIC MINERALIZATION

The areas characterized by negative SP values in Figure 7.1 are interpreted as mineralized zones that consist, in part, of nickel, copper, magnetite, and other metallic minerals. SP is a shallow tool with a maximum depth of approximately 40 m, and it can be used to map areas where oxidation and reduction reactions are occurring. Areas in Figure 7.1 characterized by SP values more negative than -30 mV are interpreted as being comprised, in part, of higher concentrations of conductive metals.

The magnetic method is used to image the subsurface to depths greater than those available with the SP tool. The magnetic tool is used to map the presence of nickel, magnetite, and other magnetically susceptible minerals. In Figure 7.2, areas characterized by positive high magnetic intensity (intensities greater than 16.3 nT) are interpreted as higher concentrations of magnetically susceptible minerals.

The TDEM tool, as applied to the study area, was used to generate a suite of 2D resistivity profiles of the subsurface. These 2D profiles were used to generate a suite of plan view maps, each of which depicts the resistivity of the subsurface at specific elevations. Figure 7.3 presents a map showing the resistivity of the subsurface at a depth of 25 m. Areas of low resistivity (values lower than 1.6 Ωm) are interpreted as areas with

higher concentrations of metallic mineralization. In Figure 7.4, SP, magnetic, and TDEM maps show the distribution of metallic minerals in the study area.

7.2. GEOPHYSICAL METHODS CAN BE USED TO MAP THE ORIENTATION FAULTS

The magnetic, SP, and TDEM maps can be used to infer the orientations of faults (Figure 7.5). These interpreted faults, superposed on the suite of maps presented as Figure 7.6, generally trend NW-SE, essentially parallel to the (Rea sea trend). The assumption is that mineralization occurred along and in proximity to pre-existing faults. Geologic mapping in the area verified the legitimacy of some, but not all, of the fault interpretations (Figure 7.7).

7.3. BOREHOLE AND SURFICIAL GEOLOGICAL DATA TO VERIFY THE REASONABLENESS OF THE SP, MAGNETIC, AND TDEM INTERPRETATIONS SIGNATURES

The mineralized zones of the Wadi Al Khadra prospect have been mapped using geological, geochemical and geophysical methods. Based on the sulfide content and mineral associations, the mineralized zone is a volcanogenic massive sulfide type, which has been highly altered and metamorphosed (SGS, 2013).

The observations seem to indicate that mineralization is related to local structural zones, that it originated in mafic volcanic rocks, and that mineralization occurs as discrete disseminations along bedding and/or foliation. Oxidized outcrops are found along these faults, but they are probably directly associated with mafic volcanic rocks (SGS, 2013).

According to the geochemical analysis of surficial samples data of Ni and Cu, there are three prominent concentrations of mineralization in the study area (Figure 7.8). One zone is in the southern part of the area; the other two locations are in the central part of the study area. It is worth noting that other metallic minerals (magnetite, pyrite, pyrrhotite, and chalcopyrite) are present in the study area; however, their concentrations do not rise to industrial or extraction significance. Figure 7.9 shows the interpreted distribution of nickel and copper concentrations anomalies in the study area based on an integrated assessment of the SP, Magnetic, and TDEM.

With respect to SP results, the high-amplitude negative anomalies are almost certainly generated by the oxidization/reduction of metallic mineralization in the shallow subsurface, which means the SP anomalies in the study area are generated by nickel, copper, and associated metallic minerals, including magnetite. The depths to which the measurement reached varied along each SP line and from SP line to SP line. Line SP 425 (Figure 7.10) is in the southern part of the study area. Elevations along the profile vary between 2,120 and 2,170 m above sea level. The SP values along this line range from 50 mV to -120 mV. Based on the assay results and the drill hole data, oxidation was observed at depths greater than 8.60 m. Relatively high concentrations of copper and nickel were present in drill hole cores. In addition, magnetite, hematite, small amounts of limonite, and traces of disseminated pyrite, pyrrhotite, and chalcopyrite were identified.

The magnetic anomalies are generated by magnetically susceptible minerals in the subsurface (e.g., magnetite, nickel, iron). The high-amplitude positive magnetic anomalies identified in the study area were interpreted as being generated by nickel and associated magnetite. Magnetic Line 425 (Figure 7.11) is located along the same of the

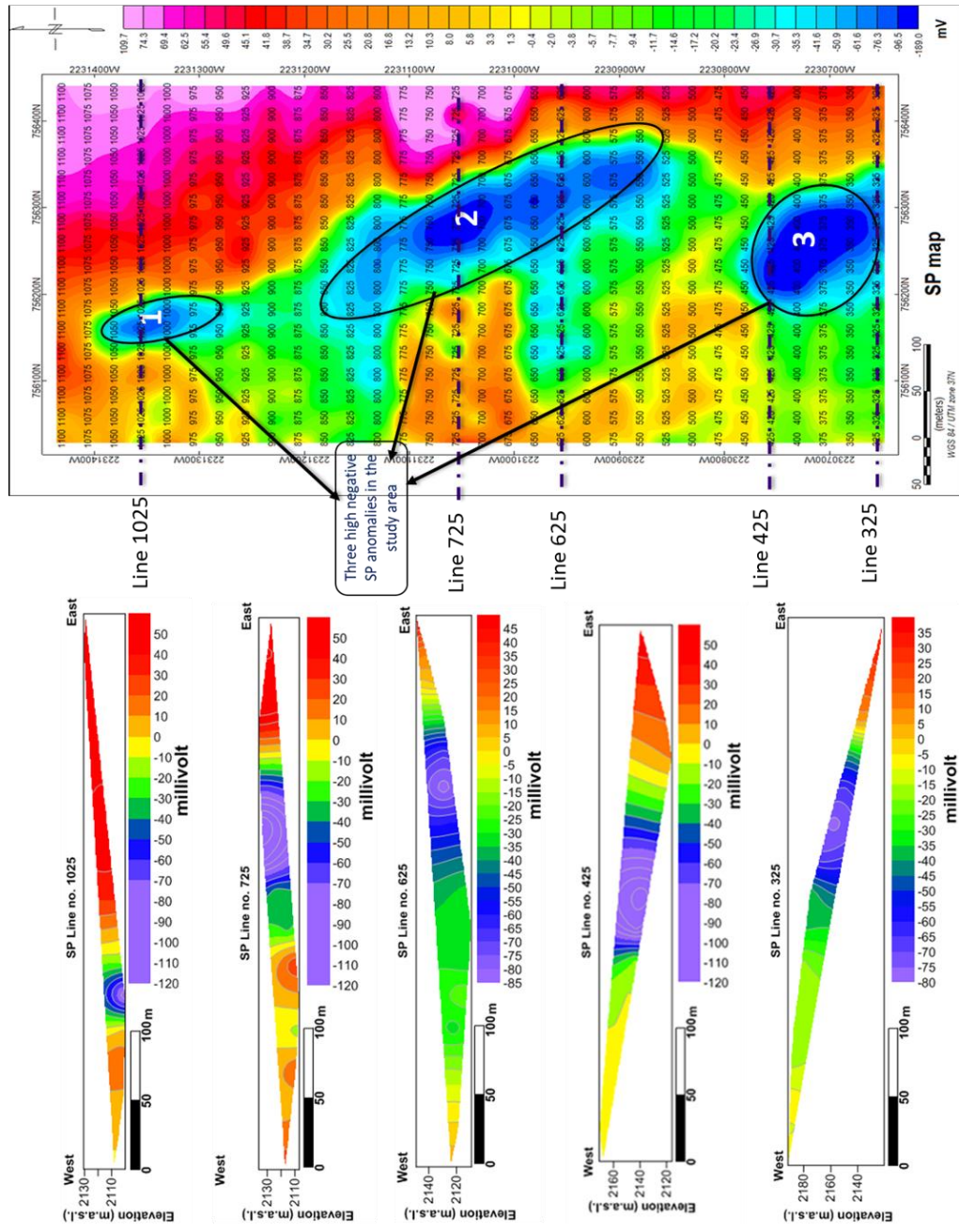


Figure 7.1 SP map showing the distribution of negative SP anomalies of the study area.

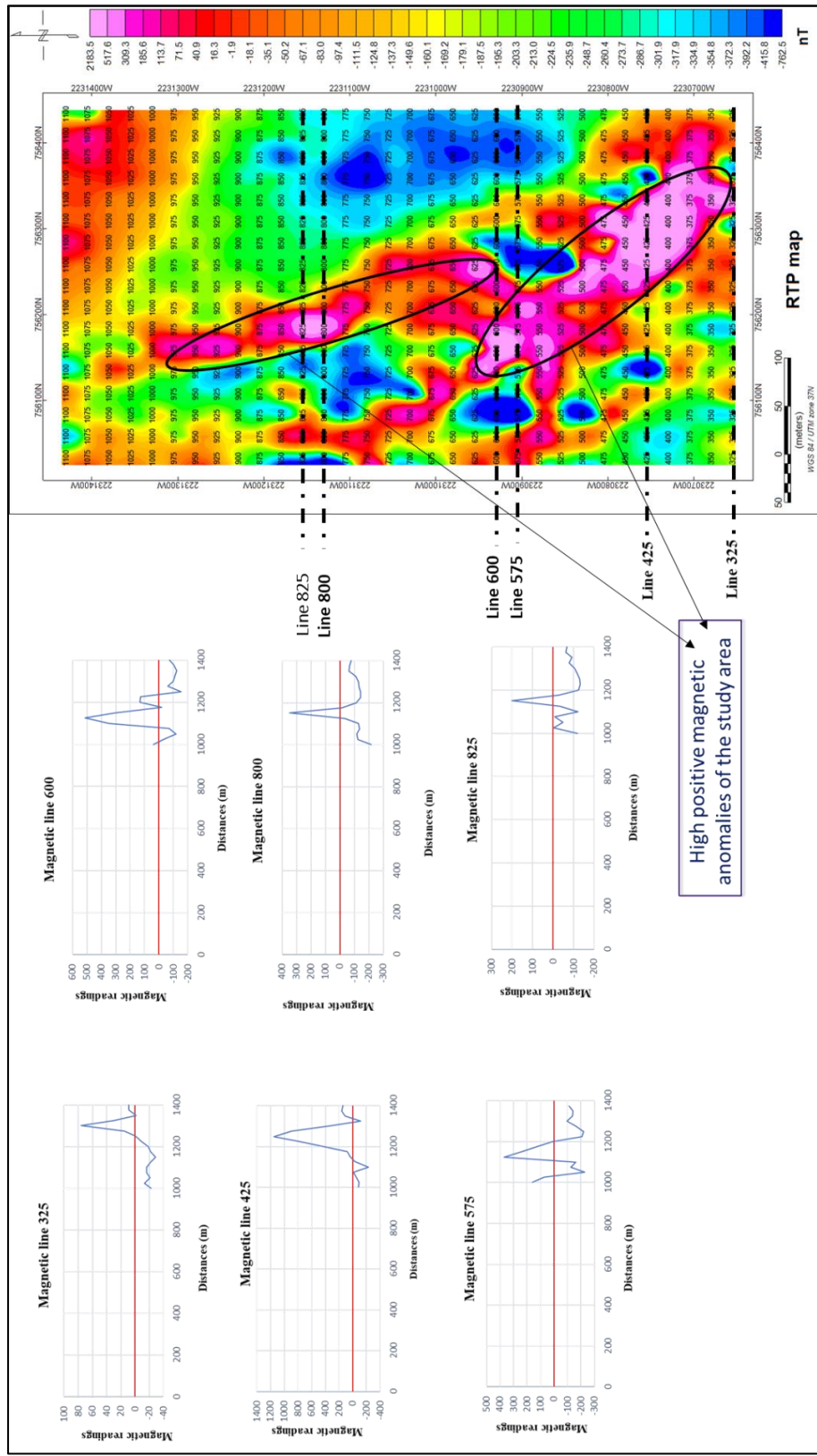


Figure 7.2 RTP map showing the distribution of positive magnetic anomalies of the study area.

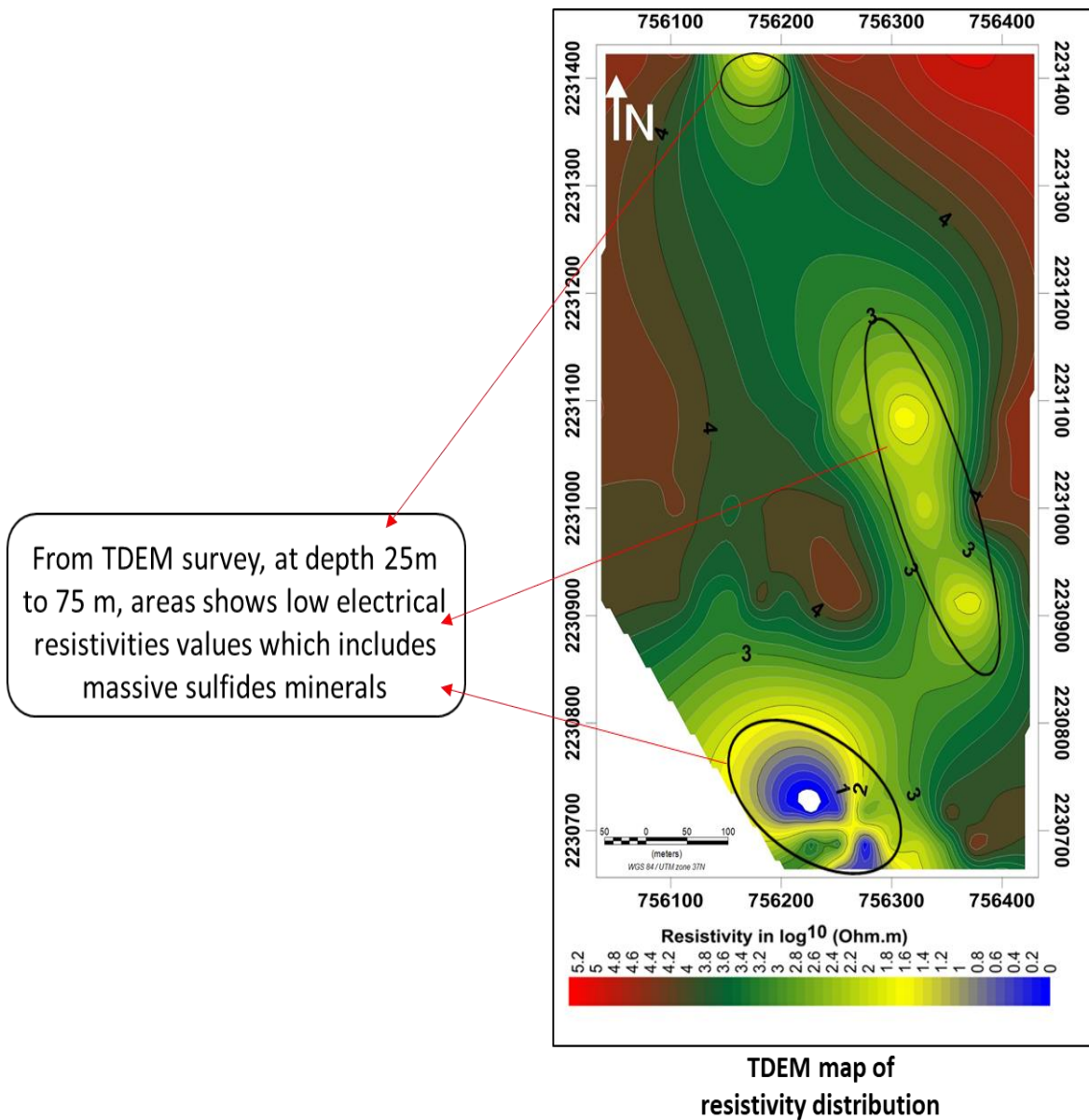


Figure 7.3 TDEM map shows a distribution at depth between 25m – 75m.

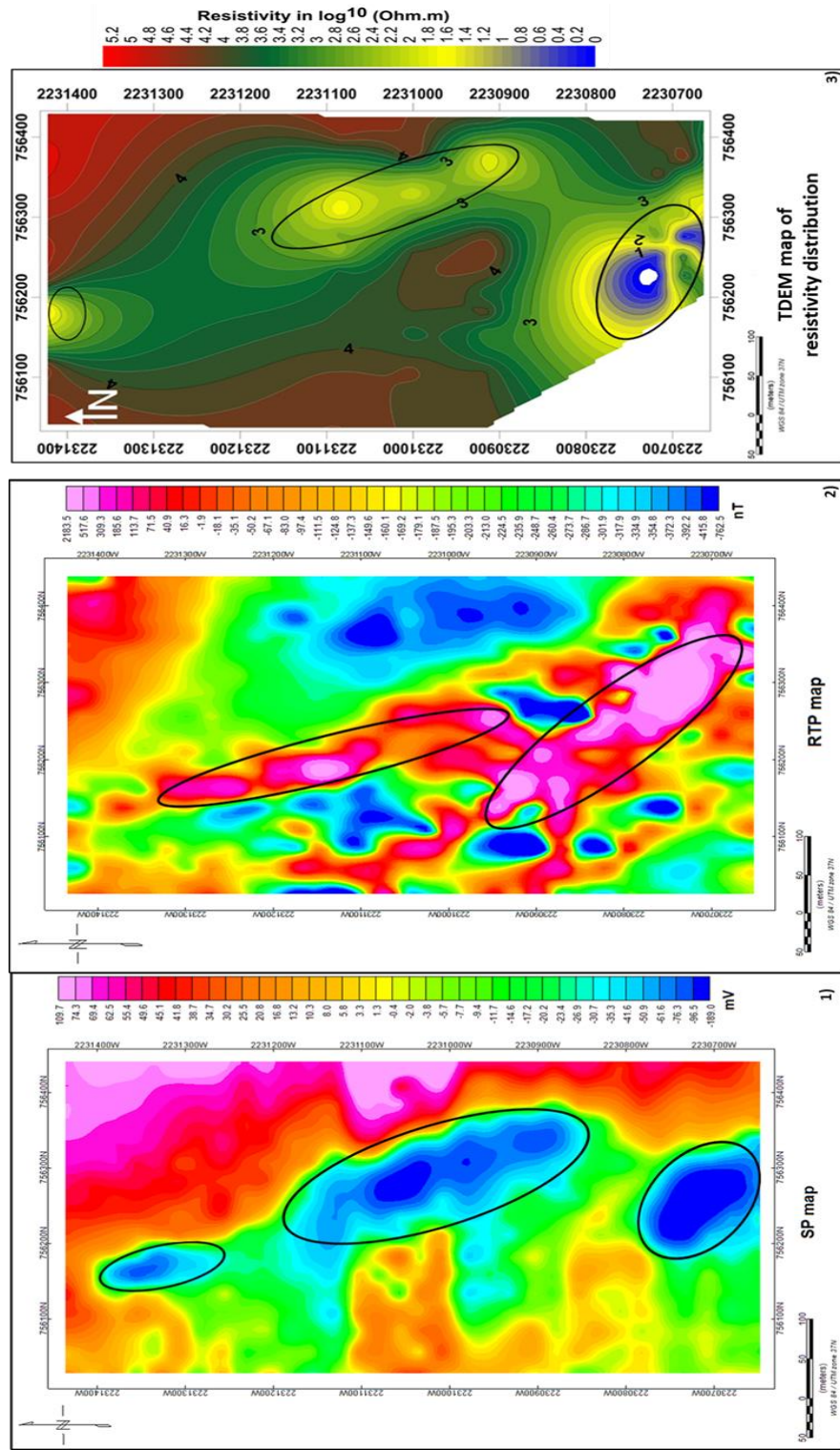


Figure 7.4 Maps from three methods showing the interpreted distribution of metallic minerals in the study area. 1) SP map (Fig.7.1), 2) RTP map (Fig.7.2), and 3) TDEM map (Fig.7.3)

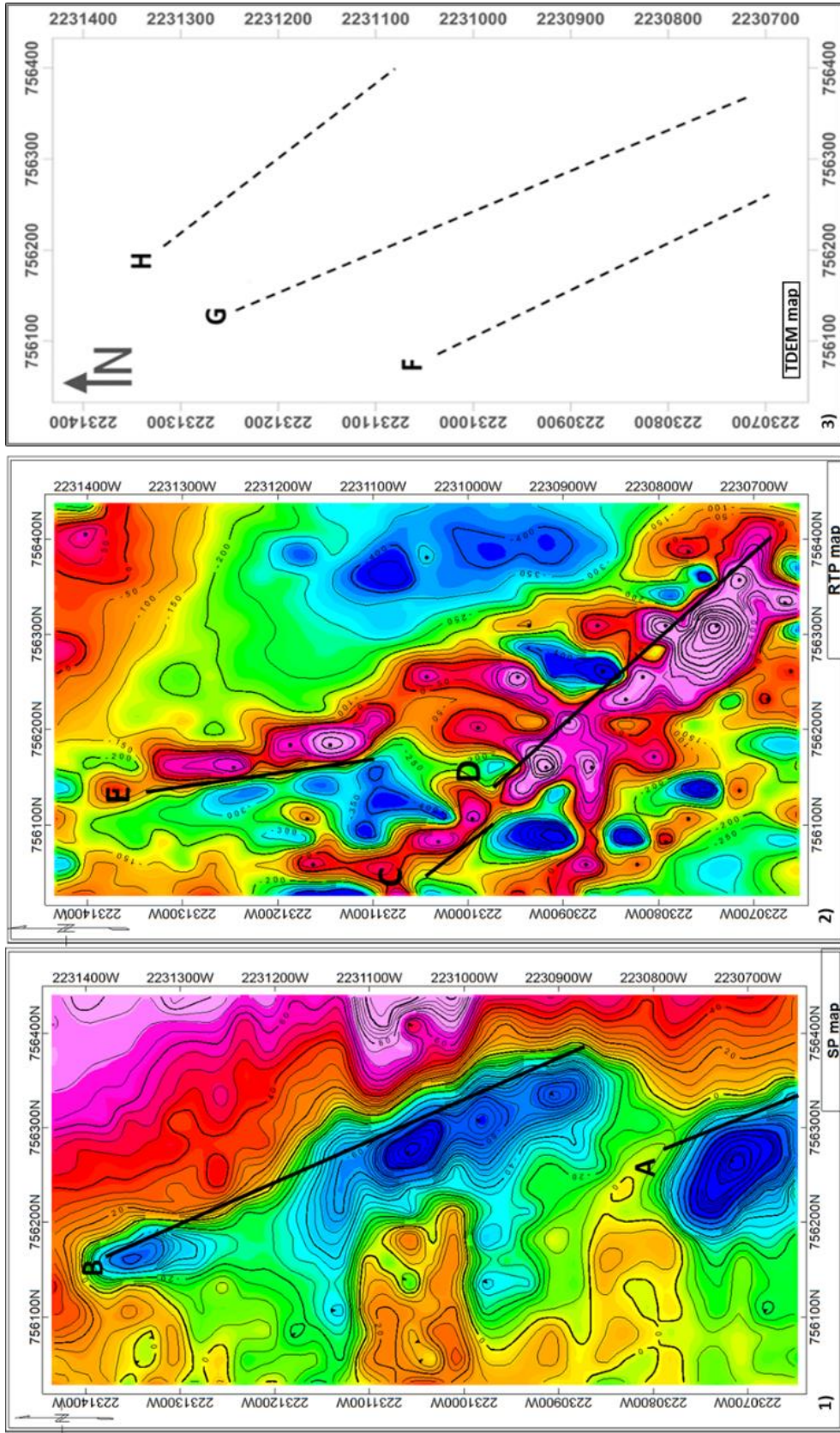


Figure 7.5 Interpreted fault trends superposed on 1) SP map, 2) RTP map, and 3) TDEM map.

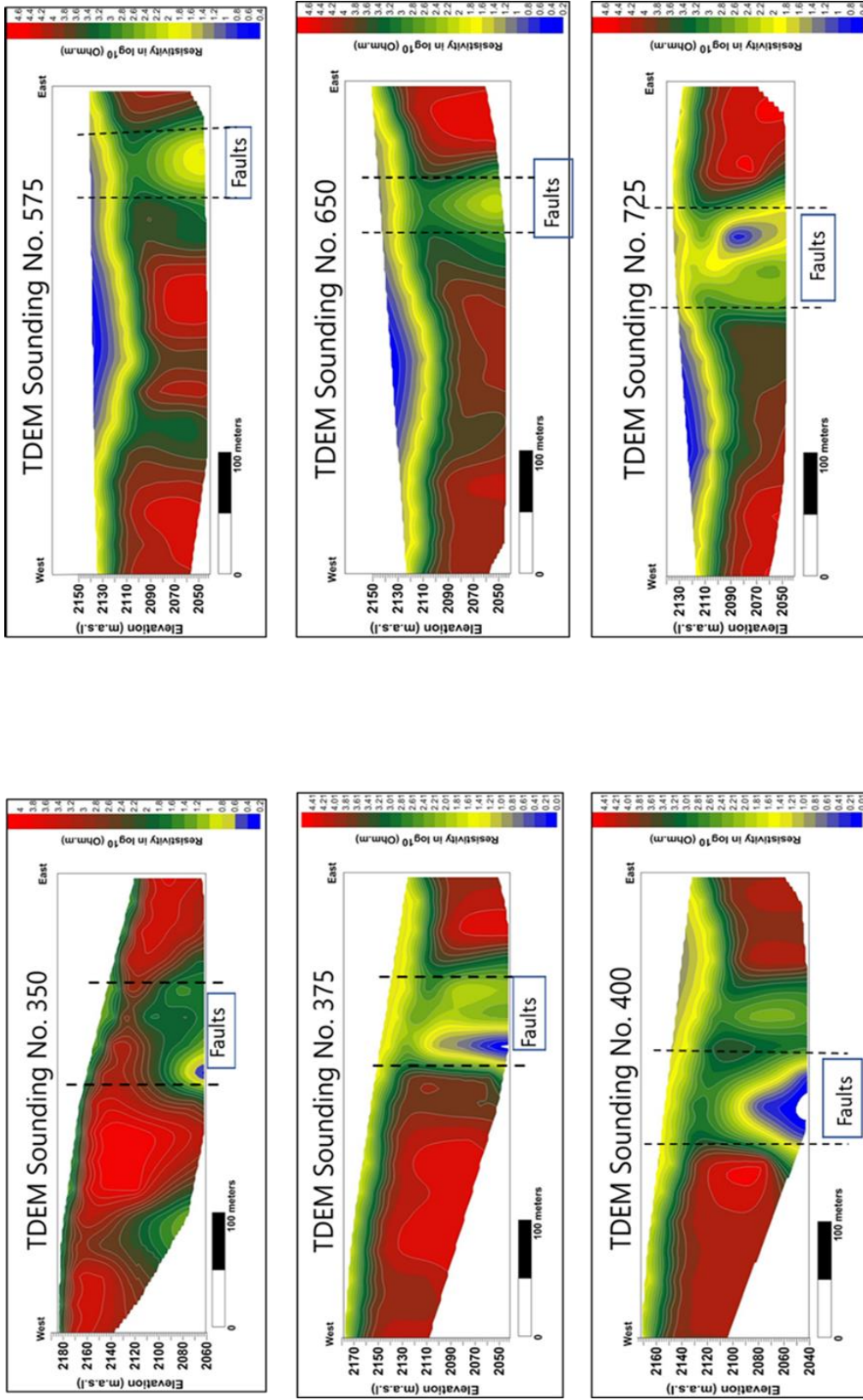


Figure 7.6 TDEM soundings showing the interpreted faults.

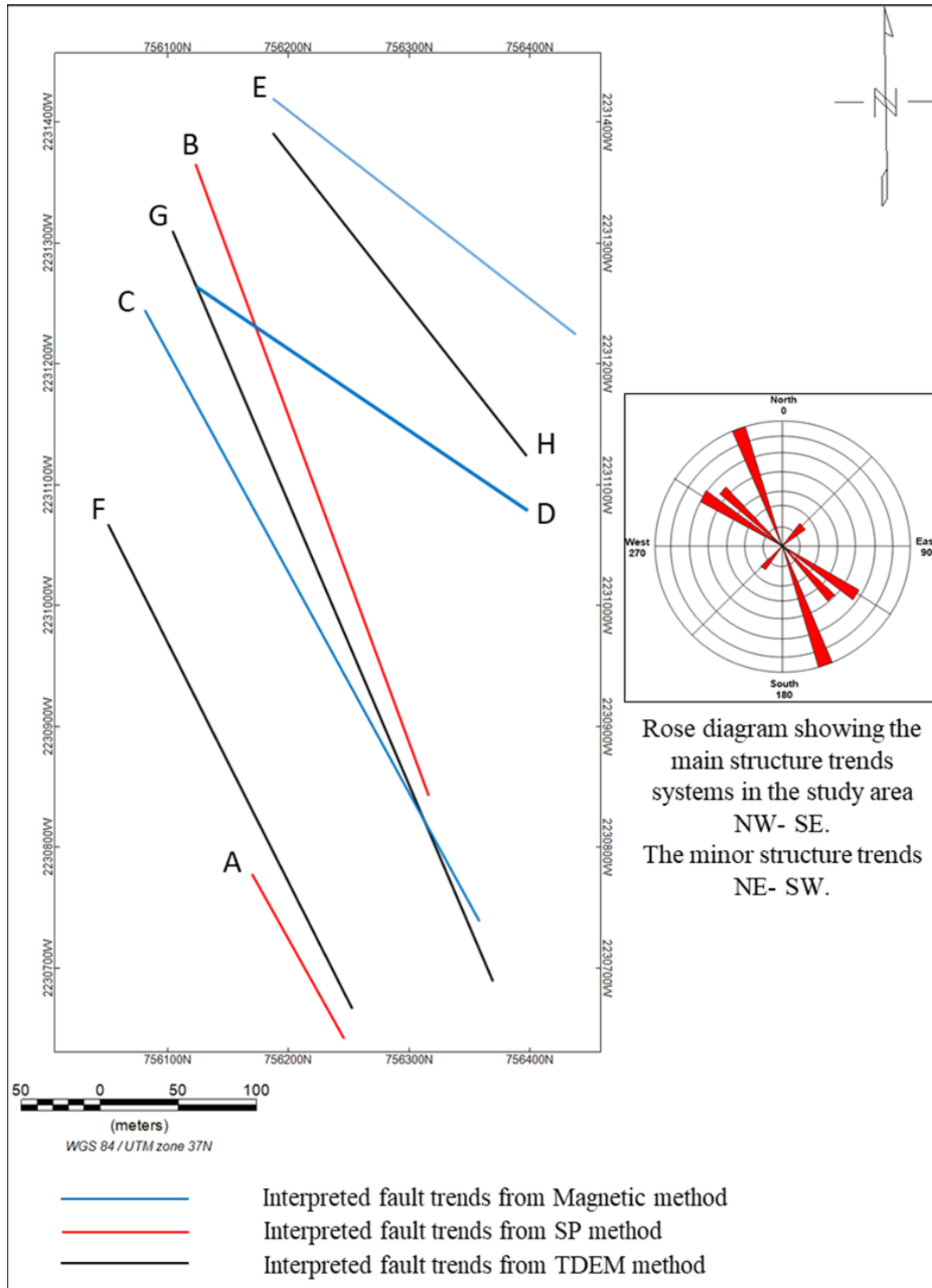


Figure 7.7 The main fault trends interpreted from geophysical data.

traverse as SP Line 425. The magnetic data values along this line range from -225 nT to 1,152 nT. The depth of sources of the anomalies can be estimated for this line using the Euler deconvolution method, and they range from approximately 5-30 m. There are also relatively high concentrations of copper and nickel, accompanied by high levels of iron to a depth of 35.40 m from the borehole data with a total depth of 250 m.

The TDEM results illustrate the distribution of resistivity values in the study area. TDEM Profile 400 (Figure 7.12) is located within 25 m of SP Line 425 and MAG Line 425. The elevation of this profile is between 2,040 and 2,160 m above sea level. Resistivity values along TDEM Profile 400 range from 0.01-1.2 Ωm . Based on the assay results and the drill hole information, it is concluded that mineralization diminishes to < 15% of massive sulfides, disseminated pyrite, and chalcopyrite. Also, there are excellent observed concentrations of copper and nickel at depths of 54.15-60 m. The lithology from Sounding 400 can be divided into three main layers based on the change in electrical resistivity values and borehole information. The first and top layer consists of ultramafic lava flows with elevation ranges from 2,140 to 2,170 m above sea level, and it has a range of electrical resistivity values between $1.21 \log^{10} \Omega\text{m}$ and $2.01 \log^{10} \Omega\text{m}$. The second layer represents ultramafic rocks with elevation ranges from 2,130 to 2,160 m above sea level, and it has a range of electrical resistivity values between $2.21 \log^{10} \Omega\text{m}$ and $4.01 \log^{10} \Omega\text{m}$. The third layer has elevation ranges from 2,040 to 2,090 m above sea level, and it has high resistivity values between above $3.0 \log^{10} \Omega\text{m}$ and in the middle there is a very low resistivities layer with 0.01 to $1.01 \log^{10} \Omega\text{m}$, which represents a massive sulfide interval with mafic rocks. Each of the geophysical methods employed contributed significantly to the generation of maps depicting the distribution of

mineralization in the study area and the location and orientation of shear zones. They clarified in one way or another the possibility of identifying rock structures.

7.4. THE DIFFERENCES AND SIMILARITIES BETWEEN THE INTERPRETATIONS OF THE SP, MAGNETIC AND TDEM DATA

Figure 7.4 presents the interpreted distributions of metallic minerals in the study area. The SP map shows the effects of minerals with low potential values (oxidation/reduction) at depths range in 10 - 40 m. The magnetic map shows high anomaly values in these areas, which are associated with nickel and magnetite at depths ranging from 5-50 m. The TDEM map shows very low resistive values in the same areas associated with massive sulfide minerals (Ni, Cu) with average shallow depths of 25 m while a deeper depth represents of 75m.

7.5. OPTIMAL ACQUISITION PARAMETERS BASED ON THE ASSESSMENT OF THE ACQUIRED DATA

In this study, a grid was designed to determine and map the structures and mineralization. The grid was controlled by the accessibility of the location which is surrounded by mountains. A grid of 80 x 40 m boxes was laid out with a spacing interval of 25 m. This interval was determined based on search for the general geological structures and the appearance of copper sulfide veins on the surface to acquire accurate, detailed information and to reduce the cost. The best coverage of data acquisition aids in mapping the structures and the changes in lithology well.

To reduce field expenses and to get the best high-resolution image of the subsurface, the magnetic survey was carried out first to provide information for the SP

and TDEM. It was easy to cover the area well to get the necessary information, but in future, it would be useful to extend the geophysical survey to the southern part of the study area.

The recommendation for any future geophysical explorations survey is to start the survey with the magnetic tool, which is a quick use tool that can operate in a continuous mode. In the continuous mode, more readings can be acquired within a short time, covering more areas.

7.6. OPTIMAL PROCESSING PARAMETERS BASED ON THE ASSESSMENT OF THE ACQUIRED DATA

Powerful software was used to process the geophysical data effectively. Geosoft Oasis Montaj™ software was used in the SP mapping, and some correction and filtrations were applied. In the magnetic survey, the data were processed with Geosoft Oasis Montaj™ and Golden Software's Surfer, while the TDEM data were processed with Zond EM 2D software.

The magnetic data processing included the use of multiple filters to enhance the final maps. Many filters were applied to the RTP map, which worked very well. For example, the Euler deconvolution filter worked well to map the depths of the anomalies. The 2D model showed the faults and layers, whereas the downward filter did not work very well. There were also many ways to process the TDEM data, and they were largely dependent upon the instrument system used to acquire the original data. Most TEM systems record the transient voltage at several discrete intervals during the voltage decay, after the applied current is switched off. Each time the current is applied and then stopped

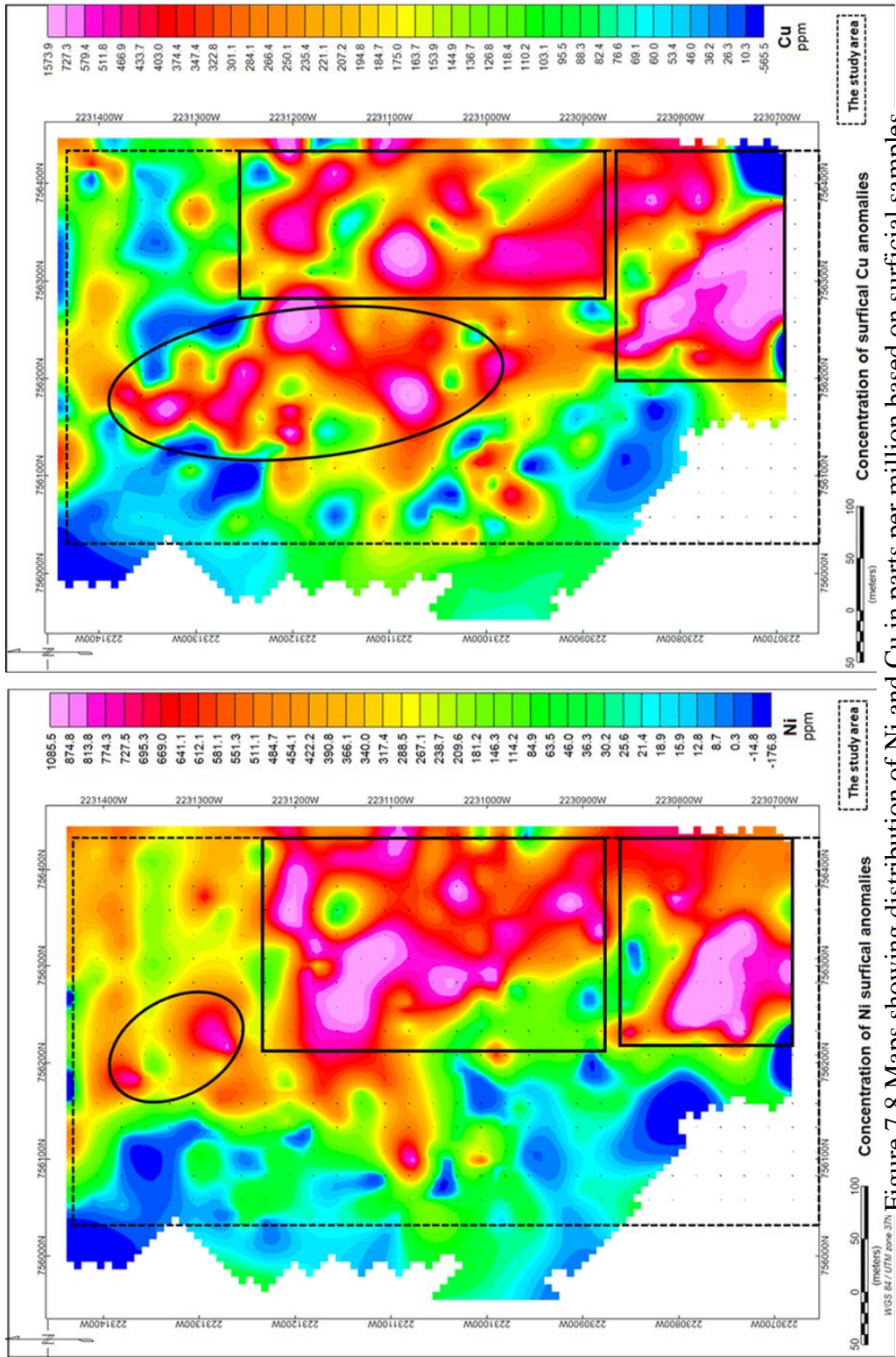


Figure 7.8 Maps showing distribution of Ni and Cu in parts per million based on surficial samples acquired in the study area.

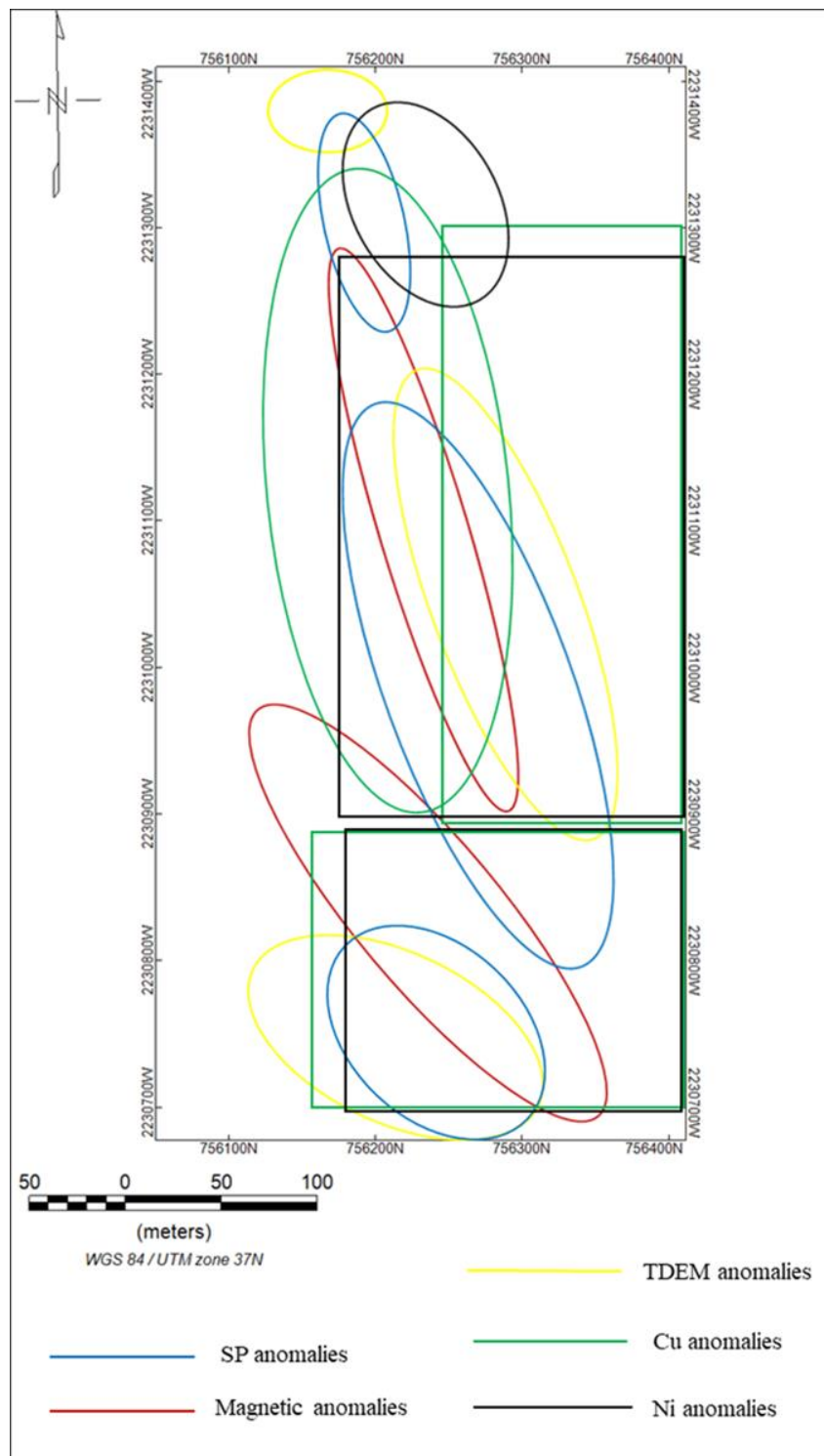


Figure 7.9 Map showing the distribution of Nickel/Copper deposits in the study area from surficial samples and using integrated geophysical data from SP, Mag, and TDEM methods.

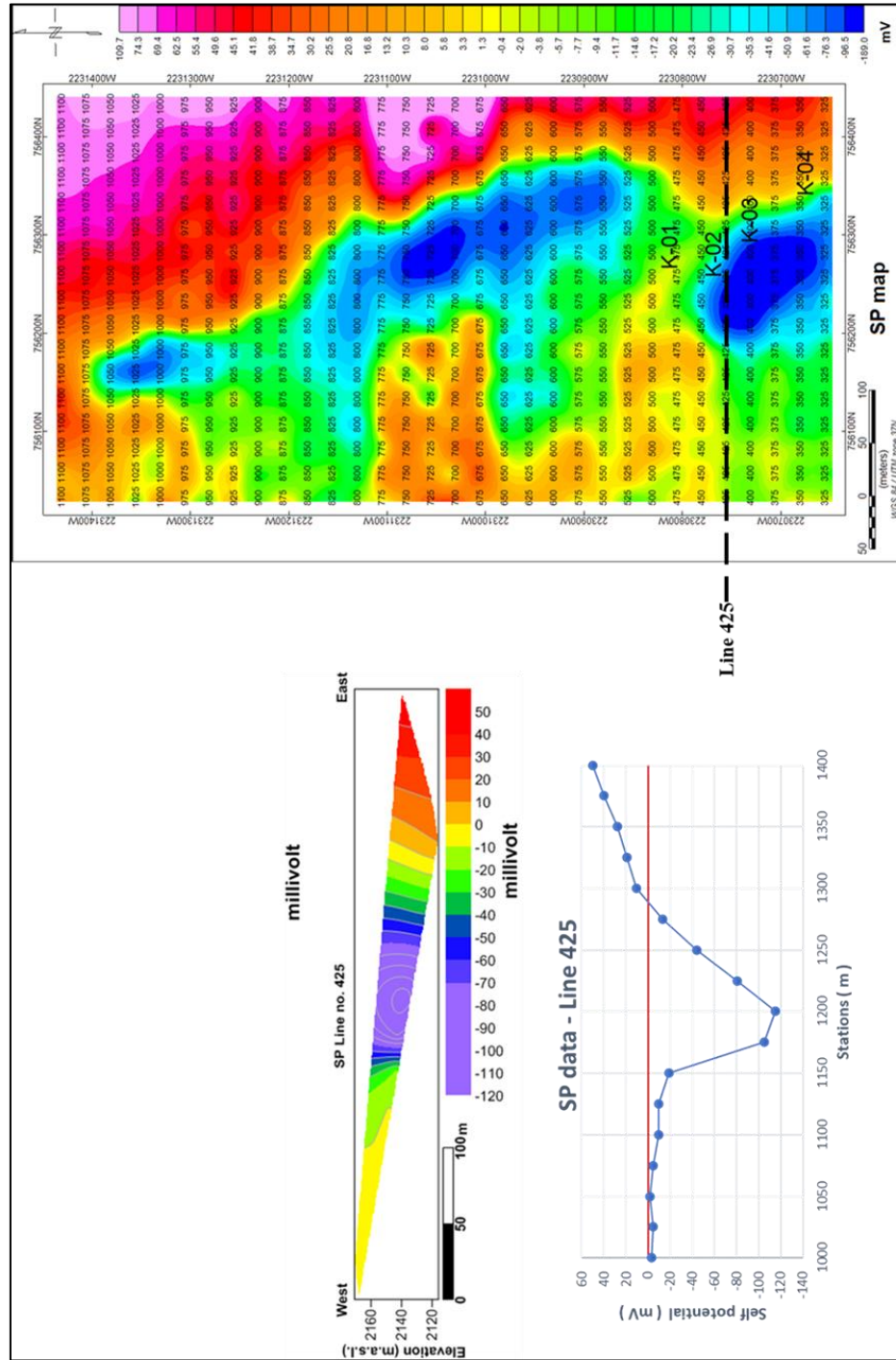


Figure 7.10 SP map shows all lines of survey, a line 425 SP profile showing negative values.

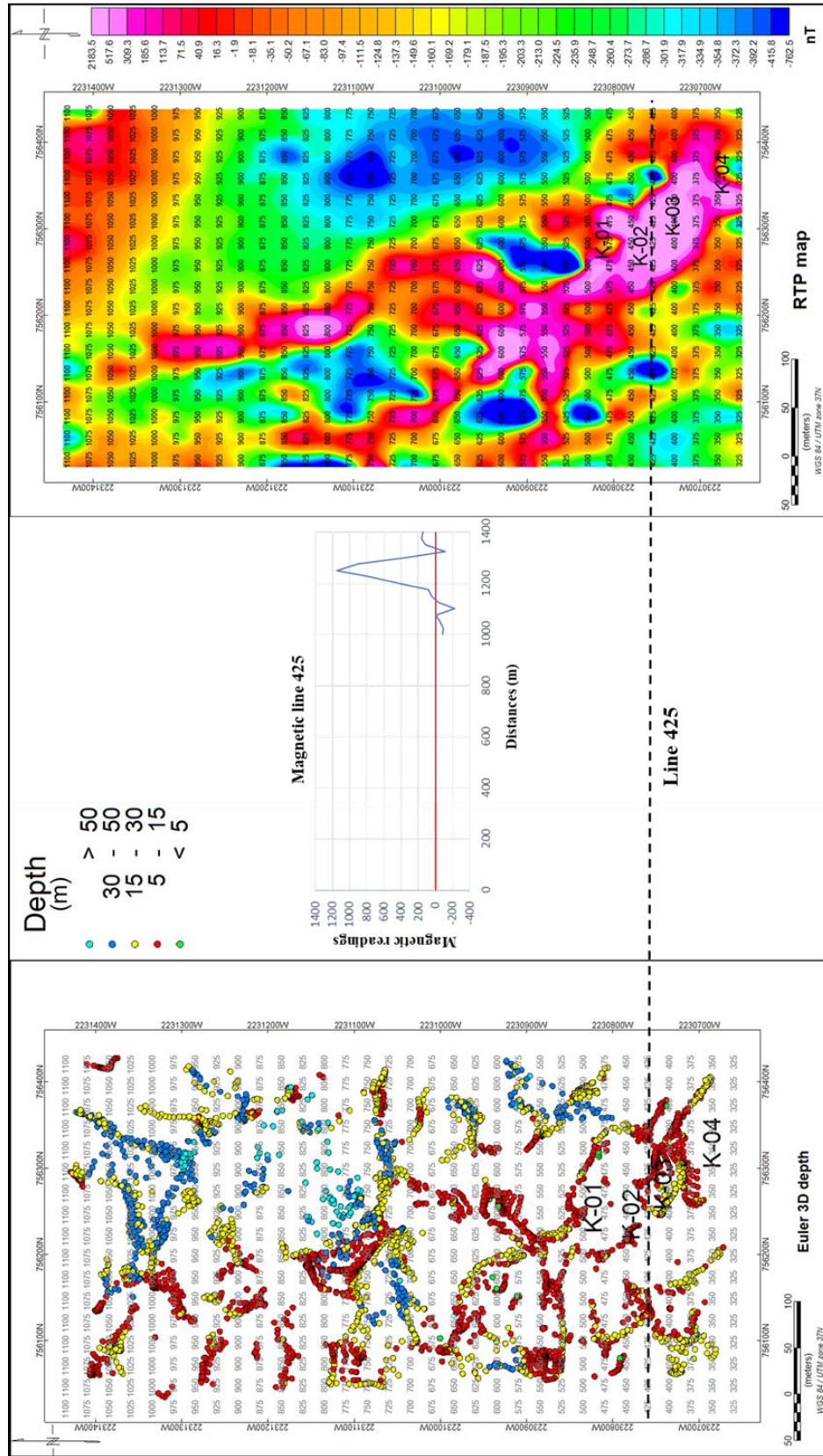


Figure 7.11 RTP map shows all magnetic lines compared with Euler depth map, a line 425 magnetic profile showing high positive amplitudes values.

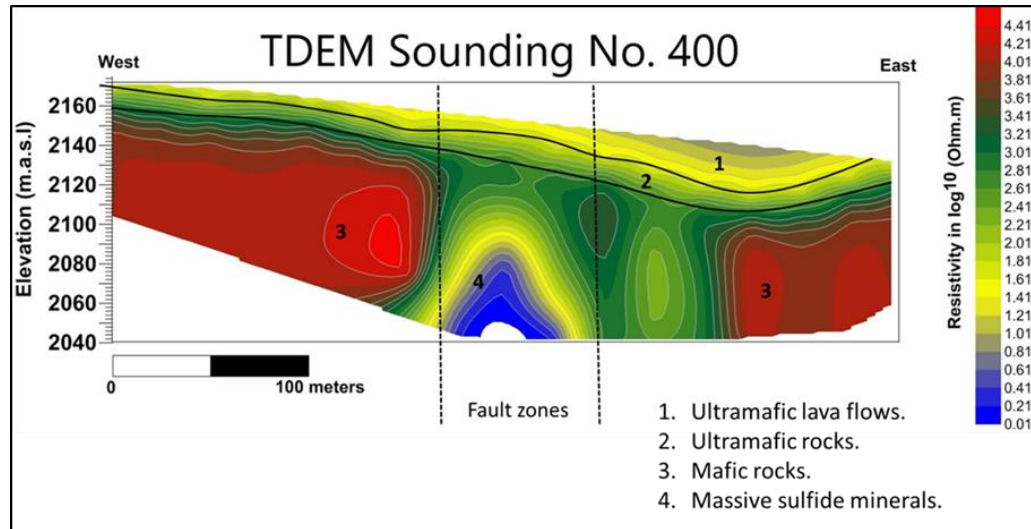


Figure 7.12 TDEM Sounding 400 showing the lithological.

measurements are taken; when the current is applied again and switched off, and a repeat set of measurements is taken. This process may be repeated many tens of times at a given location, with all the data are being logged automatically. Consequently, these data can be processed to improve the signal-to-noise ratio. After processing the geophysical data using different tools, we noticed that many Geosoft filters clarified the anomalies well for magnetic data, except the downward filter, which did not give good results. This may be from the result of the shallow targets.

7.7. OPTIMAL INTERPRETATION PARAMETERS BASED ON THE ASSESSMENT OF THE ACQUIRED DATA

Each geophysical method measures one of the physical properties of the relevant materials. For instance, in magnetic data, total magnetic intensities are measured in nT to differentiate the different types of rocks. However, a high total magnetic intensity may indicate igneous rocks. In contrast, a low anomaly may indicate sedimentary rocks. The

magnetic data provide a clear image of the differences in lithology and mapping structures. The SP measurements indicate areas with high and low voltages, which may indicate sources of minerals. TDEM data interpretation may utilize the differences in resistivity values of the subsurface. A high resistivity layer may indicate the existence of igneous rocks, and lower values may indicate sedimentary rocks. From both magnetic and TDEM data, different types of rocks and structures can be mapped. To interpret the data accurately, ground constraints should be considered in any interpretation. In addition, interpretation relies on experience.

7.8. STRENGTHS AND LIMITATIONS OF THE GEOPHYSICAL METHODS

The SP method measures the natural potential difference between two locations on the surface of the earth, and it is widely used in mineral exploration, groundwater, and geothermal investigations. It is usually relatively easy to acquire SP data in the field. A one- or two-person crew is generally sufficient to complete the survey. SP is an excellent, non-intrusive, fast, and relatively inexpensive reconnaissance tool, and it requires a voltmeter and non-polarizing electrodes. In spite of this, this method has some limitations. Data can be interpreted only qualitatively. Additionally, the tool images the subsurface to a depth less than 40 m. Also, SP anomalies can result from factors other than the oxidization/reduction of minerals. For example, water seepage can cause SP anomalies. Borehole data indicate that the study area anomalies were generated by oxidation/reduction. Water was not encountered in the core holes.

Magnetic methods measure spatial variations in the magnetic field of the earth, and they can be used to estimate relative variations in the concentration of magnetically

susceptibility minerals, to determine the location and orientation of subsurface geological structures, and for general geological mapping. It is relatively simple, inexpensive, and efficient to record in the field, where the data can be acquired rapidly by a one-person crew. Magnetic surveys can be land-based, underwater, or airborne, where magnetometers respond to the presence and concentration of magnetically susceptible material and provide a signal when an anomaly is detected. However, there are certain limitations of the magnetic method. Magnetometers only respond to metals that are magnetically susceptible. Anomalies are generally very complex, and they may be extremely difficult to interpret quantitatively. The interpretation of data is usually qualitative. Magnetic methods cannot detect copper, but they can find magnetite.

TDEM soundings are measures of subsurface electrical conductivity, and they can identify subsurface mineralization. There are multiple tools (shallow to deep). They are cost-effective means of establishing regional control, and they do not need to be coupled to the earth, so data can be acquired rapidly and inexpensively. Also, the interpretation of the data can be remarkably accurate, especially if constrained by drill hole data or other subsurface controls.

TDEM is useful for locating and mapping subsurface metals, as it responds to the presence of electrically conductive materials such as metallic mineralization and geological mapping. It generally provides more precise depth estimates if the target depth is greater than about 50 m, and it can obtain the vertical distribution of the resistivity of the ground. It is an efficient method to investigate the vertical distribution of ground resistivity. Based on borehole data that show the existence of minerals at different depths. No well log data are available to confirm fully whether there were any effects of water.

However, there are many limitations to this method. It can be affected by cultural features, e.g., metal fences, buried pipelines, or electric power lines, as the metal objects in the vicinity of the sounding site will create electromagnetic fields that the receiver coil will detect. This will distort the data from the ground, and it may produce data that are not interpretable.

7.9. CONCLUSIONS

In this dissertation, the aim was to aid government organizations, researchers, and private companies that are working in mining industries in best decision making. It has:

1. Demonstrated that the geophysical methods can be used to map the distribution of metallic mineralization.
2. Demonstrated that the geophysical methods can be used to map structures.
3. Used borehole and surficial geological data to verify the reasonableness of the SP, Magnetic, and TDEM interpretations signatures.
4. Demonstrated and explained differences and similarities between the interpretations of the SP, MAG and TDEM data.
5. Designed optimal acquisition parameters based on the assessment of the acquired data.
6. Designed optimal processing parameters based on the assessment of the acquired data.
7. Designed optimal interpretation processes based on the assessment of the acquired data.

8. Summarized the strengths and limitations of the geophysical methods.

The primary objectives were realized on this research. The interpretation of this study follows:

The study area has a rocky composition of metagabbro, which can contain many metal clusters of copper and nickel elements. To confirm these results, a geophysical survey was carried out. The best ways to search for metals include SP, Magnetic, and TDEM, because all these methods depend on the extent of the measured anomalies, which are highly responsive to the mineral elements in the rocks of the region. The mineralization zones in the study area are characterized by low resistivity values in TDEM, high negative voltages in SP, and high-amplitude positive anomaly values in Magnetic.

The SP method showed clear, relatively high negative values in three locations, which indicated the zones where subsurface metals are present.

The magnetic method (by RTP) detected high positive magnetic anomalies in two locations, which indicated the zones where there are subsurface metals.

TDEM measurement showed that there are three places with mineral accumulations. These places correspond to specific places identified by the magnetic method, and the structures derived from them are clear in the 2D profiles. It is possible that there will be a difference in the extent of mineralization between shallow and deep ground. However, with the use of the SP method, it is possible to offset and reinforce the possibility of detecting minerals in places identified by the previous magnetic and TDEM methods. The results of the chemical analysis of the well samples were satisfactory, and there was an acceptable match to the results from the geophysical methods. It is worth

noting that the structures found by the magnetic method and those from the analyses of rock samples helped greatly in developing a good visualization of the places likely to hold mineral accumulations.

This study has determined and mapped structures based on the geophysical results associated with the geological map. From the magnetic method, according to the RTP map of the study area, the direction of these faults trends toward the NW-SE. The tilt derivatives have zero values close to the edges of the body for RTP. Also, upward continuation has deduced deep and shallow structure. In addition, the 2D magnetic modeling technique indicated the major horst and graben structures.

The depth of the source bodies in the study area, found by the Euler anomalies, was about 94m. A close inspection of the Euler anomaly cluster indicates that the shallower trends are in the central part of the study area extending in a SW direction, while the deepest trends are in the central part of the study area extending in the NE direction.

The average depth levels of the magnetic sources obtained from a 2D radially average power spectrum indicates that the deeper sources have an average elevation of about 2,097 m above sea level, the intermediate sources are about 2,100 m above sea level, and the shallow or near surface sources is are about 2,191 m above sea level. Moreover, the average elevation in the selected area of ground magnetic survey ranged from 2,097 m to 2,191 m above sea level.

From the TDEM soundings, the northerly anomaly source is at a shallow depth of 25m, while the stronger southern anomaly source present at deep depth of around 75m.

From SP profiles, the depth of anomaly sources is around 10 – 40m. From magnetic, the depth of the source bodies in the study area from 5 – 50m.

The interdependence and complementarity between geological and geophysical methods indicates the ideal way for mineral exploration. This integration increases with the knowledge of structures and the chemical analyses of drilled core samples. It is very important to point out that the choice of geophysical methods to measure similar physical properties strengthens and supports the conclusions that relate to the most important point, which is the determination of places, depths, and thicknesses of the target, especially when this target has economic significance, such as mineral exploration and exploitation.

Integrated results from all research methods show that there are three promising places containing clusters of copper and nickel. These specific areas may be confined within the boundaries of the study area, but it is advisable to increase the area of the study area to determine the extent of these clusters and the economic benefit of the presence of these metals.

Since magnetic sensitivity is a proportional constant without dimensions that indicates the degree of magnetization of the material in response to an applied magnetic field, and since magnetism is the ratio between the magnetic moment and the density of magnetic flux (International Union of Pure and Applied Chemistry, 1997), the density and susceptibility volume distinguish the mineral elements from each other. There is a strong convergence between the natural density of the two metals (density of copper = 8,920 kg/m³ and density of Nickel = 8,900 kg/m³), while they differ in their volume susceptibility (copper = 7.66×10^{-7} CGS and Nickel = 48 CGS). This could explain why

the magnetic anomalies changed and how affected they are by the presence of copper rather than nickel in the region. Therefore, the presence of nickel mixed in most places with copper caused a noticeable change in places with anomalous magnetic maps from SP and TDEM. The magnetic anomalies are a function of the contributions of the mineralization as a whole, so one must not lose sight of the presence of other minerals in the region, such as iron oxides, gold, silver, and zinc. Despite their small concentrations, they somehow affect the signals of the measured magnetic anomalies, and they can result in a deformation or a change in the shape of the anomalies.

7.10. RECOMMENDATIONS

- For future work, it would be useful to extend the geophysical survey to the southern part of the study area.
- For time-domain electromagnetic data, it is perfect to acquire more than two profiles in the middle of the study area, to clarify the nature of the low resistive layer.
- Would drill another 2 exploratory core holes could be in middle and northern part of the study area to additionally verify and constrain the data interpretation.

APPENDIX A.

SURFICIAL SAMPLES ASSAY RESULTS OF NICKEL AND COPPER IN

WADI AL KHADRA PROSPECT AREA

Table A.1. Surficial samples assay results of Ni and Cu in Wadi Al Khadra prospect area.

Surficial sample No.	GPS READINGS			UTM Coordinates		Cu	Ni
	LAT.	LONG.	Altitude (m)	Easting	Northing	1.00 ppm	1.00 ppm
KAD-01	20.157	41.454	2137	756381.7	2230805.1	341	452
KAD-02	20.157	41.454	2133	756372.4	2230801.6	5,017	935
KAD-03	20.157	41.453	2130	756342.2	2230787.9	204	513
KAD-04	20.157	41.453	2126	756309	2230771.9	19,672	4,581
KAD-05	20.157	41.453	2125	756314.2	2230776.4	968	995
KAD-06	20.157	41.453	2145	756265.5	2230744.6	1,020	1,179
KAD-07	20.157	41.453	2150	756257.2	2230736.8	1,370	1,173
KAD-08	20.157	41.452	2154	756251.2	2230722.3	6,654	4,128
KAD-09	20.157	41.452	2157	756230.2	2230724.2	8,306	2,224
KAD-10	20.157	41.452	2157	756230.2	2230724.2	23,611	2,850
KAD-11	20.157	41.452	2158	756224	2230721.9	11,335	6,521
KAD-12	20.157	41.452	2158	756224	2230721.9	461	271
KAD-13	20.156	41.453	2153	756284.2	2230680.7	5,584	7,319
KAD-14	20.156	41.453	2164	756256.8	2230693.6	3,922	434
KAD-15	20.156	41.452	2152	756245	2230715.5	17,671	3,051
KAD-16	20.157	41.452	2152	756218.7	2230726.2	48,227	1,388
KAD-17	20.157	41.452	2152	756219.7	2230726.2	16,982	1,297
KAD-18	20.156	41.454	2135	756382.7	2230708.8	149	483
KAD-19	20.156	41.453	2126	756355	2230705	979	358
KAD-20	20.156	41.453	2147	756327.8	2230701	2,166	1,579
KAD-21	20.156	41.453	2148	756321.9	2230700.9	1,418	1,328

Table A.1. Surficial samples assay results of Ni and Cu in Wadi Al Khadra prospect area (Cont.)

KAD-22	20.156	41.453	2149	756310.2	2230703.9	4,556	3,029
KAD-23	20.156	41.453	2150	756301.5	2230706.7	2,207	1,060
KAD-24	20.156	41.453	2162	756284	2230706.5	2,119	1,357
KAD-25	20.156	41.453	2166	756278.3	2230706.4	1,870	1,036
KAD-26	20.156	41.453	2161	756257.9	2230703.1	1,708	1,664
KAD-27	20.156	41.452	2171	756240.7	2230696.6	2,353	1,709
KAD-28	20.156	41.452	2167	756234.8	2230699.7	116	99
KAD-29	20.156	41.452	2171	756217.2	2230702.5	100	49
KAD-30	20.16	41.453	2130	756293	2231082	2,037	1,005
KAD-31	20.16	41.453	2136	756272.7	2231084.8	238	615
KAD-32	20.16	41.453	2140	756264	2231078.5	188	615
KAD-33	20.16	41.453	2140	756261.1	2231081.5	7,668	1,299
KAD-34	20.16	41.453	2140	756258.2	2231081.5	1,509	337
KAD-35	20.16	41.453	2138	756255.3	2231081.4	1,296	808
KAD-36	20.16	41.453	2142	756255.3	2231081.4	12,355	3,866
KAD-37	20.16	41.452	2141	756243.6	2231084.4	2,128	1,139
KAD-38	20.16	41.452	2141	756243.6	2231084.4	9,563	1,622
KAD-39	20.16	41.452	2138	756240.7	2231081.2	6,532	2,841
KAD-40	20.16	41.452	2131	756240.7	2231081.2	306	187
KAD-41	20.157	41.454	2125	756381.8	2230733.1	135	420
KAD-42	20.157	41.454	2121	756373.4	2230732.9	143	422
KAD-43	20.157	41.453	2126	756349.3	2230732.6	639	1,115
KAD-44	20.157	41.453	2130	756343.1	2230732.5	458	977

Table A.1. Surficial samples assay results of Ni and Cu in Wadi Al Khadra prospect area (Cont.)

KAD-45	20.157	41.453	2124	756341	2230732.5	680	1,077
KAD-46	20.157	41.453	2125	756338.9	2230732.4	917	917
KAD-47	20.157	41.453	2128	756329.5	2230732.3	995	1,066
KAD-48	20.157	41.453	2132	756314.8	2230732.1	1,161	1,010
KAD-49	20.157	41.453	2134	756310.6	2230732	717	814
KAD-50	20.157	41.453	2136	756296	2230731.8	4,731	1,364
KAD-51	20.157	41.453	2140	756279.3	2230731.5	2,292	1,051
KAD-52	20.157	41.453	2145	756258.4	2230731.2	853	1,492
KAD-53	20.157	41.452	2147	756255.2	2230731.2	3,812	763
KAD-54	20.157	41.452	2154	756231.2	2230730.8	1,802	940
KAD-55	20.157	41.452	2156	756221.7	2230730.7	7,538	4,388
KAD-56	20.157	41.452	2157	756207.1	2230730.5	2,726	2,744
KAD-57	20.157	41.452	2156	756218.7	2230726.2	10,982	6,888
KAD-58	20.157	41.452	2156	756218.7	2230726.2	16,774	2,131
KAD-59	20.157	41.452	2156	756218.7	2230726.2	8,199	4,785
KAD-60	20.157	41.452	2156	756218.7	2230726.2	396	380
KAD-61	20.157	41.454	2126	756379.3	2230760.7	251	545
KAD-62	20.157	41.453	2119	756354.2	2230760.3	173	516
KAD-63	20.157	41.453	2124	756315.5	2230759.8	1,364	1,100
KAD-64	20.157	41.453	2128	756307.1	2230759.6	934	1,081
KAD-65	20.157	41.453	2128	756302.9	2230759.6	601	925
KAD-66	20.157	41.453	2130	756291.4	2230759.4	550	936
KAD-67	20.157	41.453	2135	756279.9	2230759.2	553	1,094

Table A.1. Surficial samples assay results of Ni and Cu in Wadi Al Khadra prospect area (Cont.)

KAD-68	20.157	41.453	2138	756269.4	2230759.1	638	1,311
KAD-69	20.157	41.452	2141	756234.9	2230758.6	6,170	634
KAD-70	20.157	41.452	2144	756225.5	2230758.4	1,077	620
KAD-71	20.157	41.452	2144	756223.4	2230758.4	362	137
KAD-72	20.157	41.452	2145	756219.2	2230758.4	1,001	622
KAD-73	20.157	41.452	2145	756218.2	2230758.3	345	361
KAD-74	20.157	41.454	2136	756379	2230780.6	618	719
KAD-75	20.157	41.453	2131	756359.1	2230780.3	138	582
KAD-76	20.157	41.453	2129	756347.6	2230780.2	117	539
KAD-77	20.157	41.453	2128	756345.5	2230780.1	748	807
KAD-78	20.157	41.453	2127	756327.7	2230779.9	209	482
KAD-79	20.157	41.453	2119	756312	2230779.7	1,124	1,874
KAD-80	20.157	41.453	2123	756298.4	2230779.5	1,003	1,598
KAD-81	20.157	41.453	2125	756291.1	2230779.3	16,540	3,891
KAD-82	20.157	41.453	2129	756288	2230779.3	515	1,169
KAD-83	20.157	41.453	2130	756271.2	2230779.1	547	1,282
KAD-84	20.157	41.452	2132	756247.2	2230778.7	425	2,016
KAD-85	20.157	41.452	2136	756237.8	2230778.6	419	938
KAD-86	20.157	41.452	2137	756231.5	2230778.5	174	283
KAD-87	20.157	41.452	2138	756227.3	2230778.4	205	405
KAD-88	20.157	41.452	2140	756222.1	2230778.3	610	222
KAD-89	20.157	41.452	2143	756208.5	2230778.1	226	136
KAD-90	20.157	41.453	2125	756321	2230808.6	1,900	325

Table A.1. Surficial samples assay results of Ni and Cu in Wadi Al Khadra prospect area (Cont.)

KAD-91	20.157	41.453	2121	756312.7	2230806.3	320	70
KAD-92	20.157	41.453	2119	756307.4	2230808.4	1,300	1,986
KAD-93	20.157	41.453	2113	756291.7	2230809.3	490	1,095
KAD-94	20.157	41.453	2114	756281.3	2230806.9	920	1,551
KAD-95	20.157	41.453	2126	756265.6	2230806.7	540	1,260
KAD-96	20.157	41.453	2129	756257.2	2230806.5	890	1,207
KAD-97	20.157	41.452	2137	756231.1	2230806.2	100	685
KAD-98	20.157	41.452	2145	756220.6	2230807.1	151	200
KAD-99	20.158	41.454	2141	756407.4	2230835.3	310	644
KAD-100	20.157	41.454	2134	756380.3	2230830.5	680	612
KAD-101	20.158	41.454	2133	756363.5	2230834.7	300	80
KAD-102	20.158	41.453	2132	756346.8	2230832.2	280	227
KAD-103	20.158	41.453	2134	756334.2	2230834.3	190	120
KAD-104	20.157	41.453	2126	756311.3	2230827.3	230	126
KAD-105	20.158	41.453	2129	756297.6	2230834.8	100	24
KAD-106	20.158	41.453	2118	756285.1	2230830.2	195	96
KAD-107	20.157	41.453	2121	756274.7	2230828.9	790	1,053
KAD-108	20.157	41.452	2128	756247.6	2230824.1	760	1,453
KAD-109	20.158	41.452	2138	756218.1	2230833.7	270	71
KAD-110	20.158	41.452	2140	756206.7	2230831.3	140	278
KAD-111	20.158	41.452	2143	756181.6	2230829.8	120	39
KAD-112	20.158	41.452	2145	756179.5	2230828.7	10	29
KAD-113	20.158	41.451	2151	756115.2	2230860.9	10	6

Table A.1. Surficial samples assay results of Ni and Cu in Wadi Al Khadra prospect area (Cont.)

KAD-114	20.158	41.451	2150	756123.6	2230861.1	10	12
KAD-115	20.158	41.452	2145	756157.1	2230856	90	35
KAD-116	20.158	41.452	2131	756203.2	2230852.3	90	44
KAD-117	20.158	41.452	2130	756217.9	2230851.4	80	157
KAD-118	20.158	41.452	2130	756217.9	2230851.4	420	558
KAD-119	20.158	41.452	2125	756232.5	2230853.8	720	880
KAD-120	20.158	41.452	2121	756251.3	2230854.1	80	19
KAD-121	20.158	41.452	2122	756253.4	2230855.2	60	28
KAD-122	20.158	41.453	2123	756269	2230858.8	190	87
KAD-123	20.158	41.453	2130	756309.8	2230858.3	100	72
KAD-124	20.158	41.453	2133	756325.5	2230857.4	150	33
KAD-125	20.158	41.453	2137	756348.4	2230864.4	5,000	3,587
KAD-126	20.158	41.454	2138	756378.5	2230882.5	580	586
KAD-127	20.158	41.453	2136	756345.1	2230878.7	3,800	3,880
KAD-128	20.158	41.453	2135	756330.4	2230880.7	4,600	2,334
KAD-129	20.158	41.453	2137	756309.4	2230883.7	40	28
KAD-130	20.158	41.453	2130	756282.3	2230880	120	83
KAD-131	20.158	41.453	2126	756270.8	2230879.8	50	37
KAD-132	20.158	41.453	2121	756255.1	2230879.6	70	37
KAD-133	20.158	41.452	2119	756237.2	2230886	1,500	163
KAD-134	20.158	41.452	2117	756225.7	2230885.8	200	60
KAD-135	20.158	41.452	2121	756234.1	2230882.6	500	311
KAD-136	20.158	41.452	2123	756242.5	2230881.6	46	30

Table A.1. Surficial samples assay results of Ni and Cu in Wadi Al Khadra prospect area (Cont.)

KAD-137	20.158	41.452	2123	756244.7	2230879.5	140	99
KAD-138	20.158	41.453	2125	756256.1	2230881.8	225	42
KAD-139	20.158	41.453	2131	756265.7	2230872	54	60
KAD-140	20.158	41.453	2132	756270.8	2230882.1	64	25
KAD-141	20.158	41.453	2134	756282.3	2230880	312	54
KAD-142	20.158	41.453	2135	756307.4	2230880.4	800	542
KAD-143	20.158	41.453	2141	756331.5	2230880.7	1,600	871
KAD-144	20.158	41.453	2140	756350.3	2230881	2,300	1,280
KAD-145	20.158	41.454	2141	756381.7	2230881.5	325	605
KAD-146	20.158	41.454	2151	756432.6	2230904.4	95	529
KAD-147	20.158	41.454	2144	756407.4	2230906.2	232	715
KAD-148	20.158	41.454	2139	756383.3	2230909.2	298	708
KAD-149	20.158	41.454	2133	756360.3	2230908.9	1,800	945
KAD-150	20.158	41.453	2127	756349.9	2230906.5	2,200	651
KAD-151	20.158	41.453	2136	756323.8	2230906.1	1,100	425
KAD-152	20.158	41.453	2130	756310.1	2230910.3	470	473
KAD-153	20.158	41.453	2124	756281	2230894.4	19	6
KAD-154	20.158	41.452	2116	756210.9	2230901.1	375	186
KAD-155	20.158	41.452	2116	756208.8	2230898.9	84	8
KAD-156	20.158	41.452	2120	756193	2230904.2	202	17
KAD-157	20.158	41.452	2132	756166.9	2230906	46	43
KAD-158	20.158	41.451	2134	756144.9	2230902.4	70	25
KAD-159	20.158	41.451	2138	756139.8	2230900.1	171	22

Table A.1. Surficial samples assay results of Ni and Cu in Wadi Al Khadra prospect area (Cont.)

KAD-160	20.158	41.451	2142	756118.7	2230905.3	117	24
KAD-161	20.158	41.451	2146	756111.4	2230905.2	93	20
KAD-162	20.158	41.451	2146	756067.5	2230902.3	27	23
KAD-163	20.158	41.451	2146	756048.7	2230904.3	110	15
KAD-164	20.158	41.45	2142	756041.2	2230913	85	10
KAD-165	20.159	41.452	2115	756217	2230981	610	226
KAD-166	20.159	41.452	2111	756191.1	2230964	215	51
KAD-167	20.159	41.452	2130	756150.3	2230964.5	198	41
KAD-168	20.159	41.454	2162	756432.6	2230970.8	225	70
KAD-169	20.159	41.451	2108	756110.6	2230963.9	19	11
KAD-170	20.159	41.451	2111	756103.3	2230962.7	20	7
KAD-171	20.159	41.451	2114	756068.7	2230962.1	2,500	1,340
KAD-172	20.159	41.451	2117	756061.4	2230962	1,900	1,950
KAD-173	20.159	41.45	2124	756039.5	2230961.7	128	43
KAD-174	20.159	41.45	2128	756014.3	2230964.7	95	28
KAD-175	20.159	41.453	2119	756274.4	2230988.4	203	645
KAD-176	20.159	41.452	2120	756209.6	2230989.7	1,400	742
KAD-177	20.159	41.452	2118	756201.1	2230997.3	422	224
KAD-178	20.159	41.452	2117	756193.9	2230989.5	520	206
KAD-179	20.159	41.451	2107	756092.4	2230990.2	39	15
KAD-180	20.159	41.451	2108	756052.6	2230990.7	2,860	1,660
KAD-181	20.159	41.45	2117	756019.2	2230991.3	111	30
KAD-182	20.159	41.45	2104	755961.6	2230990.5	77	23

Table A.1. Surficial samples assay results of Ni and Cu in Wadi Al Khadra prospect area (Cont.)

KAD-183	20.159	41.454	2158	756434.6	2230979.7	265	646
KAD-184	20.159	41.454	2157	756426.2	2230981.8	184	676
KAD-185	20.159	41.454	2153	756408.4	2230981.6	173	631
KAD-186	20.159	41.454	2145	756374.9	2230983.3	122	588
KAD-187	20.159	41.453	2146	756354	2230980.8	150	556
KAD-188	20.159	41.453	2146	756337.3	2230982.7	600	833
KAD-189	20.159	41.453	2145	756305.9	2230982.3	1,400	1,362
KAD-190	20.159	41.453	2144	756296.5	2230983.2	3,200	1,080
KAD-191	20.159	41.453	2141	756293.4	2230977.7	334	201
KAD-192	20.159	41.453	2134	756293.5	2230972.1	1,100	809
KAD-193	20.159	41.453	2133	756282.8	2230987.5	1,100	798
KAD-194	20.159	41.453	2132	756279.8	2230977.5	185	45
KAD-195	20.159	41.452	2124	756251.5	2230981.5	380	245
KAD-196	20.159	41.452	2120	756243.2	2230979.1	116	54
KAD-197	20.159	41.452	2116	756191.9	2230981.7	230	186
KAD-198	20.159	41.452	2120	756149	2230983.3	74	13
KAD-199	20.159	41.451	2122	756139.6	2230983.1	48	8
KAD-200	20.159	41.451	2124	756138.6	2230980.9	96	4
KAD-201	20.159	41.451	2121	756128.2	2230975.2	244	45
KAD-202	20.159	41.451	2124	756120.8	2230979.5	2,100	1,206
KAD-203	20.159	41.451	2131	756099.9	2230974.8	2,600	1,612
KAD-204	20.159	41.451	2128	756084.2	2230980.1	500	73
KAD-205	20.159	41.451	2129	756052.8	2230981.9	68	24

Table A.1. Surficial samples assay results of Ni and Cu in Wadi Al Khadra prospect area (Cont.)

KAD-206	20.159	41.45	2132	756033.9	2230981.6	124	17
KAD-207	20.159	41.454	2148	756432.1	2231004.1	129	30
KAD-208	20.159	41.454	2149	756408.1	2231005.9	295	721
KAD-209	20.159	41.454	2151	756402.9	2231003.6	205	554
KAD-210	20.159	41.454	2148	756387.1	2231005.6	97	515
KAD-211	20.159	41.454	2148	756373.5	2231006.5	460	684
KAD-212	20.159	41.454	2149	756368.3	2231008.7	240	727
KAD-213	20.159	41.453	2146	756332.7	2231008.1	158	552
KAD-214	20.159	41.453	2150	756319.1	2231005.7	425	547
KAD-215	20.159	41.453	2147	756300.3	2231005.5	1,000	774
KAD-216	20.159	41.453	2147	756289.8	2231007.5	2,800	1,896
KAD-217	20.159	41.453	2145	756277.3	2231007.3	2,600	1,368
KAD-218	20.159	41.453	2144	756272.1	2231005	1,250	425
KAD-219	20.159	41.453	2138	756264.8	2231004.9	500	247
KAD-220	20.159	41.453	2140	756259.5	2231007.1	86	40
KAD-221	20.159	41.453	2124	756256.4	2231007	225	118
KAD-222	20.159	41.453	2133	756259.5	2231004.8	207	159
KAD-223	20.159	41.453	2129	756256.4	2231004.8	45	19
KAD-224	20.159	41.452	2129	756251.2	2231004.7	163	85
KAD-225	20.159	41.452	2128	756248	2231004.7	53	37
KAD-226	20.159	41.452	2126	756243.8	2231006.8	90	114
KAD-227	20.159	41.452	2124	756235.5	2231004.5	67	13
KAD-228	20.159	41.452	2125	756230.3	2231004.4	344	95

Table A.1. Surficial samples assay results of Ni and Cu in Wadi Al Khadra prospect area (Cont.)

KAD-229	20.159	41.452	2121	756228.2	2231004.4	153	53
KAD-230	20.159	41.452	2119	756225	2231004.3	348	128
KAD-231	20.159	41.451	2120	756136.1	2231003	83	56
KAD-232	20.159	41.451	2123	756130.9	2231002.9	287	393
KAD-233	20.159	41.451	2123	756128.8	2231007.3	59	39
KAD-234	20.159	41.451	2124	756112	2231007.1	474	255
KAD-235	20.159	41.451	2125	756107.9	2231004.8	189	129
KAD-236	20.159	41.451	2125	756101.6	2231004.7	1,332	787
KAD-237	20.159	41.451	2120	756089	2231007.9	247	73
KAD-238	20.159	41.451	2122	756076.5	2231006.6	177	74
KAD-239	20.159	41.451	2124	756049.3	2231004	68	36
KAD-240	20.159	41.45	2127	756036.8	2231003.8	98	28
KAD-241	20.159	41.454	2144	756431.8	2231029.5	289	665
KAD-242	20.159	41.454	2148	756378.4	2231028.8	560	929
KAD-243	20.159	41.453	2147	756334.5	2231030.3	155	603
KAD-244	20.159	41.453	2147	756284.3	2231029.6	1,652	1,046
KAD-245	20.159	41.453	2138	756266.5	2231031.5	1,947	810
KAD-246	20.159	41.452	2127	756233	2231032.1	199	98
KAD-247	20.159	41.452	2118	756190	2231035.9	23	25
KAD-248	20.159	41.452	2113	756180.6	2231035.8	326	84
KAD-249	20.159	41.451	2118	756123.2	2231029.4	18	12
KAD-250	20.159	41.451	2117	756116.9	2231032.6	99	201
KAD-251	20.159	41.451	2116	756109.6	2231032.5	133	165

Table A.1. Surficial samples assay results of Ni and Cu in Wadi Al Khadra prospect area (Cont.)

KAD-252	20.159	41.451	2117	756099.1	2231034.6	89	22
KAD-253	20.159	41.451	2120	756081.3	2231029.9	4	49
KAD-254	20.159	41.451	2121	756052.1	2231023.9	105	52
KAD-255	20.16	41.454	2141	756428.3	2231053.9	226	442
KAD-256	20.16	41.454	2140	756402.1	2231056.8	355	450
KAD-257	20.16	41.454	2147	756357.1	2231055	73	514
KAD-258	20.16	41.453	2144	756334.1	2231054.7	357	646
KAD-259	20.16	41.453	2140	756263	2231054.7	1,399	1,350
KAD-260	20.16	41.452	2136	756247.3	2231056.7	8,382	2,063
KAD-261	20.16	41.452	2138	756239.9	2231056.6	557	391
KAD-262	20.16	41.452	2129	756236.8	2231056.6	329	397
KAD-263	20.16	41.451	2115	756121.8	2231054.9	233	289
KAD-264	20.16	41.451	2118	756103.9	2231057.9	144	64
KAD-265	20.16	41.451	2121	756072.6	2231056.4	32	11
KAD-266	20.16	41.451	2120	756058.9	2231059.5	24	12
KAD-267	20.16	41.451	2123	756054.8	2231057.2	178	194
KAD-268	20.155	41.454	2139	756431	2231084	390	830
KAD-269	20.16	41.454	2136	756406.9	2231081.2	164	731
KAD-270	20.16	41.454	2131	756370.4	2231077.4	297	1,169
KAD-271	20.16	41.453	2130	756331.7	2231076.8	918	1,373
KAD-272	20.16	41.453	2138	756263.6	2231082.4	15,104	1,519
KAD-273	20.16	41.453	2137	756253.2	2231081.2	12,348	12,397
KAD-274	20.16	41.452	2134	756241.6	2231086.5	6,869	3,804

Table A.1. Surficial samples assay results of Ni and Cu in Wadi Al Khadra prospect area (Cont.)

KAD-275	20.16	41.452	2127	756226	2231080.8	349	426
KAD-276	20.16	41.452	2120	756208.2	2231080.5	388	312
KAD-277	20.16	41.452	2120	756187.3	2231080.2	997	1,451
KAD-278	20.16	41.451	2112	756116	2231093.6	4,081	4,036
KAD-279	20.16	41.451	2113	756100.5	2231078.9	290	971
KAD-280	20.16	41.451	2117	756067	2231079.5	66	186
KAD-281	20.159	41.451	2120	756045	2231012.8	262	69
KAD-282	20.16	41.454	2142	756430.6	2231107.1	632	787
KAD-283	20.16	41.454	2128	756404.5	2231106.7	216	1,080
KAD-284	20.16	41.454	2130	756401.3	2231108.8	1,300	1,286
KAD-285	20.16	41.453	2122	756345.9	2231108	323	1,075
KAD-286	20.16	41.453	2127	756333.4	2231105.6	664	861
KAD-287	20.16	41.453	2130	756277.9	2231104.8	215	717
KAD-288	20.16	41.453	2133	756257	2231108.9	294	637
KAD-289	20.16	41.452	2138	756228.8	2231106.3	1,548	1,090
KAD-290	20.16	41.452	2124	756179.6	2231105.6	407	633
KAD-291	20.16	41.452	2117	756157.6	2231107.5	186	338
KAD-292	20.16	41.451	2116	756085.4	2231107.5	139	33
KAD-293	20.16	41.451	2119	756075.1	2231100.7	170	74
KAD-294	20.16	41.451	2120	756056.2	2231106	225	99
KAD-295	20.16	41.451	2119	756042.8	2231090.3	121	21
KAD-296	20.16	41.454	2152	756430.3	2231131.4	121	535
KAD-297	20.16	41.454	2141	756408.3	2231131.1	2,217	764

Table A.1. Surficial samples assay results of Ni and Cu in Wadi Al Khadra prospect area (Cont.)

KAD-298	20.16	41.454	2129	756380.1	2231130.7	112	1,057
KAD-299	20.16	41.453	2124	756319.4	2231133.1	185	939
KAD-300	20.16	41.453	2128	756273.4	2231129.1	177	879
KAD-301	20.16	41.452	2130	756244.1	2231130.9	179	893
KAD-302	20.16	41.452	2133	756210.6	2231130.4	1,113	1,185
KAD-303	20.16	41.452	2131	756194.9	2231131.3	2,281	2,080
KAD-304	20.16	41.452	2125	756178.2	2231129.9	1,361	451
KAD-305	20.16	41.452	2123	756165.6	2231130.8	195	75
KAD-306	20.16	41.452	2119	756152	2231130.6	128	117
KAD-307	20.16	41.451	2117	756079.9	2231129.6	99	9
KAD-308	20.16	41.451	2121	756048.5	2231131.3	111	39
KAD-309	20.16	41.45	2119	756040.1	2231133.4	125	27
KAD-310	20.16	41.454	2141	756439.3	2231157	88	487
KAD-311	20.16	41.454	2140	756407.9	2231156.6	641	772
KAD-312	20.16	41.454	2129	756371.3	2231156	152	131
KAD-313	20.16	41.453	2117	756320.1	2231155.3	104	734
KAD-314	20.16	41.453	2128	756256.3	2231156.5	1,013	1,165
KAD-315	20.16	41.452	2133	756230.1	2231156.2	602	793
KAD-316	20.16	41.452	2133	756194.6	2231155.6	4,674	2,493
KAD-317	20.16	41.452	2130	756178.8	2231157.6	3,383	1,026
KAD-318	20.16	41.452	2121	756167.4	2231155.2	5,817	1,362
KAD-319	20.16	41.452	2120	756144.4	2231154.9	6,054	468
KAD-320	20.16	41.451	2120	756130.8	2231152.5	1,265	236

Table A.1. Surficial samples assay results of Ni and Cu in Wadi Al Khadra prospect area (Cont.)

KAD-321	20.16	41.451	2114	756113	2231154.4	189	111
KAD-322	20.16	41.451	2122	756057.5	2231156.9	15	17
KAD-323	20.16	41.453	2119	756348.2	2231161.2	112	22
KAD-324	20.161	41.454	2122	756433.7	2231181.3	65	511
KAD-325	20.161	41.454	2121	756408.6	2231180.9	312	690
KAD-326	20.161	41.454	2123	756381.4	2231182.8	470	785
KAD-327	20.161	41.453	2121	756332.3	2231179.8	442	806
KAD-328	20.161	41.453	2121	756308.2	2231179.5	71	863
KAD-329	20.161	41.453	2119	756303	2231179.4	140	148
KAD-330	20.161	41.453	2118	756290.4	2231181.4	531	923
KAD-331	20.161	41.452	2127	756248.6	2231180.8	606	764
KAD-332	20.161	41.452	2126	756219.2	2231185.9	277	728
KAD-333	20.162	41.452	2128	756185.2	2231365.9	516	844
KAD-334	20.161	41.452	2126	756170.1	2231180.7	2,305	608
KAD-335	20.161	41.452	2116	756144	2231180.4	123	191
KAD-336	20.161	41.451	2121	756138.7	2231184.7	255	35
KAD-337	20.161	41.451	2116	756115.7	2231179.9	148	52
KAD-338	20.161	41.451	2112	756105.2	2231185.3	187	33
KAD-339	20.161	41.451	2118	756041.4	2231183.3	121	23
KAD-340	20.161	41.454	2132	756433.3	2231206.8	822	734
KAD-341	20.161	41.454	2123	756405.1	2231205.3	90	854
KAD-342	20.162	41.454	2115	756370.3	2231296.7	304	715
KAD-343	20.161	41.453	2120	756347.5	2231207.7	596	922

Table A.1. Surficial samples assay results of Ni and Cu in Wadi Al Khadra prospect area (Cont.)

KAD-344	20.161	41.453	2117	756313	2231209.4	141	182
KAD-345	20.161	41.453	2116	756293.2	2231206.9	1,174	1,337
KAD-346	20.161	41.453	2118	756256.6	2231204.2	926	1,121
KAD-347	20.161	41.452	2126	756172.9	2231207.4	158	139
KAD-348	20.161	41.452	2125	756166.6	2231207.3	702	384
KAD-349	20.161	41.452	2123	756148.8	2231207	175	99
KAD-350	20.161	41.451	2121	756140.5	2231206.9	995	330
KAD-351	20.161	41.451	2120	756127.9	2231207.8	33	11
KAD-352	20.161	41.451	2116	756115.3	2231209.8	344	16
KAD-353	20.161	41.451	2115	756109.1	2231207.5	150	51
KAD-354	20.161	41.451	2111	756098.6	2231207.4	260	44
KAD-355	20.161	41.454	2134	756431.9	2231231.1	133	464
KAD-356	20.161	41.454	2128	756416.3	2231229.8	7	9
KAD-357	20.161	41.454	2121	756374.4	2231232.5	256	500
KAD-358	20.161	41.453	2116	756339.9	2231232	276	527
KAD-359	20.161	41.453	2115	756277.1	2231234.4	88	85
KAD-360	20.161	41.452	2122	756229	2231232.6	235	273
KAD-361	20.161	41.452	2123	756184	2231229.7	1,840	1,114
KAD-362	20.161	41.452	2126	756156.8	2231231.5	96	407
KAD-363	20.161	41.451	2121	756141.1	2231232.4	191	146
KAD-364	20.161	41.451	2119	756114	2231229.8	44	33
KAD-365	20.161	41.451	2116	756105.6	2231228.5	81	30
KAD-366	20.161	41.451	2115	756100.4	2231227.3	127	59

Table A.1. Surficial samples assay results of Ni and Cu in Wadi Al Khadra prospect area (Cont.)

KAD-367	20.161	41.451	2115	756094	2231232.8	19	19
KAD-368	20.161	41.451	2113	756092	2231231.7	52	16
KAD-369	20.161	41.451	2112	756052.2	2231233.3	89	61
KAD-370	20.161	41.45	2112	756038.6	2231234.2	15	6
KAD-371	20.161	41.45	2113	756031.3	2231231.9	99	10
KAD-372	20.161	41.454	2133	756433.6	2231257.7	231	389
KAD-373	20.161	41.454	2126	756408.5	2231257.4	113	376
KAD-374	20.161	41.453	2118	756329.1	2231256.2	84	353
KAD-375	20.161	41.453	2119	756307.1	2231255.9	322	262
KAD-376	20.161	41.453	2115	756270.5	2231257.5	16	465
KAD-377	20.161	41.452	2108	756232.8	2231254.8	97	272
KAD-378	20.161	41.452	2115	756206.7	2231253.3	621	465
KAD-379	20.161	41.452	2119	756181.6	2231256.2	500	508
KAD-380	20.161	41.451	2112	756125.1	2231256.5	334	142
KAD-381	20.161	41.451	2113	756118.8	2231256.4	5	12
KAD-382	20.161	41.451	2111	756112.5	2231258.5	9	13
KAD-383	20.161	41.451	2108	756053.9	2231258.8	144	61
KAD-384	20.161	41.451	2110	756042.4	2231260.8	110	12
KAD-385	20.161	41.45	2111	756032	2231256.2	71	34
KAD-386	20.162	41.454	2130	756433.3	2231282.1	151	389
KAD-387	20.162	41.454	2122	756383.1	2231280.3	106	370
KAD-388	20.162	41.454	2119	756352.7	2231280.9	111	175
KAD-389	20.162	41.453	2116	756280.6	2231277.6	125	386

Table A.1. Surficial samples assay results of Ni and Cu in Wadi Al Khadra prospect area (Cont.)

KAD-390	20.162	41.453	2113	756264.9	2231279.6	27	562
KAD-391	20.162	41.452	2112	756217.9	2231273.4	4,573	972
KAD-392	20.162	41.452	2116	756200	2231279.8	95	272
KAD-393	20.162	41.452	2116	756163.4	2231279.2	538	504
KAD-394	20.162	41.452	2119	756157.1	2231280.2	1,335	666
KAD-395	20.162	41.451	2114	756138.3	2231282.2	55	71
KAD-396	20.162	41.451	2108	756116.3	2231280.8	53	23
KAD-397	20.162	41.451	2108	756110.1	2231279.6	14	20
KAD-398	20.162	41.451	2107	756067.2	2231280	13	15
KAD-399	20.162	41.454	2122	756395.3	2231302.6	106	374
KAD-400	20.162	41.454	2122	756368	2231307.7	240	438
KAD-401	20.162	41.453	2120	756346.2	2231301.9	114	324
KAD-402	20.162	41.452	2110	756211.1	2231307.6	335	543
KAD-403	20.162	41.451	2110	756102.4	2231301.6	198	92
KAD-404	20.162	41.452	2111	756167.3	2231302.5	1,545	1,370
KAD-405	20.162	41.452	2113	756149.5	2231305.6	47	17
KAD-406	20.162	41.452	2112	756142.2	2231304.4	73	24
KAD-407	20.162	41.451	2104	756113.9	2231307.3	51	15
KAD-408	20.162	41.451	2105	756096.1	2231308.1	64	39
KAD-409	20.162	41.454	2130	756430.5	2231330.8	101	255
KAD-410	20.162	41.454	2129	756388.6	2231330.2	42	235
KAD-411	20.162	41.454	2127	756352	2231328.5	49	247
KAD-412	20.162	41.453	2126	756329	2231330.4	31	258

Table A.1. Surficial samples assay results of Ni and Cu in Wadi Al Khadra prospect area (Cont.)

KAD-413	20.162	41.453	2118	756292.4	2231328.8	85	227
KAD-414	20.162	41.452	2107	756196.2	2231327.3	102	290
KAD-415	20.162	41.452	2106	756177.4	2231328.2	3,214	1,772
KAD-416	20.162	41.452	2108	756165.8	2231329.1	746	329
KAD-417	20.162	41.451	2111	756137.6	2231330.9	82	24
KAD-418	20.162	41.451	2109	756129.2	2231330.8	14	15
KAD-419	20.162	41.454	2133	756430.1	2231355.2	129	308
KAD-420	20.162	41.454	2139	756413.2	2231362.7	31	168
KAD-421	20.162	41.454	2133	756391.4	2231353.5	66	225
KAD-422	20.162	41.454	2131	756355.8	2231357.4	56	201
KAD-423	20.162	41.453	2129	756328.6	2231358.1	35	202
KAD-424	20.162	41.453	2122	756298.3	2231356.5	141	180
KAD-425	20.162	41.453	2115	756256.4	2231357	33	232
KAD-426	20.162	41.452	2113	756190.6	2231353.8	85	94
KAD-427	20.162	41.452	2105	756161.2	2231357.8	325	207
KAD-428	20.162	41.452	2109	756155	2231354.4	6,345	1,039
KAD-429	20.162	41.451	2108	756135.1	2231354.1	179	56
KAD-430	20.162	41.454	2144	756433.8	2231384	55	556
KAD-431	20.162	41.454	2145	756406.7	2231382.5	303	541
KAD-432	20.163	41.454	2135	756353.3	2231386.2	160	500
KAD-433	20.162	41.453	2131	756323.1	2231378	81	474
KAD-434	20.163	41.453	2121	756269.6	2231383.8	190	476
KAD-435	20.163	41.452	2116	756209	2231382.9	212	492

Table A.1. Surficial samples assay results of Ni and Cu in Wadi Al Khadra prospect area (Cont.)

KAD-436	20.163	41.452	2115	756161.9	2231382.2	64	378
KAD-437	20.162	41.451	2107	756124.3	2231379.5	58	21
KAD-438	20.163	41.451	2108	756054.2	2231384	7	11
KAD-439	20.163	41.451	2113	756051.1	2231380.6	96	14
KAD-440	20.163	41.454	2158	756430.5	2231398.4	88	354
KAD-441	20.163	41.454	2154	756416.8	2231404.8	439	616
KAD-442	20.163	41.454	2159	756413.7	2231405.9	16	13
KAD-443	20.163	41.454	2154	756389.6	2231405.5	88	363
KAD-444	20.163	41.453	2141	756331	2231405.8	154	304
KAD-445	20.163	41.453	2132	756281.9	2231405	228	193
KAD-446	20.163	41.452	2121	756221.2	2231406.4	202	362
KAD-447	20.163	41.452	2115	756168.9	2231408.9	197	457
KAD-448	20.163	41.451	2113	756060.1	2231407.3	6	10
KAD-449	20.163	41.451	2115	756052.8	2231406.1	30	14
KAD-450	20.163	41.454	2162	756430	2231432.7	183	500
KAD-451	20.163	41.454	2170	756397.6	2231428.9	145	358
KAD-452	20.163	41.453	2145	756339.1	2231428	67	361
KAD-453	20.163	41.453	2133	756285.7	2231430.6	75	284
KAD-454	20.163	41.453	2131	756279.4	2231432.7	57	40
KAD-455	20.163	41.452	2111	756166.5	2231429.9	58	90
KAD-456	20.163	41.451	2106	756130.9	2231431.6	283	455
KAD-457	20.163	41.451	2104	756113.1	2231430.2	2,138	358
KAD-458	20.163	41.451	2112	756050.3	2231430.4	20	19

APPENDIX B.

MINERALIZATION ZONES OF DRILL HOLES IN WADI AL KHADRA

PROSPECT AREA

Table B.1. Mineralization zones of drill hole Co01

Depth (meter)	Drill KAD - Co01	
	Mineralization	
0.00 – 4.90 m	<ul style="list-style-type: none"> • Oxidation zone is observed down to 8.60m. • Hematite and small amount of limonite are observed only along the fractures. • Traces of disseminated pyrite, pyrrhotite, and chalcopyrite are found scattered. 	
4.90 – 26.50 m	<ul style="list-style-type: none"> • From 5 to 6m, micro veins of milarite, chalcopyrite and pyrite <4% finely disseminated in the metamorphosed groundmass. • From 9.30 to 9.40m, a pyrite and chalcopyrite micro vein is found associated to chlorite follow the axis of the core. <4%. • From 9.40 to 26.50 m, mineralization interval with massive sulfides comprised by 10% of pyrrhotite, 15% of pyrite, 10% of chalcopyrite ,and traces of sphalerite. 	
26.50 – 32.50 m	<ul style="list-style-type: none"> • Massive lava flow layer only metamorphosed; some pyrrhotite, pyrite and pyrite along foliation <5%. 	
32.50 – 34.10 m	<ul style="list-style-type: none"> • Stringer and veinlets vary from 1cm to 6 cm in thickness; comprise by pyrrhotite, pyrite, chalcopyrite <45% with increasing associated quartz content <15% 	
34.10 – 66.10 m	<ul style="list-style-type: none"> • Traces of cubic pyrrhotite and pyrite along stringers, blebs and veinlets of chlorite which are sub parallel to the incipient foliation 	
66.10 – 80.20 m	<ul style="list-style-type: none"> • pyrrhotite, pyrite and magnetite <3% in grains along fractures 	

Table B.2. Mineralization zones of drill hole Co02

Depth (meter)	Drill KAD - Co02
	Mineralization
0.00 – 39.72 m	<ul style="list-style-type: none"> • Oxidation zone is observed down to 17.80m. • Hematite and small amount of limonite are observed only along the fractures. • Traces of disseminated pyrite, pyrrhotite, and magnetite are found scattered.
39.70 – 43.05 m	<ul style="list-style-type: none"> • Hematitic (oxides) veinlets diminishes < 2% with a thickness of about 2mm. • Traces of pyrite in small grains in groundmass
43.05 – 48.80 m	<ul style="list-style-type: none"> • Traces of pyrrhotite along foliation
48.80 – 62.80 m	<ul style="list-style-type: none"> • Traces of disseminated cubic pyrite
62.80 – 70.40 m	<ul style="list-style-type: none"> • Strong chloritization and silicification. • Quartz micro veinlets and micro veins < 5%, Traces of pyrrhotite. • Epidote increases <10%
71.40 – 78 m	<ul style="list-style-type: none"> • Traces of pyrrhotite along the texture of veinlets
78.40 – 83.23 m	<ul style="list-style-type: none"> • Traces of pyrrhotite and pyrite along the texture of veinlets
83.23 – 92.10 m	<ul style="list-style-type: none"> • Chlorite and silicification < 20%
92.10 – 102.45 m	<ul style="list-style-type: none"> • Pyrite and chalcopyrite are seen in traces along the foliation < 3%

Table B.3. Mineralization zones of drill hole Co03

Depth (meter)	Drill KAD - Co03	
	Mineralization	
0.00 – 4.80 m	<ul style="list-style-type: none"> • Iron oxides < 10% comprised by hematite and some goethite • Oxidation zone affecting also some pyroxenes • Traces of pyrite and chalcopyrite are found along foliation 	
4.80 – 8.20 m	<ul style="list-style-type: none"> • Traces of pyrrhotite and magnetite 	
8.20 – 18.65 m	<ul style="list-style-type: none"> • Traces of disseminated magnetite and pyrrhotite 	
21.29 – 21.55 m	<ul style="list-style-type: none"> • Disseminated pyrrhotite along rock and along thin CO₃ veinlets < 3% 	
21.55 - 23.55 m	<ul style="list-style-type: none"> • Mineralization diminishes to a stringer < 15% of massive sulfides 	
23.55 – 34.80 m	<ul style="list-style-type: none"> • Zone of mineralization, abundant of sulfide, stringers, pyrrhotite + presence of chalcopyrite, sph along fractures with CO₃ 	
34.80 – 68.90 m	<ul style="list-style-type: none"> • Disseminated pyrite and chalcopyrite along the foliation and disseminated in the groundmass 	
68.90- 80 m	<ul style="list-style-type: none"> • Sulfides decreases to traces along foliation and filled plagioclase-quartz 	
80 – 92.34 m	<ul style="list-style-type: none"> • Traces of pyrrhotite and pyrite disseminated bordering the plagioclase cloths 	
92.34 – 95 m	<ul style="list-style-type: none"> • Traces of pyrrhotite and pyrite disseminated in groundmass 	

Table B.4. Mineralization zones of drill hole Co04

Depth (meter)	Drill KAD - Co04	
	Mineralization	
0.00 – 7.10 m	<ul style="list-style-type: none"> • Traces of pyrite are found along fractures but highly oxidized <4%. • Oxidation zone close to the surface. 	
7.10 – 8.40 m	<ul style="list-style-type: none"> • Oxidation zone traces of pyrite and chalcopyrite along foliation. • Oxidized millerite are found along foliation <3% 	
8.40 – 12.60 m	<ul style="list-style-type: none"> • Traces of pyrite, chalcopyrite, and pyrrhotite are found in this oxidation zone 	
12.60 – 19.75 m	<ul style="list-style-type: none"> • Oxidation is found along the fracture walls <10% and in blebs within the ground mass. Pyrite and chalcopyrite associated are seen <3% , and some copper oxides are seen <2% 	
19.75 – 23.10 m	<ul style="list-style-type: none"> • Strong chlorite, quartz and plagioclase alteration <60%. • Pyrite and chalcopyrite in discreet and elongated grains <4% 	
23.10 – 32.10 m	<ul style="list-style-type: none"> • Traces of pyrite, chalcopyrite, and pyrrhotite 	
32.10 – 47 m	<ul style="list-style-type: none"> • Traces of epidote and pyrrhotite 	
47 – 54.90 m	<ul style="list-style-type: none"> • Pyrrhotite and pyrite are found disseminated and stringers <3% along foliation and fractures of average 2mm. 	
54.90 - 72 m	<ul style="list-style-type: none"> • Pyrite (15%), chalcopyrite (10%), millerite(2%) and Pyrrhotite are among the most common sulfides present in these veins and magnetite < 2% 	
72 – 118 m	<ul style="list-style-type: none"> • Traces of po along induced foliation. Also, chalcopyrite and pyrite grains <2%. • Traces of magnetite crystals. 	

REFERENCES

- James E. Quick & Paul S. Bosch. (1990). Tectonic History of the Northern Nabatah Fault Zone, Arabian Shield, Kingdom of Saudi Arabia. USGS , Denver, CO: Report prepared by the U.S. Geological Survey in cooperation with the Deputy Ministry for Mineral Resources, Saudi Arabia.
- ADE-HALL. (n.d.). The magnetic properties of some submarine oceanic lavas. *Geophys*, JI 9 (1): 85-92.
- Adel A.R. Zohdy, G. P. (1974). Application of surface geophysics to ground-water investigations. USGS.
- Affleck, J. (1963). MAGNETIC ANOMALY TREND AND SPACING PATTERNS. SEG.
- Agency, U. E. (2016). Time - Domain Electromagnetic methods.
- Alamta Singarimbun, Mitra Djamal, and Fitri Meliaweti. (n.d.). Self-Potential Methods on Geothermal Exploration (Case study: Mount Patuha, West Java, Indonesia). Recent Researches in Geography, Geology, Energy, Environment and Biomedicine.
- Al-Awsat, A. (2018). Saudi Arabia: Minerals Geological Storage Exceeds. Asharq Al-Awsat, <https://aawsat.com/english/home/article/1325596/saudi-arabia-minerals-geological-storage-exceeds-13-trillion>.
- Aljahdali.N,Fscarrach.R,Khalil.I,Jinadi.E,Bokhari.T,Siddiqui.A,Kattu.G,Alamoudi.O. (2015). Geology and Mineralization of Wadi Al Khadra Cu-Ni Ore Prospect, Wadi Bidah District, Southwest Region, Kingdom of Saudi Arabia. Saudi Geological Survey.
- Al-quorashi, H.E., Al-ghamdi, M.A., and Al-Eissa, A.M. (1989). Assessment of prospects at Umm Ad Damar (23/41A). Saudi Arabian Directorate General of Mineral Resources .

- Alshanti, A. M. (2009). *Geology of the Arabian Shield of Saudi Arabia*. Jeddah, Saudi Arabia: Scientific Publishing Center - King Abdulaziz University.
- Alshanti, P. A. (2009). *Mineral Deposits of the Kingdom of Saudi Arabia*.
- Al-Zahrani, A. A. (2014). *MINING IN AL-BAHA REGION, SOUTH-WESTERN SAUDI ARABIA, IN ISLAMIC-ERA: THE ARCHAEOLOGY OF ASHAM*. UK: PhD dissertation, UNIVERSITY OF YORK, ARCHAEOLOGY.
- Anne Marie Helmenstine, P. (2019). *Copper Facts: Chemical and Physical Properties*. ThoughtCo.
- Anne Marie Helmenstine, P. (Updated 2019). *Nickel Element Facts and Properties*. Thoughtco.
- Azunna, Daniel. E., and Chukwu, Godwill. U. (May, 2018). *Investigation of Graphite and Sulphide Minerals in Some Parts of Southern Umuahia Using Self Potential Anomalies*. *Journal of Geography, Environment and Earth Science*.
- Blakely, R. (1995). *Potential Theory in Gravity & Magnetic Applications*. Cambridge: Cambridge University Press.
- Bournant, G. (1981). *Jabal Sayid copper-zinc deposits, synthesis of work and results of 1971-1974*. Saudi Arabian Deputy Ministry for Mineral Resources.
- Carter, R.B., and Tayeb, J. (1989). *Jabal Mardah: Examples of low-temperature volcanogenic pyrite and millerite-polydymite-veasite nickel deposits*, Kingdom of Saudi Arabia. Saudi Arabian Directorate.
- Chemistry, R. S. (2019). *Periodic Table*. Retrieved from <http://www.rsc.org/periodic-table>
- Chevremont, P., and Johan, Z. (1981). *Wadi Kamal-Wadi Murratijah ultramafic-mafic layered complex*. Deputy Ministry for Mineral Resources Open-File Report BRGM-OF-01-36, 143 p.
- Cluster, I. (2019). *Natural Resources*. Retrieved from ic.gov.sa.

CSA. (2008). Discovery Guides, A Brief History of Copper.

Database, I. A. (2010). CRC Handbook of Chemistry & Physics (18th Ed.) .

Donzeau, M. (1980). Geological study of the Jabal Ash Shizm prospect. French Bureau dr Recherches Geologiques et Minieres .

export.gov. (2018). Saudi Arabia - Mining and Minerals. Retrieved from <https://www.export.gov/article?id=Saudi-Arabia-Mining-and-Minerals>.

Fred W. Cater and Peter R. Johnson. (1986). The explanatory notes to the Geologic map of the Jabal Ibrahim quadrangle. Jeddah, Saudi Arabia: Ministry of Petroleum and Mineral Resources.

Greenwood, W. (1975 a). Geology of the Jabal Ibrahim quadrangle, sheet 20/41C , Kingdom of Saudi Arabia, with section on Economic geology by R.G. Worl and Greenwood: Saudi Arabian Directorate General of Mineral Resources Geoscience Map GM-22, 18 p., scale: 100,000.

Haldar, S. K. (2013). Mineral Exploration , Principles and Applications.

JONATHAN E. NYQUIST,CHARLES E. CORRY. (2002). Self-potential: The ugly duckling of environmental geophysics. THE LEADING EDGE.

Keary P, B. M. (1991). An Introduction to geophysical exploration, Second Edition. London,UK: Blackwell Scientific Publication.

Khalid S. Essa and Marc Munschy. (2019). Mineral Exploration from the Point of View of Geophysicists. IntechOpen.

Lange's Handbook of Chemistry . (1952).

Lidiak, E.G., Hinze, W.J., Keller, G.R., Reed, J.E., Braile, L.W. and Johnson, R.W. (1985). Geologic Significance of Regional Gravity and Magnetic Anomalies in the East-Central Midcontinent. In: Hinze, W.J., Ed., The Utility of Regional Gravity and Magnetic Anomaly Maps,. Tulsa, 287-307: Society of Exploration Geophysicists.

- Lowrie, W. (2007). *Fundamentals of Geophysics*. Cambridge University Press.
- LUO, Y., XUE, D.-J., & WANG, M. (2010). Reduction to the Pole at the Geomagnetic Equator. *Chinese Journal of Geophysics*, 53(6), 1082-1089.
- Massaro, E. J. (2002). *Handbook of Copper Pharmacology and Toxicology*. Humana Press. ISBN 0-89603-943-9.
- Mendonca, C.A. and Silvia, B.C. (1993). A Stable Truncated Series Approximation of the Reduction-to-the Pole Operator. *Geophysics*, 58, 1084-1090.
- Meshref, W. (1990). *Tectonic Framework of Egypt*. A.A. Balkema, Rotterdam, Brookfield, p. 734.
- Michael Dentith, Stephen Mudge. (2014). *Geophysics for the Mineral Exploration Geoscientist*. Cambridge University Press.
- Mickus, K. (2014). *MAGNETIC METHOD*.
- Miller, H. G., and Singh, V.,. (1994). Potential field tilt – a new concept for location of potential field sources:. *Journal of Applied Geophysics*, 32, 213–217.
- Ministry of Energy and Industry And Mineral Resources, D. M. (Reprinted, 2016). *Mineral Resources of Saudi Arabia*. Kingdom of Saudi Arabia.
- Minstry of Energy, I. a.-D. (n.d.). *Mineral Information , A handbook of some of the Varied range of Minerals in the kingdom*. Jeddah: Deputy Ministry for Mineral Resources.
- Nyquist, J.E. and CORRY, C.E. (2002). *Self-Potential, The Ugly Ducking of Enviromental Geophysics*.
- Peter Hood and D. J. McClure. (1965). Gradient Measurements in Ground Magnetic Prospecting. *GEOPHYSICS*, p.403- 410.

- Puffett, W.P., Flanigan, V.J., Merghelani, H., Kiilsgaard, T.H., Gonzalez, L., Schmidt, D.I., and Hadley, D.G., (1975). Exploration for nickel at Jabal Jedair southeast of Ranyah, Kingdom of Saudi Arabia. U.S Geological survey Saudi Arabian project Report 199, 36 p.
- Ravat, D. (1996). Analysis of the Euler Method and Its Applicability in Environmental Investigations. *Journal of Environmental and Engineering Geophysics*, 1, 229-238.
- Ravat, D. (2007). Reduction to Pole. In: Gubbins D., Herrero-Bervera E. (eds) *Encyclopedia of Geomagnetism and Paleomagnetism*. Springer, Dordrecht.
- Reeves, C. (2005). E-Book on Aeromagnetic Surveys: Principles, Practice and Interpretation. Retrieved March 2, 2017, from <http://www.geosoft.com/news/news-releases/e-book%09aeromagnetic-surveys%09principles-practice-and-interpretati>.
- Reynolds, J. M. (1995). *An Introduction to Applied and Environmental Geophysics*. North Wales, UK.
- RJ., B. (1995). *Potential theory in gravity and magnetic applications*. New York, USA: Cambridge University Press.
- S.J. Balch, T.J. Crebs, A. King, and M. Verbiski. (SEG 1998). *Geophysics of the Voisey's Bay Ni-Cu-Co Deposits*. Paper .
- Said, R. (1962). *The Geology of Egypt*. Elsevier, New York, p. 377.
- Salem, A., Williams, S., Fairhead, D., Ravat, D., and Smith, R., (2007). Tilt-Depth method: A simple depth estimation method using first-order magnetic derivatives. *The Leading Edge*, 26, 1502–1505.
- Smith, C.W., Anderson, R.F., and Dehlavi, M.R. (1977). *Geology and ore deposits of the Kutam mine, Kingdom of Saudi Arabia*. U.S. Geological survey Saudi Arabian Mission Project Report 211, 51 p.
- Spector, A. a. (1970). Statistical models for interpretation of aeromagnetic data. *Geophysics*, 35: 293 - 302.

survey, B. G. (2008). Nickel. Retrieved from Natural Environment Research Council.

Syd Visser *, SJ Geophysics Ltd., E. Trent Pezzot, S.J.V. Consultants Ltd., Nicholas C. Carter, Consultant. (2002). Time domain EM and magnetic mapping of the Ferguson Lake Nickel-Copper-Cobalt-PGE. SEG Int'l Exposition and 72nd Annual Meeting * Salt Lake City, Utah * October 6-11, 2002.

Syd Visser,E. Trent Pezzot,Nicholas C. Carter. (2002). Time domain EM and magnetic mapping of the Ferguson Lake Nickel-Copper-Cobalt-PGE. SEG Int'l Exposition and 72nd Annual Meeting .

Verduzco, B. F. (2004). New insights into magnetic derivatives for structural mapping. *The Leading Edge*, 23, 116–119.

W.M. Meshref, H.S. Sadek, S.H. Abdel El-Baki, A.H. El-Serafi, M.A. El-Kattan, M.A. El-Meliegy, M.N. El-Sheikh. (1980). Structural geophysical interpretation of basement rocks of the north Western Desert of Egypt. *Ann. Geol. Survey, Egypt*, X, pp. 920-939.

W.M.Telford,L.P.Geldart,R.E.Sheriff. (1990). *Applied Geophysics*. Cambridge University Press.

W.W. Guo,M.C. Dentith. (1998). Geophysical signature of the Jinchuan Ni-Cu-PGE deposit, Gansu Province,China. Article in *Exploration and Mining Geology*.

Witherly, K. (2009). Geophysical response of the Munali Ni-Cu deposit , Zambia. ASEG/PESA Conference - Adelaide, South Australia.

Worl, R.G. and Wynn, J.C. (1982). Preliminary exploration report and drilling proposal for the Wadi al khadra prospect, Wadi Bidah district, Kingdom of Saudi Arabia: Saudi Arabian Deputy Ministry for Mineral Resources . USGS-OF-02-9,18 p.

Yarger, H. (1985). Kansas Basement Study Using Spectrally Filtered Aeromagnetic Data. In: Hinze, W.J., Ed., *The Utility of Regional Gravity and Magnetic Anomaly Maps*. Tulsa, 213-232: Society of Exploration Geophysicists.

VITA

Abdulrahman Aljabbab was born in 1986 in Saudi Arabia. He received his Bachelor of Science in Geology in 2008 from King Saud University, Saudi Arabia. He started his job in 2008 as a researcher at Oil and Gas center, King Abdulaziz City for Science and Technology (KACST). In 2010, he received a scholarship to complete his graduate studies.

In May 2013, he received his Master of Science in Petroleum Engineering from Missouri University of Science and Technology.

Mr. Aljabbab began the Ph.D. program in Geological Engineering with an emphasis in Geophysics of Mineral Exploration at Missouri University of Science and Technology during the Fall semester of 2017.

In May 2020, Mr. Aljabbab received his Ph.D. in Geological Engineering from Missouri University of Science and Technology.